

SUSCEPTIBILITY MODELLING OF RAINFALL INDUCED
LANDSLIDES

By

KOSKEI KIPYEGON

Reg. Grad. Eng., B. Tech (Hons) Moi University

A THESIS SUBMITTED IN PARTIAL FULFILMENT OF THE
REQUIREMENTS OF THE AWARD OF THE DEGREE OF MASTER OF
SCIENCE IN WATER ENGINEERING TO THE DEPARTMENT OF
CIVIL AND STRUCTURAL ENGINEERING, SCHOOL OF
ENGINEERING OF MOI UNIVERSITY.

AUGUST, 2013

DECLARATION

DECLARATION BY THE CANDIDATE

This thesis is my original work and has not been presented for a degree in any other University. No part of this thesis may be reproduced without the prior written permission of the author and/or Moi University

.....
Koskei Kipyegon
TEC/PGCS/02/09

.....
Date

DECLARATION BY THE SUPERVISORS

This thesis has been submitted for examination with our approval as University Supervisors.

.....
Dr. C. M. W. Sitters
Moi University,
School of Engineering,
Department of Civil and Structural Engineering,
P.O. Box 3900 Eldoret, Kenya.

.....
Date

.....
Dr. Joel K. Kibiiy
Moi University,
School of Engineering,
Department of Civil and Structural Engineering,
P.O. Box 3900 Eldoret, Kenya.

.....
Date

DEDICATION

To my parents, brothers, sisters, and friends, without whose love and support the completion of this work would not have been possible.

ABSTRACT

Occurrence of rainfall induced landslides coincides in time with the period of high persistence of heavy wet spells and in spatial locations where vegetative cover has been denuded. As the rain water percolates into the slope it increases the soil water content and reduces in situ suction, followed by built-up of pore water pressures resulting in a decrease in the effective stress in the slope soils, and may induce to slope failure. The state of soil moisture content is a function of soil type, land use, soil thickness and rainfall intensity. The highest infiltration capacities are observed in loose, sandy soils while heavy clay or loamy soils have considerable smaller infiltration capacities. Vegetation cover is known to stabilize slopes majorly by roots reinforcement of soils. In this study a model was formulated to simulate previous landslide occurrence and then used in scenario analysis to establish the effects of wet spell persistence and land use changes on the stability of slope in the western stretch of Kerio escarpment. The April and May rainfall data for region's rainfall stations were applied in the analysis whereby HYDRUS 1D model was used in soil moisture analysis, formulated Markov chain/event based models was used in stochastic rainfall generation, formulated Ms-EXCEL infinite slope model was used in sensitivity and factor of safety analysis, ArcGIS tool was use in maps preparation and ILWIS GIS tool was used in mapping spatial distribution of slope stability. Results indicated that rainsum of wet spell greatly influences soil moisture condition and weekly antecedent rainfall best describes expectation of unstable areas when two rainfall patterns are being compared. Statistical assessment of unstable areas under different land use revealed the importance of vegetation cover in slope stabilization since the scenario that the study area was completely forested, the percentage of unstable and critical areas were 0.05% and 1.81% respectively while for the scenario that it was completely denuded (agriculture), the percentage of unstable and critical areas were 0.69% and 5.35% respectively. It was concluded that landslide prediction model was successfully developed and should be adopted in generation of landslide hazard maps when heavy rainfall is anticipated. The generated hazard maps was recommended as a basis tool for decision making to residents (in identifying habitable areas), environmentalists (in showing importance of tress), rescuers (e.g. Red Cross, in marshal resources) and engineers (in establishing major projects) so as to reducing, preventing and mitigating losses caused by landslides.

Keyword(s): Landslides, sensitivity analysis, Wet spell persistence, Land use, Markov chains, HYDRUS 1D, ArcGIS and ILWIS

LIST OF ABBREVIATIONS

a.s.l	- above sea level
ANOVA	- Analysis Of Variance
CDF	-Cumulative Density Function
DEM	-Digital Elevation Model
ESRI	- Environmental Systems Research Institute
F _s	-Factor of Safety
GA	-Green Ampt model
GAR	-Green Ampt model with redistribution
GIS	-Geographic Information System
GPS	-Global Positioning System
IDW	- Inverse Distance Weighting
ILWIS	-Integrated Land and Water Information System
KMD	- Kenya Meteorological Department
LPM	-Landslide Prediction Model
OCHA	- Office for the Coordination of Humanitarian Affairs
PDF	-Probability Density Function
RAR	- Root Area Ratio
RTS	- Root Tensile Strength
SMA	-Suction Matric Analysis model
SWCC	-Soil Water Characteristic Curve
TTEST	- Student t- Test
UNDP	- United Nations Development Programme

TABLE OF CONTENTS

DECLARATION	i
DEDICATION	ii
ABSTRACT.....	iii
LIST OF ABBREVIATIONS	iv
TABLE OF CONTENTS	v
LIST OF FIGURES	ix
LIST OF TABLES	xii
LIST OF PLATES	xiii
ACKNOWLEDGEMENT.....	xiv
CHAPTER ONE: INTRODUCTION.....	1
1.1 THE PROBLEM OF LANDSLIDES	1
1.2 RECENT LANDSLIDE OCCURRENCES IN THE WORLD.....	2
1.3 OCCURENCE OF LANDSLIDES IN KENYA	3
1.4 LANDSLIDE PRONE ZONES IN KENYA.....	5
1.5 TYPES OF LANDSLIDES MOVEMENT	5
1.6 PROBLEM STATEMENT.....	7
1.7 JUSTIFICATION	8
1.8 OBJECTIVE OF RESEARCH.....	8
1.8.1 Specific Objectives	8
1.9 STUDY APPROACH.....	8
1.10 THESIS OUTLINE.....	9
1.11 STUDY AREA	9
1.11.1 Location.....	9
1.11.2 Climate	10
1.11.3 Topography and Land Use	11
CHAPTER TWO: LITERATURE REVIEW.....	12

2.1 LANDSLIDE CAUSATIVE FACTORS	12
2.2 RAINWATER INFILTRATION AND ITS EFFECTS ON SLOPE STABILITY	14
2.2.1 Infiltration and Soil Water Movement	14
2.2.2 Soil Water Profile	17
2.2.3 Rainfall and Slope Stability	18
2.3 LAND USE AND ITS EFFECTS ON STABILITY OF SLOPES	21
2.3.1 Vegetation and Slope Stability	21
2.3.2 Land Use Changes and its Effects on Slope Stability	22
2.4 OVERVIEW OF LANDSLIDE ASSESSMENT METHODS	23
2.4.1 Hydrological Modelling	23
2.4.2 Slope Stability Modelling	26
2.4.3 Preview of Models Applied in the Study	29
CHAPTER THREE: METHODOLOGY	31
3.1 INTRODUCTION	31
3.2 WATERSHED DELINEATION	32
3.3 STOCHASTIC GENERATION OF DAILY RAINFALL	33
3.3.1 Introduction	33
3.3.2 Rainfall Data	34
3.3.3 Potential Evapo-Transpiration data	39
3.3.4 Markov Chains Application in Stochastic Rainfall Generation	39
3.3.5 Event Based Synthetic Rainfall Generation Method	43
3.4 PHYSICAL PROPERTIES OF SOIL	47
3.4.1 Soil as a Three Phase System	47
3.4.2 Porosity, Volumetric Water Content and Degree of Saturation	47
3.4.3 Density, Specific Gravity and Unit Weight	49
3.4.4 Gravimetric water content	50

3.4.5 Soil Water Conservation Curve (SWCC).....	51
3.5 HYDRUS 1D MODEL.....	54
3.5.1 Uniform Water Flow	54
3.5.2 Numerical Solution of Variably Saturated Flow Equation in HYDRUS 1D	55
3.5.3 Model Parameters, Inputs and Outputs	57
3.6 SLOPE STABILITY ASSESSMENT USING INFINITE SLOPE MODEL	59
3.6.1 Infinite Slopes and Mode of Failure	59
3.6.2 Determination of Root Cohesion Strength Using Wu Method	60
3.6.3 Rainfall Occurrence.....	64
3.6.4 Matric Suction and Suction Stress in Absence of a Water Table.....	65
3.6.5. Formulation of Generalized Infinite Slope Stability Function	70
3.7 SLOPE STABILITY ASSESSMENT AND HAZARD MAPPING.....	73
3.7.1 ILWIS GIS Tool Data inputs.....	73
3.7.2 Formulation of ILWIS GIS Mapping Function.....	81
3.8 FORMULATION OF LANDSLIDE PREDICTION MODEL (LPM).....	85
3.9 MODELS FORMUALTION ALGORITHMS.....	89
3.10 MODELLING STEPS	94
CHAPTER FOUR: RESULTS AND DISCUSSIONS.....	97
4.1 INTRODUCTION	97
4.2 GENERATION AND ANALYSIS OF SPATIAL RAINFALL.....	97
4.2.1 Analysis of Rainfall Data	97
4.3 SIMULATING LANDSLIDE OCCURRENCE IN MOKWO AREA	100
4.3.1 Soil Moisture Redistribution and Water Flow Flux	101
4.3.2 Suction Stress Analysis:	102
4.3.3 Sensitivity Analysis and Model Correction.....	103
4.3.4 Spatial Mapping Using ILWIS GIS MODEL	106
4.3.5 Discussion.....	106

4.4 SCENARIO ANALYSIS FOR SLOPE STABILITY ASSESSMENT	108
4.4.1 Evaluating Effects of Wet Spell Persistence on Slope Stability.....	108
4.4.2 Evaluating Effects of Land Use Change on Slope Stability.....	121
4.5 GROUND TRUTHING OF GENERATED HAZARD MAPS	125
CHAPTER FIVE: CONCLUSIONS AND RECOMMENDATIONS	126
5.1 CONCLUSIONS	126
5.1.1 Developing Model for Rainfall Induced Landslides:	126
5.1.2 Sensitivity of Slope Stability to Change in Variables	127
5.2 RECOMMENDATIONS.....	127
REFERENCES.....	129
APPENDICES.....	138
Appendix A (i): Formulated ILWIS GIS soil cohesion strength function	138
Appendix A (ii): Formulated ILWIS GIS landslide hazard mapping function	138
Appendix A (iii): Temporal parameters required by ILWIS GIS Functions in every section of soil.....	140
Appendix A (iv): Raster maps required by mapping functions in ILWIS GIS	141
Appendix B: Modelled suction stress results for areal rainfall data.....	142
Appendix C: Modelled soil water content for areal rainfall data	145
Appendix D: landslide prone areas of Kenya.....	148
Appendix E: Root tensile strength for various plant species.....	149
Appendix F: Rainfall data applied in analysis.....	151
Appendix G: Moi University Rainfall Occurrence Charts	153

LIST OF FIGURES

Figure 1. 1: Types of landslides movements	6
Figure 1. 2: Location of Study area (Western stretch of Kerio escarpment)	10
Figure 2. 1: Main forces on a block of soil on a slope	13
Figure 2. 2: Infiltration regime and net storm rain	15
Figure 2. 3: Soil moisture distribution with depth for infiltration into initially dry soil.	17
Figure 2. 4: Plot of pore water pressure response to rainfall at various soil depths.	19
Figure 2. 5: Plot of matric suction recovery with time during a dry spell	20
Figure 2. 6: Effect of rainfall on degree of saturation in different soils	20
Figure 3. 1: Procedure for watershed delineation using ArcGIS tool.	33
Figure 3. 2: Distribution of rainfall stations along western stretch of Kerio escarpment	36
Figure 3. 3: Definitions for event based analysis	44
Figure 3. 4: The three phases of a natural soil mass.	47
Figure 3. 5: Comparison plot of SWCC models	51
Figure 3. 6: spatial and temporal discretization used in solving Richards's equation	55
Figure 3. 7: Descritization of soil layer in Hydrus 1D model and an illustration of infiltration/percolation front.	58
Figure 3. 8: Comparative assessment of mean monthly rainfall data for various stations	65
Figure 3. 9: Forces in saturated slope under parallel seepage flow condition	71
Figure 3. 10: Slope map in degrees for the study area	74
Figure 3. 11: Land use map for the study area	75
Figure 3. 12 (a): RAR variation with soil depth for trees, herbs and reed	76
Figure 3. 12 (b): RAR variation with soil depth for shrubs	76

Figure 3. 12 (c): RAR variation with soil depth for Grasses	77
Figure 3. 13: Point interpolation results	79
Figure 3. 14: flow chart for Event based stochastic rainfall generator	89
Figure 3. 15: Flow chart of Suction stress analysis (MSA) model	90
Figure 3. 16: Flow chart of modified infinite slope stability model	91
Figure 3. 17: Flow chart of spatial mapping in ILWIS GIS Tool	92
Figure 3. 18: Flow chart of extracting and clipping maps using GIS	93
Figure 3. 19: Summary flow chart of Landslide Prediction Model, LPM	96
Table 4. 2: Rainfall station and their weights as used in areal rainfall generation	99
Figure 4. 1: Thiessen polygon for calculating areal rainfall	100
Figure 4. 2: Some of historical landslide occurrence sites in study area	101
Figure 4. 3: Soil water redistribution curve for loam with soil thickness of 1.5 m	102
Figure 4. 4: Variation of suction stress for loam soil of depth 1.5m	103
Table 4. 3: Sensitivity of model to parameter change	104
Figure 4. 5: Variation of F_s for loam soil of slope 40 degrees and depth of 1.5 m.	105
Figure 4. 6: Calibrated variation of F_s with time for soils in Mokwo area	105
Figure 4.7: Hazard map for Mokwo area as on 29 th April 2007.	106
Figure 4.8 (1): Fitting events to Poisson PDF distribution	110
Figure 4.8 (2): Fitting events to Poisson CDF distribution	110
Figure 4.8(3): Fitting events duration to Geometric PDF distribution	111
Figure 4.8(4): Fitting events duration to Geometric CDF distribution	111
Figure 4.8(5): Fitting daily rainfall depths to Gamma PDF distribution	112
Figure 4.8(6): Fitting daily rainfall depths to Gamma CDF distribution	112

Figure 4.8(7): Fitting inter-events to Geometric PDF distribution	113
Figure 4.8(8): Fitting inter-events to Geometric CDF distribution	113
Figure 4. 9: Plots of generated skewed and evenly distributed rains	114
Figure 4.10 (a): Volumetric moisture content curves for clay loam with soil thickness of 1 m in analysis using skewed rainfall pattern.	115
Figure 4.10(b): Volumetric moisture content curves for sandy loam with soil thickness of 1 m in analysis using skewed rainfall pattern.	115
Figure 4.10(c): Volumetric moisture content curves for clay loam with soil thickness of 2 m in analysis using evenly rainfall pattern.	116
Figure 4.10(d): Volumetric moisture content curves for sandy loam with soil thickness of 2 m in analysis using evenly rainfall pattern.	116
Figure 4.11 (a): Variation of Suction stress with time for clay loam soil with depth of 1m, under evenly distributed rainfall	117
Figure 4.11(b): Variation of Suction stress with time for sandy loam soil with depth of 1m, under evenly distributed rainfall	117
Figure 4.11(c): Variation of Suction stress with time for clay loam soil with depth of 2m, under evenly distributed rainfall	118
Figure 4.11(d): variation of Suction stress with time for sandy loam soil with depth of 2m, under skewed distributed rainfall	118
Figure 4. 12: Probability distribution of rainfall occurrence	121
Figure 4.13: Hazard map for complete forestation of study area as on 29 th April 2007	123
Figure 4.14: Hazard map for complete denudation of study area as on 29 th April 2007	124
Figure 4.15: 3D display of generated hazard map in Tot area	125

LIST OF TABLES

Table 1. 1: Causes of landslides	1
Table 3. 1: Location coordinates of rainfall stations	35
Table 3. 2: Lambda constant for calculating RAR distribution with depth	77
Table 3. 3: Plant properties used in calculating root cohesion strength	78
Table 3. 4: Soil properties table	79
Table 3. 5: Soil depth classification	80
Table 3. 6: Typical ranges of unsaturated soil parameters for various soils	81
Table 3. 7: Matric suction stress parameters	81
Table 4. 1: Mean annual rainfall for Thiessen polygons	98
Table 4. 4: Distributions fitting parameters	109
Table 4. 5: ILWIS GIS Statistical analysis for various stability classifications	119
Table 4. 6: Cumulative antecedent rainfall for Skewed and evenly rainfall	120

LIST OF PLATES

Plate 1. 1: Fatal landslide in kibigor village, Elgeyo-Marakwet County	4
--	---

ACKNOWLEDGEMENT

This study was made possible by the contributions of many people, whom I may not completely mention. I am sincerely grateful to my supervisors, Dr. C.M.W. Sitters and Dr. J.K. Kibiiy, for continual guidance from the inception of the thought to final writing. The Department of Civil and Structural Engineering and the MUK-VLIR_UOS project for financial support and a chance to undertake my MSc. studies.

I thank my fellow Msc. Students; M. A. Arot, D. K. Ndiema, and L. K. Sum for the assistance and collaboration during the study at Moi University. I also thank all staff members at the Department of Civil and Structural Engineering, Moi University, for continuous help throughout the study period.

Also grateful acknowledgements are extended to my parents, brothers, sisters and relatives for their constant encouragement and moral support. Finally to the almighty God for in him we live, move and have our being.

CHAPTER ONE: INTRODUCTION

1.1 THE PROBLEM OF LANDSLIDES

Generally, landslide is defined as movement of a mass of rock, debris or earth down a slope when the shear stress of the material is higher than its shear strength (Emba, 2010). The causes of landslides are usually related to instabilities in slopes and it is usually possible to identify one or more landslide causes and one landslide trigger. Landslide causes are listed in Table 1. 1, and include geological factors, morphological factors, physical factors and factors associated with human activity. Causes may be considered as factors that make the slope vulnerable to failure or that predispose the slope to becoming unstable.

Table 1. 1: Causes of landslides

Geological causes	Morphological causes	Physical causes	Human causes
i.Weak materials	i.Slope angle	i.Volcanic eruption	i.Excavation
ii.Weathered materials	ii.Uplift	ii.Ground water changes	ii.Deforestation
iii.Permeability contrasts	iii.Glacial erosion	iii.Soil pore water pressure	iii.Land use change
iv.Material contrasts	iv.Slope loading	iv.Earthquake	iv.Mining
	v.Vegetation change		v.Quarrying

The trigger is the single event that finally initiates the landslide. Triggering factors may either increase the shear stress, decrease the shearing resistance of the material or both. Common triggering factors of slope movements include; water infiltration (rainfall,

snowmelt, irrigation, leakage of drainage systems), erosion/excavation at the toe of the slope, surcharging and loading at the crest (by deposition or sedimentation, rapid drawdown (man-made reservoir, flood high tide, breaching of natural dams), earthquake, volcanic eruption, modification of slope geometry, fall of material (rock and debris), weathering (freeze and thaw weathering, shrink and swell weathering of expansive soils), physico-chemical changes, fatigue due to static/cyclic loading and creep, vegetation removal (by erosion, forest fire, drought or deforestation), earthquake shaking, artificial vibration (including traffic, pile driving, heavy machinery), mining and swinging of trees (Van Asch et al., 2007). In the majority of cases the main trigger of landslides is heavy or prolonged rainfall. A global survey of landslide occurrence has revealed that over 90% of landslides are triggered by heavy rainfall (Azizul, 2009). Rainfall triggers so many landslides principally because it drives an increase in pore water pressures within the soil thereby reducing the stresses between the soil particles and giving gravity force upper hand in driving landslide movement (Corominas and Moya, 1999).

Landslides represented 4.89% of the natural disasters that occurred worldwide during the years 1990 to 2005 (Kanungo et al., 2006) and this trend would be continued increasingly, if unplanned urbanization and development be increased and/or irregular deforestations are continued.

1.2 RECENT LANDSLIDE OCCURRENCES IN THE WORLD

Every few years a large earthquake or torrential rainfall event triggers landslide that kills many more people. Recent examples include Hurricane Mitch in 1998 (possibly as many as 18000 landslide fatalities), Venezuela in 1999 (up to 30000 fatalities) and Haiti/Dominican Republic in 2004 (up to 4500 fatalities in two separate events) (Petley and Bulmer, 2004).

On the 8th August, 2010 a devastating mudslide occurred in the Chinese Gansu Province after floods and torrential rainfall. Several landslides were triggered by intense rainfall that transported gravel and mud into the river and built up a temporary dam. The lake behind the dam grew to a length of 3 km before it finally broke. An estimated 1.8 million cubic meter of debris swept through three villages in Zhouqu County destroying homes and in Yueyuan village, not a single structure was left intact by the landslides (Bloomberg, 2010). The outflow slid down the valley as a wall of mud, wiping out houses and multi-story buildings, killing at least 1,144 residents (Boston Globe, 2010).

Unusually heavy rainfall in December 1999 triggered a disastrous chain of events in the several states of Venezuela, in particular in Vargas and Miranda. In the worst-hit areas, more than twice the average annual rainfall, which ranges between 400 and 900 mm, fell in the span of 72 hours. This heavy precipitation resulted in flash floods, fluvial torrents and debris flows, as well as landslides in densely populated areas. Major infrastructure including dikes, bridges, drains, and dams were undermined or destroyed, feeding into the flows. It is estimated that 30,000 people were killed, 600,000 affected and 114,000 homeless. 64,700 houses were damaged and another 23,000 destroyed (IADB 2000).

1.3 OCCURENCE OF LANDSLIDES IN KENYA

In Kenya landslides do occur during months of heavy rainfall and when it occurs people are maimed or killed and properties are destroyed by the sliding mud. A mudslide occurred in Kibigor village, Kapkosom location in Elgeyo-Marakwet County on Friday, 2nd December, 2011(see Plate 1. 1) claiming the lives of three children after a relentless rainfall (Standardmedia, 2011). On Thursday, 29th April, 2010 a landslide

struck Kitony village, Kapen location in the Marakwet district of Elgeyo-Marakwet County of Kenya, after relentless heavy rains killing more than 10 people, (BBC news 2010, Standardmedia 2010), and on Monday, 3rd May, 2010 families were rendered homeless at a village in Mathira following landslides caused by heavy rains. There are reports of whole families being buried during the long rains of April and May on 2002 and 2003 in Murang'a district (UNDP 2005). These implies that as the country anticipates periods of heavy rainfalls it should also be prepared for the likelihood of landslides occurrences and therefore the Landslide monitoring and early warning systems will have to been developed to predict and map out prone areas. Landslides occurrences in Kenya are also aggravated by human activities that are injurious to the environment thus destabilizing the already fragile slopes.



Plate 1. 1: Fatal landslide in kibigor village, Elgeyo-Marakwet County

(Source: Standardmedia, 2011)

1.4 LANDSLIDE PRONE ZONES IN KENYA

Landslides are usually experienced during months of heavy rainfall in areas around Mount Kenya region which include Muranga, Thika, Maragua, Nyeri, Kirinyaga, Nyandarua, some parts of Kiambu and also some parts of western parts of Kenya mostly the mountainous Rift Valley such as Marakwet, Kericho and Nandi hills. *Appendix D* is a map of Kenya showing areas prone to landslides and their levels of susceptibility.

1.5 TYPES OF LANDSLIDES MOVEMENT

The five primary types of landslides movement include; slides, spreads, creep, flows and fall (see Figure 1. 1), and are distinguished on the basis of the relationship between the unstable mass and the failure surface and the internal structure and deformation of the mass (Ritter, 2004).

Slides move as coherent blocks or masses along the failure plane. Slides exhibit little internal shear or deformation such that patches of turf, trees, and structures on the surface may stay relatively intact and are not incorporated into the slide (Ritter, 2004). Soil or sediment stratigraphy within the sliding mass also may be preserved.

Lateral Spreads are type of landslide associated with nearly flat topography. This type of movement is initiated by tectonic movement such as earthquakes which shakes already saturated piece of land thereby shoving aside some pieces of land.

Creep is another type of slope movement and is indicated by the bases of trees in a slope each bowing outward in the downslope direction or a situation whereby some of the retaining walls are bulging out over the sidewalks.

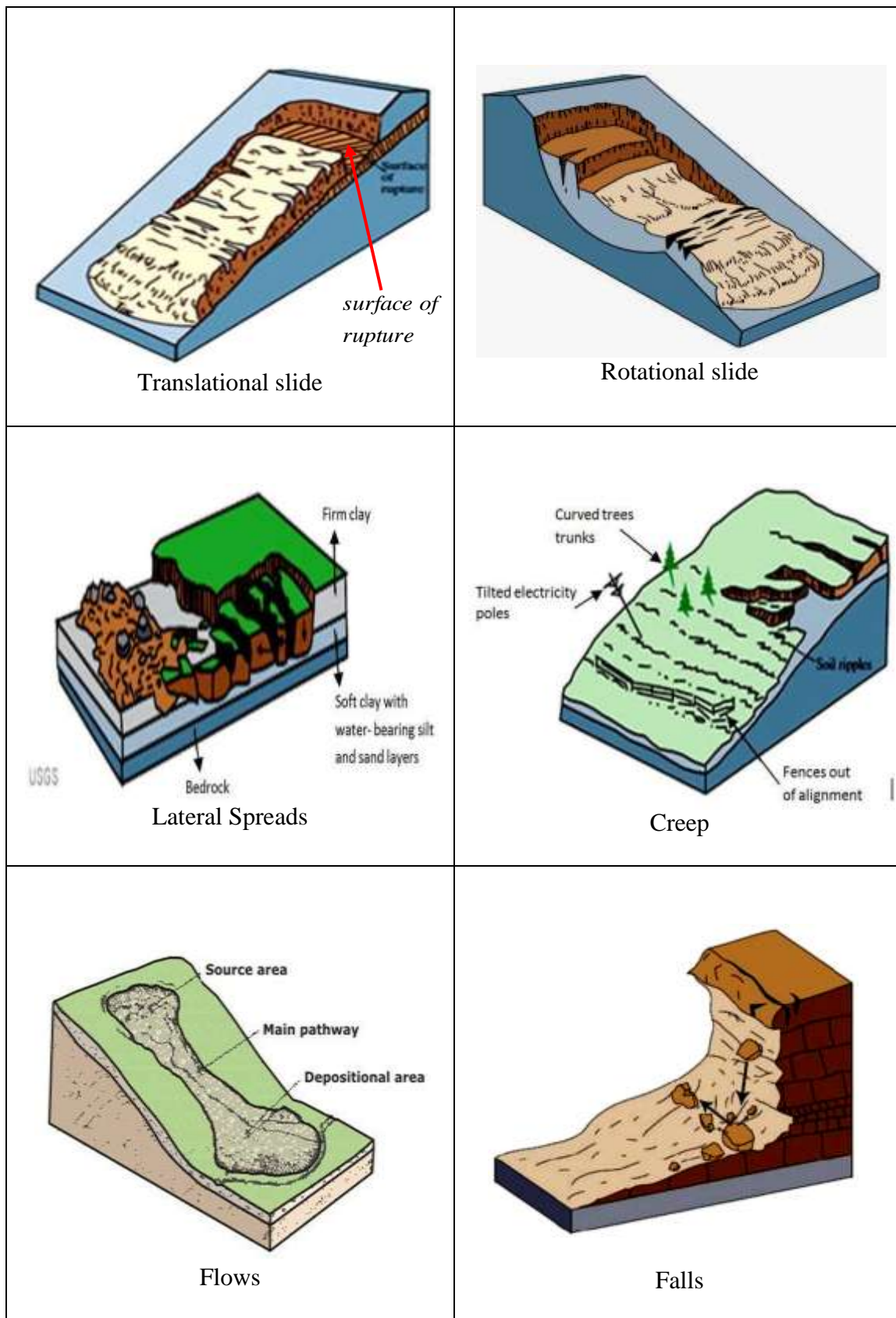


Figure 1. 1: Types of landslides movements

(Source: <http://geology.com/usgs/landslides/>)

Flows move as a coherent but constantly changing mass, involving internal shear or mixing of the mass, even sorting based on particle size and position in the flow. Surface features such as turf, shrubs, trees, and structures are incorporated into the flow (Ritter, 2004). Down slope materials and surface features may be buried by the flow mass, but they may also be incorporated into the flow as this type of slide tends to be erosive as it travels along its path.

In falls, the material may be in freefall, losing contact with the failure surface intermittently or entirely. In this type of landslide the mass moves as individual particles, with no coherent structure developing between particles (*Source: <http://geology.com/usgs/landslides/>*)

1.6 PROBLEM STATEMENT

Landslides are among the hazardous geological processes which not only cause enormous damage to roads, bridges, and houses but also lead to loss of life. Kenya is not immune to landslides as this phenomenon does occur nearly every year during months of heavy rainfall, implying that as the country anticipates periods of heavy rainfalls she should also be prepared for the likelihood of landslides occurrences. Avoidance of landslide prone areas is the easiest and cheapest option to prevent damage from mass movements, but is not an option for the cases of already existing infrastructure and settlement. Securing prone areas by grading, excavation and by adopting technical protective measures are expensive and may not be technically or economically feasible if the area is expansive. Hence, there is a need for development of landslide monitoring and early warning systems for assessing stability of slopes and consequently generating corresponding hazards maps based on anticipated rainfall. Landslides are the result of complex interaction among several factors, primarily involving geological, geomorphological, anthropological and meteorological factors.

Landslides triggered by rainfall can be predicted by modelling the relationship between rainfall and landslide occurrence, and this study endeavours to develop a model for use in assessing stability of slopes at any time based on anticipated rainfall events.

1.7 JUSTIFICATION

Landslides generally happen where they have occurred in the past, and in identifiable hazard locations and are triggered by rapid saturation of the soil which in turn reduces cohesion, matric suction and friction (UNDP 2005). The landslide prediction model formulated in this study will assist in early decision making involving relocation of people and properties from hazard prone areas reducing considerable loss of lives and properties to landslides. Also generated hazard maps will aid the government in identification of unstable areas during the establishment of major projects such as cities, railways or roads and also in human settlement.

1.8 OBJECTIVE OF RESEARCH

The main objective of this study was to develop a model for predicting occurrence of rainfall induced landslide and using it to evaluate the sensitivity of slope stability to land use and wet spell variables.

1.8.1 Specific Objectives

1. To develop Markov and Event based models for stochastically generating rainfall patterns
2. To analyze subsurface water movement
3. To develop and calibrate slope stability model
4. To assess spatial variability in stability of slopes using ILWIS GIS tool.

1.9 STUDY APPROACH

This study shall be undertaken in five levels which include; preparation of geotechnical data, models formulation, hydrological modelling, slope stability analysis and hazard

mapping. Soil, DEM and landuse maps will be collected from relevant institutions and will be used to derive morphological and geotechnical information. Hydrological modelling involves stochastic rainfall generation, soil water content analysis and water flow flux analysis and was undertaken outside the GIS software. Stochastic rainfall generation was undertaken using developed Ms-EXCEL models of Markov chains model and Event based models, water flow flux (negative infiltration) and volumetric water content was analysed using HYDRUS 1D model. The matric suction stress and infinite slope stability equations was merged into a function in both ILWIS GIS tool (for spatial mapping) and Ms-EXCEL Landslide prediction model (for identification of critical mapping day). The mapping function in ILWIS GIS tool shall be formulated taking into consideration spatial variation in components of hydrology and topography that affects stability of slopes and these components include; water flow flux, soil moisture, slope, land use and soil type.

1.10 THESIS OUTLINE

This study is designed to provide a systematic understanding of procedure used in formulating, calibrating and application of a model in simulation of rainfall induced landslide. Chapter 2 summarizes the principles of slope instability and landslides occurrences while chapter 3 presents the materials and methodology applied in the study. Results and discussions are presented in Chapter 4 and chapter 5 presents conclusion and recommendation for further studies.

1.11 STUDY AREA

1.11.1 Location

Western stretch of Kerio escarpment is located in Elgeyo-Marakwet County (Figure 1. 2). Geographically, Elgeyo-Marakwet County lies between latitude $0^{\circ} 51'N$ to $1^{\circ} 19'N$ and longitude $35^{\circ} 29'E$ to $35^{\circ} 43'E$ and occupies an area of 30sq km. The altitude

in Elgeyo-Marakwet county ranges from 1000 meters above sea level (a.s.l) in Kerio Valley floor to about 3000 meters a.s.l in the highlands of the Keiyo Escarpment (Muchemi, 2002). At the highlands, Kerio Valley is clearly seen with Kerio River meandering through it. The Kerio River originates from the Elgeyo escarpment and runs through Marakwet and East Pokot before emptying to Lake Turkana. The river runs in the north direction parallel to the escarpments, which are about 2400 meters a.s.l at Kamariny and the Tugen mountain range in Baringo District. East and west from the river's banks lays a stretch of flat land, about a 1.5 Kilometres each (Kalenjinonline, 2012).

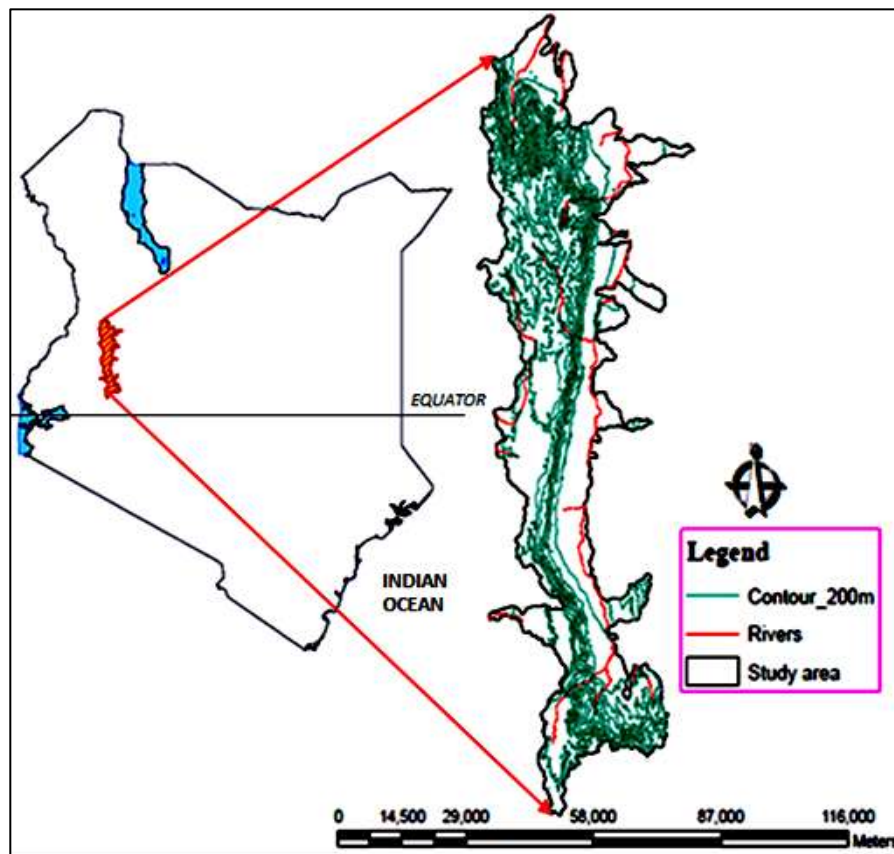


Figure 1. 2: Location of Study area (Western stretch of Kerio escarpment)

1.11.2 Climate

The highlands are characterized by high bimodal rainfall figures ranging between 1,200 mm to 1,700 mm while rainfall in the escarpment ranges between 1,000 mm to

1,400 mm per year. The Kerio Valley receives between 700 mm to 1,000 mm. However, the rainfall pattern in the valley is quite erratic and figures as low as 220 mm per year have been recorded (Muchemi, 2002). The average annual temperature at the valley is around 26 degrees Celsius and between 6 to 18 degrees Celsius at the highlands (Kalenjinonline, 2012). Rainfall distribution is highly influenced by topography. Mean annual evaporation rate is about 2000 mm in the valley and 1300 mm in the highlands. The highlands are generally wet while the valley floor is dry and semi-arid (KAGOECH, 2012).

1.11.3 Topography and Land Use

The Great Rift Valley is associated with steep escarpments and mountains. Kerio escarpment has steep rolling slopes of thinner loamy textured soils. Increasing population and lack of employment opportunities in other sectors have forced farmers to cultivate on steeper slopes. Forests have been cleared to give way to farmland and this has resulted in degradation of water sources, rampant soil erosion, and declining soil fertility (Muchemi, 2002). During heavy rains, the escarpment (tumoo) and the middle zone (mosop and korget) suffer from landslides, mudslides, and soil erosion while the valley floor (soin) suffer from floods and gaping/deep gullies, and all these threaten the suitability and sustainability of the environment (KAGOECH, 2012).

The valley floor is sparsely covered with mainly Acacia trees (sesia) and other indigenous trees and is generally used for grazing indigenous breeds of livestock mainly cattle, sheep and goats. The highlands are generally green with forests and meadows and are suitable for agricultural activities. In some parts of the highlands (escarpment) there are indigenous forests and trees such as Bamboo (tegat), cedar (torokwet), periplica or sycamore (sinendet). (KAGOECH, 2012).

CHAPTER TWO: LITERATURE REVIEW

2.1 LANDSLIDE CAUSATIVE FACTORS

Numerous natural factors such as meteorological factors (concentrated rainfall events), anthropogenic factors (deforestation and slope excavation), and geological factors (earthquakes and undercutting of banks by flood) contribute to slope failures by decreasing shear strength or increasing shear stress of the soil mass. However, most of the slope failures coincide with the period of intensive rainfall (Lakhan, 2009).

Rainfall-induced landslides pose significant hazards in many parts of the world especially in mountainous areas during periods of intense rainfall as these phenomena occur frequently. It is widely known that rainfall induces a rise of the groundwater level decreasing the stresses between the soil particles thus decreasing the soil strength and that may results in slope failure. However, how much the groundwater level has to rise to trigger the observed slope failures is still unknown. To obtain the stresses between the soil particles, pore water pressure is required. If this pressure is negative with respect to the ambient atmospheric pressure it is called matric suction. Matric suction increases the strength of the soil. If the pore water pressure is positive with respect to the ambient atmospheric pressure because of rainfall, it reduces the strength of the soil. Measurements of matric suction can be made in situ using tensiometers (Fredlund and Rahardjo, 1993). In order to determine indirectly the increase or decrease of the matric suction, the relationship between the matric suction of the soil and the water content is required. This relationship is called the soil water characteristic curve, SWCC (Yeh et al., 2008). The amount of rainfall that infiltrates the slope during a wet spell is obtained using infiltration models such as Green-Ampt, Richards's and Horton's models.

The general procedure applied in analyzing the stability of a slope is to compute the shearing resistance available along a critical sliding surface and to compare this with the driving forces present along the surface. The critical surface will be assumed planar though can be circular depending upon the type of soil, depth to bedrock or layering sequences. If the comparison, called a factor of safety (F_s), results in a value less than or equal to unity, the slope will or is likely to fail. In general equation form,

$$F_s = \frac{\text{resisting forces}}{\text{driving forces}}$$

The major driving force present in any slope is the combined weight of the soil mass and water. The fully mobilized shear resistance along the critical failure surface is the major resisting force.

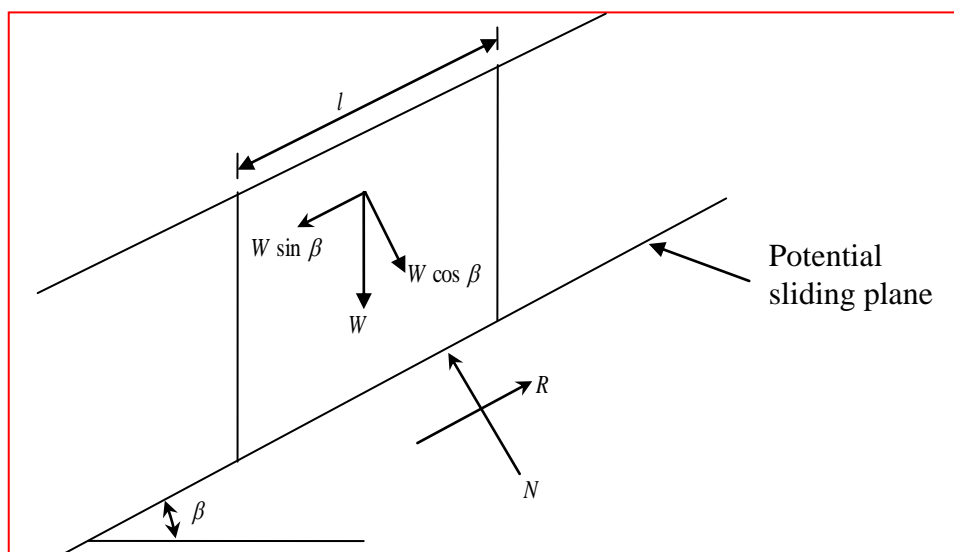


Figure 2. 1: Main forces on a block of soil on a slope

(Source: http://www.tulane.edu/~sanelson/Natural_Disasters/slopestability.htm)

Infinite slopes usually fail by sliding linearly along the firm surface. Figure 2. 1 illustrates the main forces acting on a block of soil on a slope. The weight of the block is W and the force that tries to drive the block down the slope is $W \sin \beta$, where β is the angle of the slope. The resistance R of the potential sliding plane should be larger

than $W \sin \beta$ to have a stable situation. The resistance R is composed of two contribution; a contribution origination from the cohesion of the soil and a contribution which is proportional to the normal force, $N = W \cos \beta$ (coulomb's law of friction). When the slope fills up with water the fluid pressure provides the block with buoyancy reducing the normal force N and thus the resistance R . This reduces the stability and R may become smaller than $W \sin \beta$ and thus inducing a landslide. The Factor of safety F_s , will thus be the ratio of the resistance R , to that promoting movement, $W \sin \beta$, that is $F_s = R/W \sin \beta$.

2.2 RAINWATER INFILTRATION AND ITS EFFECTS ON SLOPE STABILITY

2.2.1 Infiltration and Soil Water Movement

Infiltration refers to the movement of water into the soil layer. The rate of this movement is called the infiltration rate. The total amount of water entering the soil since the start of infiltration into the soil is referred to as the cumulative infiltration. Movement of water into the soil is controlled by gravity, capillary action, and soil porosity. Of these factors soil porosity is most important (Gustafson et al, 2005). A soil's porosity is controlled by its texture, structure, and organic content. Coarse textured soils have larger pores and fissures than fine-grained soils and therefore allow for more water flow. The rate of infiltration normally declines rapidly during the early part of a rainstorm event and reaches a constant value after several hours of rainfall. A number of factors are responsible for this phenomenon (Gustafson et al, 2005), including:

- i. The filling of small pores on the soil surface with water reduces the ability of capillary forces to actively move water into the soil.

- ii. Hydraulic gradient decreases as soil saturation increases.
- iii. As the soil moistens, the micelle structure of the soil particles absorbs water causing them to expand thus reducing the size of soil pores.
- iv. Raindrop impact breaks large soil clumps into smaller particles which clog soil surface pores reducing the movement of water into the soil.
- v. Also the rate of water entry into the soil depends on the amount of water in the soil and the wetter the soil, the lower is the rate of water infiltration into the soil.

If rainfall intensity is greater than the infiltration rate, water will accumulate on the surface (ponding) and runoff will begin. Ponding starts at a point when rainfall rate is greater than infiltration rate and ends at point when rainfall rate is less than infiltration rate. Figure 2. 2 illustrate ponding process and the region shaded blue represent ponded water.

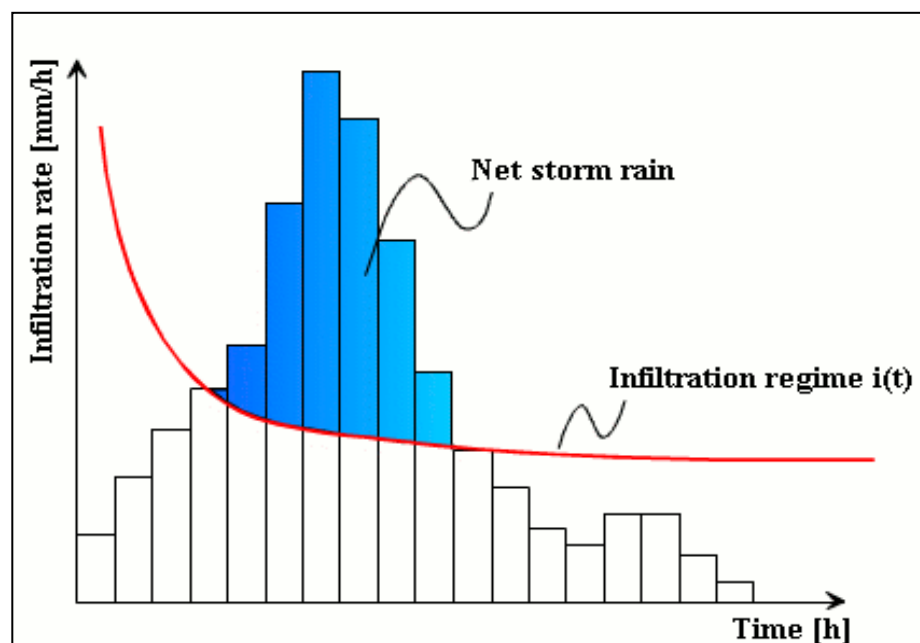


Figure 2. 2: Infiltration regime and net storm rain

(Source: Musy, 2001)

Water can move through the soil in all directions, but (between two points) it always moves from a point at higher potential (i.e., higher total hydraulic head) to a point at lower potential (Trotta et al, 2004). The difference between the soil water potential or total hydraulic head (ΔH) between two points determines the direction of water flow, and the rate of change of the hydraulic head along the flow path between the points, referred to as gradient ($\Delta H/L$, where L is the length of the flow path), determines the rate of movement of water between them. The rate of water movement between the two points also depends on the hydraulic conductivity of the medium. Hydraulic conductivity, K , can be defined as a measure of the ability of soil (or any porous medium) to transport water.

Darcy's law (see equation 2.1) simply states that the rate of movement of water through a soil is proportionally related to the hydraulic gradient (i.e., the driving force acting on water) and the hydraulic conductivity of the medium (i.e., a measure of the ability of soil to transmit water) (Gustafson et al, 2005).

$$Q/\Delta t = v = K \cdot \Delta H/L \quad (2.1)$$

When the soil is fully saturated, most of the water passes through large tubular pores created by roots and animals or the planar voids between soil macropores. Although the inter-particle pores or pores inside soil peds (matrix pores) may be filled up with water, the rate of water movement is relatively slow in these pores as compared to the macropores. Under saturated conditions the hydraulic conductivity (i.e., K_s) of the soil is a constant value at any given time for any given point within the soil body. During the drainage process of a saturated soil volume with no water input (dry spell), water initially moves out of the larger pores due to gravity. Subsequently, water moves out of the smaller pores due to the reduction in soil water pressure head resulting from vertical drainage, plant root uptake and evaporation from the surface. As water moves

out of this volume of soil, the soil water content decreases and the tendency of the soil for holding to water increases (i.e., pressure head, h , decreases). Consequently, the flow path for water becomes narrower and the ability of the soil to transmit water (i.e. hydraulic conductivity, K) decreases as the soil water content decreases (Trotta et al, 2004).

2.2.2 Soil Water Profile

When the rate of water application to the soil equals or exceeds the maximum rate of infiltration into the soil the zone immediately below the surface where water is applied becomes saturated (Trotta et al, 2004). This zone is called saturation zone (see Figure 2. 3). The volume of the soil below this saturation zone is referred to as the transmission zone. In this unsaturated zone soil water content is fairly uniform (for a uniform soil). At the other end of the transmission zone is the wetting front zone where water content decreases rapidly. At the edge of the wetting front zone the hydraulic gradient is relatively high and the wetted zone advances into the dry soil despite the low hydraulic conductivity (Trotta et al, 2004).

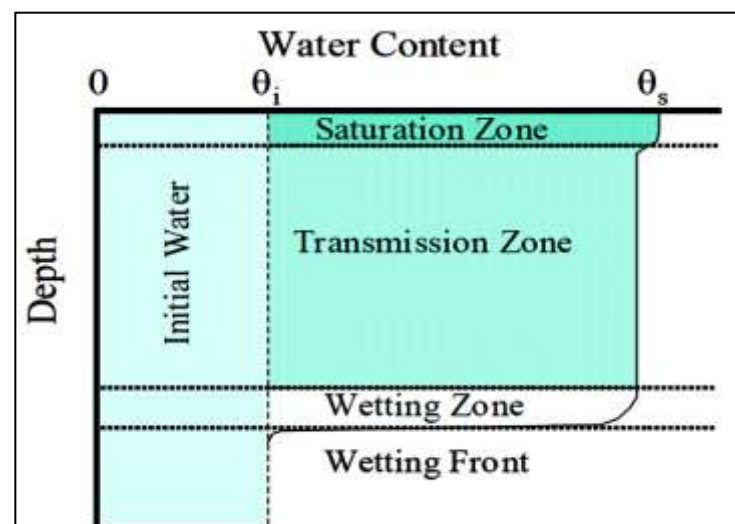


Figure 2. 3: Soil moisture distribution with depth for infiltration into initially dry soil.

(Source: Gustafson et al, 2005)

2.2.3 Rainfall and Slope Stability

Rainfall is the main cause of majority of landslides that occurs in regions experiencing high seasonal rainfall. In most cases, the rainfall induced landslides occurring in residual soils consist of relatively shallow slip failure above the groundwater table. Corominas and Moya (1999) noted that landslides are triggered when a critical pore water pressure threshold is being exceeded, and according to Van Asch and Sukmantalya (1993), landslide occurrence is as a result of increased weight of the saturated soil. The mechanism that leads to slope failures is the matric suction (i.e. *negative pore water pressures*) that starts to decrease when water begins to infiltrate the unsaturated soil (Yeh et al., 2004). The loss of matric suction decreases the shear strength of the soil below the mobilized shear strength along the potential slip surface. Matric Suction decreases with increase in depth of soil. During the dry spell, the matric suction values at the shallower depth are always larger than the suction values at the deeper soil depths, and upon rain (wet spell), there is a decrease of suction in all cases. The drop in suction at the deeper depth can be noticed after a long wet period, indicating longer time is required by the water to percolate the soil. Higher rainfall intensity would results in larger drop in suction, particularly at the shallow depth and after the cessation of the rain, suction at the shallow depth will show a faster recovery compared with the deeper depth (EJGE, 2005).

In Figure 2. 4, the matric suction appears to fluctuate considerably and reflects a mirror-image with the rainfall. The matric suction response to antecedent rainfall is less significant as the depth increases. The suction at the shallower depth (33 cm) drops to only about 0 KPa, while the minimum recorded values of suction at deeper depths (95 cm and 170 cm) are much higher. The drop in suction over the entire period in the shallower depth (33 cm) shows a mirror image response to the rain plot.

From Figure 2. 5, it can be established that the suction at the shallow depth recovers faster (steeper increases in suction) compared with the deeper depths (92 cm and 124 cm) during the dry spell. In Figure 2. 6, the level of soil saturation (i.e. the ratio of volume of water in soils to volume of voids in soils) after a rainfall event will depend directly on the rainfall amount and the type of soil under consideration. Soils that have high permeability (sand) will have a low saturation level after a rainfall event compared to low permeability soils (clay).

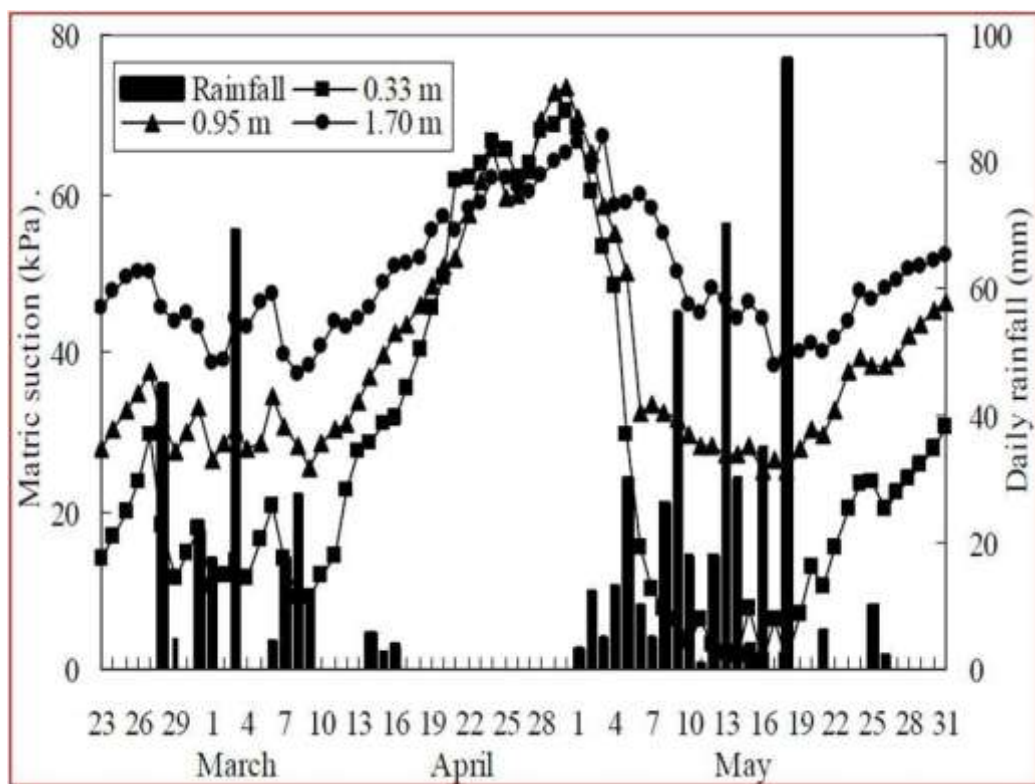


Figure 2. 4: Plot of pore water pressure response to rainfall at various soil depths.

(Source: Rahardjo *et al*, 2003)

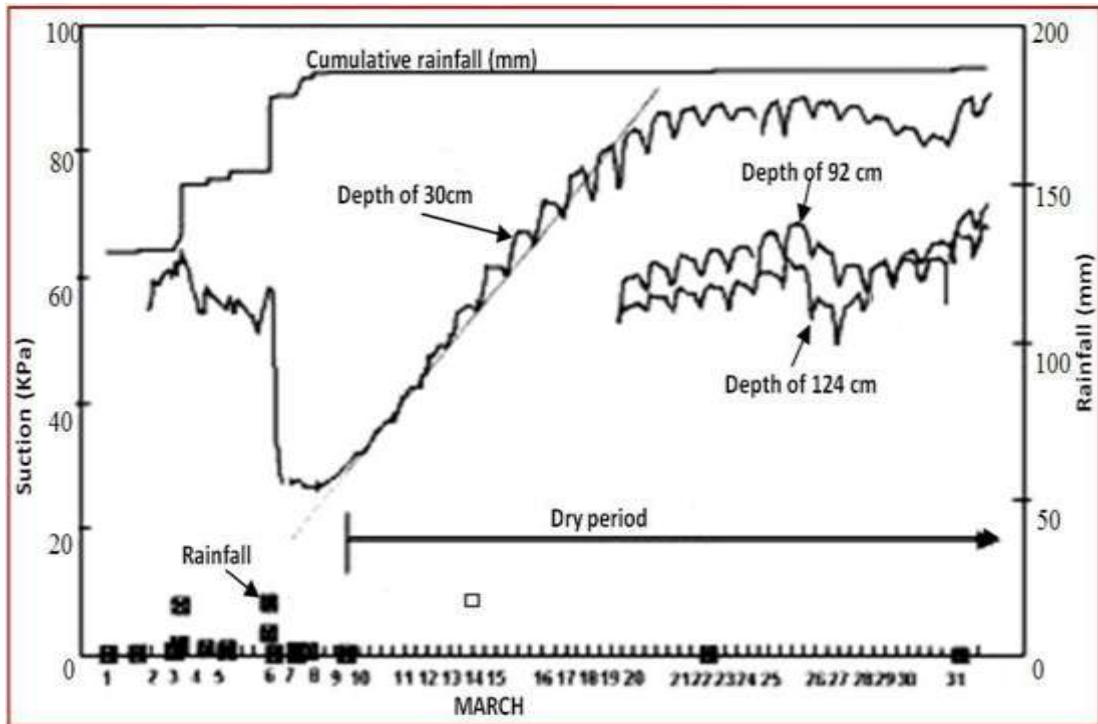


Figure 2. 5: Plot of matric suction recovery with time during a dry spell

(Source: EJGE, 2005)

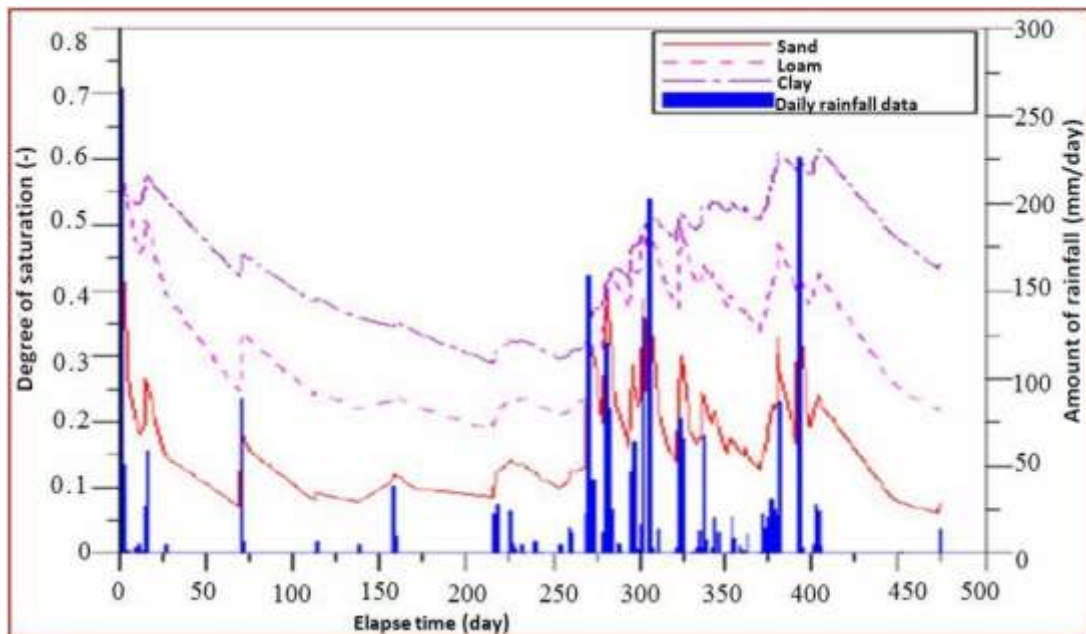


Figure 2. 6: Effect of rainfall on degree of saturation in different soils

(Source: Yeh et al, 2008)

2.3 LAND USE AND ITS EFFECTS ON STABILITY OF SLOPES

Land use is the arrangements, activities and inputs people undertake in a certain land cover type to produce, change or maintain it (FAO, 1997a; FAO/UNEP, 1999). The major effect of land use on land cover since 1750 has been deforestation while the more recent significant effects include urban sprawl, soil erosion, soil degradation, salinization, and desertification. According to Karsli et al. (2008), land use change has been recognized as the most important factor influencing the occurrence and re-activation of landslides triggered by rainfalls. In a heavily rainy environment, the relation between landslide and vegetation cover is extremely important and it should not be underestimated, since vegetation can influence the slope stability parameters, such as cohesion, internal friction angle, weight of the slope-forming material and pore-water pressure.

Vegetation can both enhance effective soil cohesion due to root matrix reinforcement and soil suction or negative water pressure through evapotranspiration and interception; and from these effects, vegetation can increase soil shear-strength up to 60% depending on the tree species. Landslides activity increases up to 15% in places where the original land cover has been removed or altered (Emba, 2010).

2.3.1 Vegetation and Slope Stability

Vegetation and slope stability are interrelated as the plants growing on slopes tends to promote the stability of the slope. The relationship is a complex combination of the type of soil, the rainfall regime, the plant species present, the slope aspect, and the steepness of the slope. Vegetation majorly influences slope stability through the removal of water and mechanical reinforcement of roots.

2.3.1.1 Removal of water

Vegetation influences slope stability by removing water through transpiration. Transpiration is the vaporization of liquid water contained in plant tissue and the vapour removal to the air (FAO, 2007). The major effect of transpiration is the reduction of soil pore water pressures which counteracts the loss of strength which occurs through wetting. Osman and Barakbah (2006) notes that there exist significant relationships between root density, soil water content and ultimately slope stability. He established that slopes that had high root density (due to dense vegetation on the surface) were less likely to undergo slope failure because a high root length density results in low soil water content which in turn results in an increase in shear strength and a decrease in soil permeability.

2.3.1.2 Mechanical reinforcement of roots

According to Cammeraat et al. (2005) and Morgan (2007), roots reinforce the soil through growing across failure planes and root columns acting as piles. When roots grow across the plane of potential failure there is an increase in shear strength by binding particles. The roots anchor the unstable soils in the surface to the deeper stable layers or bedrock (Mattia et al., 2005). Perry et al (2003) noted that the strength exerted by roots only extends down to 1m while most failures occur between 1.2 – 1.5m soil depth and thus cannot be associated with slope stability.

2.3.2 Land Use Changes and its Effects on Slope Stability

Conversion of land from current state of forestry to agricultural or urban uses can cause enormous change in the stability of slopes. When vegetation is removed or replaced to create space for urban development, the slope morphology is affected and construction increases loading of slopes which lead to an increased likelihood of slope failures.

Sidle et al. (1985) notes that conversion of land from forests to pastures results in substantially higher slope movements within the pastures. Roots are frictionally coupled to the surrounding soil and contribute to soil shear resistance that varies between 3 and 150 kPa, and can represent up to 100% of the cohesive strength of hillslope soils (Hales et al, 2009). Eigenbrod and Kaluza (1997) established that shallow slope failures occurred after forest clearing in Northern Ontario due to a decrease in evapotranspiration and decaying of the root system. He noted that the slopes peak instability after forest removal was about 6 years and this time delay was for the decomposition of the root system left behind during lumber harvesting. Sidle et al., (1985) also established that decreasing evapotranspiration results in a higher saturation within the soil leading to reduced slope stability.

2.4 OVERVIEW OF LANDSLIDE ASSESSMENT METHODS

The aim of this section is to give an overview on the methods most used in landslide modelling practice and to highlight their advantages and disadvantages in their modelling capabilities. In this section also, an introduction to models adopted for this study will be given. Prediction of landslide involves hydrological and slope stability modelling.

2.4.1 Hydrological Modelling

Crosta and Frattini, (2008) notes that the most important trigger in both shallow and deep-seated landslides is intense rainfall, as rain water percolating the soil increases pore water pressures at hydrologic boundaries, which subsequently decreases shear strength. Positive pore water pressure may occur directly caused by infiltration and percolation, or may be the result of perched groundwater tables (Terlien, 1998).

Vadose or unsaturated zone is the dynamic area that controls the flux of water between the surface and groundwater and partitions rainfall into infiltration, runoff,

groundwater recharge and evapotranspiration. Unsaturated flow can best be described by combining Darcy's law (1856) with the continuity equation, resulting in a theoretical partial differential equation known as Richards' equation (Gowdich, 2007), (see equation 2.2).

$$\frac{\partial \theta}{\partial t} = \frac{\partial}{\partial z} \left(K(h) \frac{\partial h}{\partial z} + 1 \right) \quad (2.2)$$

Richards' equation does not have a general analytical solution, and therefore must be solved numerically in many practical applications or approximated using physically based models.

2.4.1.1 Finite difference solution to Richards's equation

The head-based formulation of Richards' equation (Equation 2.2) allows solution in both saturated and unsaturated conditions. The numerical solution of Richards' equation is generally computationally intensive, require extensive soil property data, and involve parameterization and fine spatial and temporal discretization which can result in errors (Gowdich, 2007), and in addition, certain conditions can present problems of instability and errors of convergence that compromise the solutions. Despite drawbacks associated with the use of Richards' equation in hydrologic predictions, the equation has been successfully used in field scale and watershed scale models of soil moisture and runoff (Šimůnek et al 2009; Dawes and Hatton, 1993; Refsgaard and Storm, 1995).

2.4.1.2 Approximate methods of Richards's equation

Because of instability problems and errors of convergence that compromise the numerical solutions, approximate or physically based approaches have been often used for modelling infiltration and soil water redistribution. Particularly, for the case of infiltration, the method of Green-Ampt (1911), GA, modified for unsteady rain events,

has been widely used in hydrological modelling. In spite of its apparent limitations, the method produces good results in comparison with other approximate methods if it is correctly parameterized (Gowdiss, 2007). In addition, the method presents the advantage that its parameters can be reckoned based on the soil textural classification (Rawls et al. 1982). As opposed to the complete Richards' (1931) formulation, the GA equation strictly handles infiltration. Thus, an equation for the redistribution of soil water in the profile between rainfall events is also needed. Soil water redistribution models have been proposed and used, but it is desirable that the model chosen be based on the same underlying assumptions as the GA equation. One such model is the Green-Ampt with Redistribution (GAR) method (see Figure 2. 7) and was described by Ogden and Saghafian (1997). This model is used to simulate the continuous infiltration and soil water redistribution cycle for multistorm time series (Gowdiss, 2007).

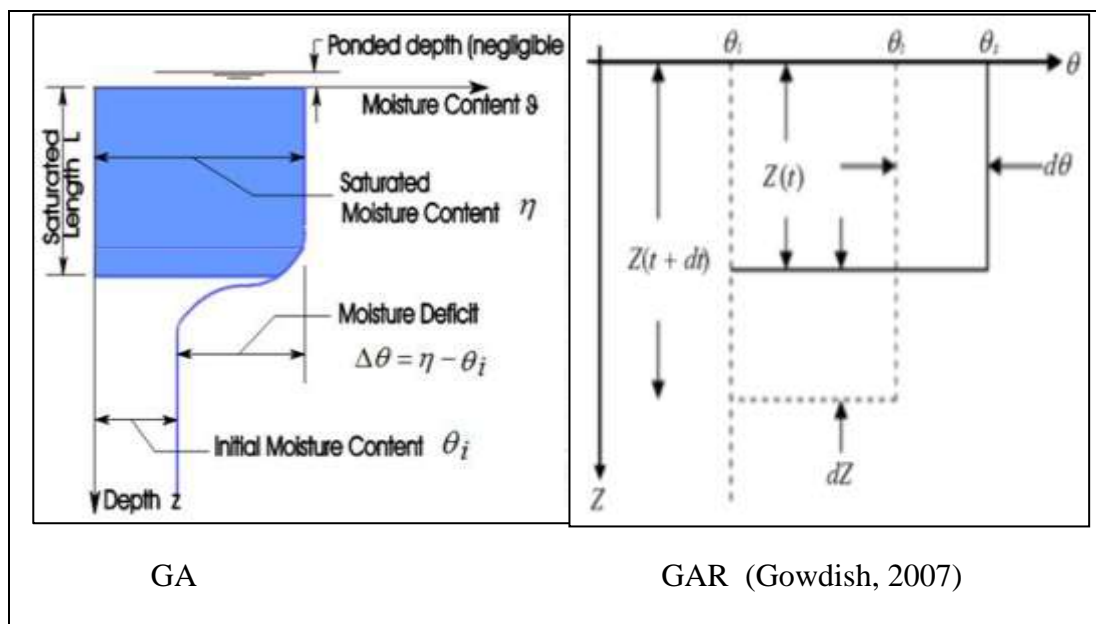


Figure 2. 7: Green Ampt models

One benefit of using the GAR model is that it requires only three soil infiltration parameters and three water contents, which can be determined from soil textural classifications (Gowdiss, 2007). In addition, the method is explicit and is therefore

easy to implement and robust when time steps are constrained to allow for convergence.

2.4.1.3 Comparison of commonly used hydrological models

All the hydrological models (numerical and approximate solutions of Richards's equation), with proper input parameters, could show high accuracies in simulating soil water movement. Finite difference method of Richards's equation always gives the best wetting front prediction compared to Green Ampt model though one should be cautious when selecting dt and dz . Green-Ampt model requires least parameters and the simplest programming and is acceptable if only the cumulative infiltration is of main concern.

Simpler methods, such as GA and GAR, are approximations of Richards' equation and do not provide detailed soil moisture profiles or simulate the movement of water from the groundwater to the unsaturated zone. Accurate representation of layered soils or soils with a water table is also difficult with the approximation methods. Application of approximation methods in simulation of surface water content in soils with larger saturated hydraulic conductivity values after a storm would give a prediction error as soil water content increases and furthermore, when method is applied to a long period of uneven storms would result in an increasing divergence from actual surface water content after subsequent redistributions (Gowdich, 2007).

Therefore numerical solution of Richards's equation (HYDRUS 1D model) was adopted for soil water analysis (hydrological modelling) in this study.

2.4.2 Slope Stability Modelling

Modelling of landslide failures can be either qualitative or quantitative (Thiebes, 2012). Qualitative approaches integrate descriptive prediction and the opinion of experts, while quantitative applications are based on numerical simulations. Landslide

modelling approaches can broadly be separated into models that are focusing on single landslide processes (local models), and models with greater spatial extent (regional models). Local approaches to landslides have a long tradition within geotechnical engineering slope stability practice, while regional applications have increasingly emerged since the wide availability of powerful computers and GIS. However, it is important to note that all models are necessarily simplified generalization and approximations of processes which are occurring in nature (Thiebes, 2012). A brief summary on regional and local approaches used in modelling landslides are discussed below.

2.4.2.1 Regional models

Regional deterministic models apply physically-based simulations to assess landslide susceptibility expressed chiefly as F_s , and provide useful insights into landslide. The most frequently applied methodology for regional deterministic modelling is based on distributed hydrological modelling and stability calculation using a simplified approach, i.e. the infinite-slope model. According to Soeters and Van Westen (1996), deterministic methods are only applicable when geomorphic and geologic conditions are fairly homogenous over the entire study area and landslide types are simple. Due to these limitations, regional deterministic models are only suitable for simple landslide processes, such as shallow translational landslides. The most widely used models for regional deterministic analyses include SINMAP, ILWIS and ASWSM.

SINMAP (Pack *et al.*, 2001) is an approach suitable for modelling slopes that have a shallow soil depth and impermeable underlying bedrock. It uses cohesion and root cohesion (for forested slopes) in the calculations. SINMAP is an ArcView extension which computes and maps slope stability index based on geographical data, especially digital elevation data. To derive the terrain stability, SINMAP requires several inputs:

slope, wetness index, gravity, soil density, ratio of transmissivity to recharge rate, cohesion, and angle of friction (Pack et al. 2005).

ILWIS GIS provides a platform for formulating mapping equations such as infinite slope model with ease. In spatial slope stability modelling, ILWIS would require raster maps of soil and topographical properties for the study area with also the inputs of soil moisture from a hydrological model. Calculation in this GIS tool is done on a pixel basis and the effect of the neighbouring pixels is not considered, and the model can be used to calculate the stability of each individual pixel resulting in a hazard map of safety factors (Van Westen, C.J. and Terlien, M.T.J., 1996).

2.4.2.2 Local models

Models for the analysis of single slope failures (local models), allow for detailed investigation of failure processes, assessing effects of triggering events, and assessment of the effectiveness of remedial measures and stabilization works. Overviews of some commercially available local landslide analysis and simulation models are presented below.

SLOPE/W model has several methods which provide a limit-equilibrium analysis of soil and rock slopes i.e. Morgenstern-Price, Spencer, Bishop, Ordinary, Janbu and more. Stability analysis may be performed using deterministic or probabilistic input parameters. However, dynamic hydrological modelling of pore pressures is not included in SLOPE/W, but can be imported from SEEP/W, a finite element software by the same company (GEOSLOPE). The use of SLOPE/W, also in combination with SEEP/W is fairly widely acknowledged in recent landslide research (Navarro et al. 2010).

CHASM (Combined Hydrology And Stability Model) is a coupled hydrology and slope stability model for limit-equilibrium analysis. The software program integrates

simulation of saturated and unsaturated hydrological processes to calculate pore water pressures, which are then incorporated into stability computation. CHASM is essentially two-dimensional but hydrological simulations can be extended to account for flow concentration at topographic hollows. Moreover, vegetation and stabilisation measures can be integrated into Janbu and Bishop Stability simulations. Common applications of CHASM include investigations of effects of rainfall on slope hydrology and subsequently on slope stability (Thiebes, 2012).

2.4.3 Preview of Models Applied in the Study

Given the spatial extend of the study area; regional landslide modelling method was applied in this study, whereby ILWIS GIS tool was applied in spatial mapping of unstable areas whereas HYDRUS 1D model was applied in hydrological modelling.

The preview of tools and models to be applied in this study are as follows;

2.4.3.1 ILWIS GIS TOOL

ILWIS is an acronym for the Integrated Land and Water Information System. It is a Geographic Information System (GIS) with Image Processing capabilities. ILWIS has been developed by the International Institute for Aerospace Survey and Earth Sciences (ITC), Enschede, The Netherlands. As a GIS and Remote Sensing package, ILWIS allows you to input, manage, analyze and present geographical data. From the data you can generate information on the spatial and temporal patterns and processes on the earth surface. The software package can be freely downloaded from; <http://52north.org/ilwis>.

2.4.3.2 HYDRUS-1D MODEL

HYDRUS-1D is a software package for simulating water, heat and solute movement in one-dimensional variably saturated porous media. The HYDRUS program numerically solves the Richards's equation for variably saturated water flow and advection-

dispersion type equations for heat and solute transport. The software package can be freely downloaded from *www.hydrus2d.com*. Flow and transport can occur in the vertical, horizontal, or a generally inclined direction. The water flow part of the model can deal with prescribed head and flux boundaries, boundaries controlled by atmospheric conditions, as well as free or deep drainage boundary conditions. The governing flow and transport equations are solved numerically using Galerkin-type linear finite element schemes (Šimůnek et al, 2009).

2.4.3.3 ArcGIS Desktop

ArcGIS Desktop is an integrated commercial suite of professional Geographic Information System, GIS applications. A geographic information system (GIS) is a computer-based tool for mapping and analyzing feature events on earth. GIS manages location-based information and provides tools for display and analysis of various statistics, including population characteristics, economic development opportunities, and vegetation types. ArcGIS Desktop includes a suite of integrated applications that allow you to perform GIS tasks, including mapping, geographic analysis, data editing and compilation, data management, visualization, and Geoprocessing.

CHAPTER THREE: METHODOLOGY

3.1 INTRODUCTION

This chapter discusses in detail methods that were used in the study. It focuses on five levels which study undertook i.e. collection and preparation of meteorological and geotechnical/ morphological data, models formulations, hydrological modelling, slope stability assessment and hazard mapping.

The data required in this study are soil map (with details of soil depths, soil type, hydraulic conductivities, unit weights, and angle of friction), landuse map (with details of forest covers, agricultural land, bare land and rocky land), DEM map, rainfall data, evapotranspiration data and calibration/ validation data (historical landslide occurrence dates and sites coordinates). Also required in this study are analysis tools and models, and include ArcGIS, ILWIS GIS, GPS (for use in Georeferencing historical landslide areas), HYDRUS 1D model, INSTANT + model and slope stability model.

Soil, DEM and landuse maps were used in derivation of morphological and geotechnical information. Hydrological modelling was undertaken outside the GIS tool and involved rainfall generation, soil moisture content and water flow flux analysis. Rainfall generation was undertaken using developed Ms-EXCEL's Markov chains model and Event based model, water flow flux and soil water redistribution was analysed using HYDRUS 1D model. The matric suction stress and slope stability was analysed using developed formulation based on Lu and Likos (2004, 2006) equation and Infinite slope model respectively and the formulation was implemented both in ILWIS GIS model (mapping function) and in Ms-EXCEL's Hydrological and Slope Stability model (for calibration and identification of critical mapping day).

The mapping function in ILWIS GIS model was formulated taking into consideration spatial variation in components of hydrology and topography that affects stability of slopes. These components include; water flow flux, soil moisture, slope, land use and soil type. The formulated LPM was calibrated by using it to predict previous landslides occurrences, and if the model is overstating or understating failure, then modelled values will be scaled by multiplying with numerical constants in the slope stability and mapping function depending on whether to raise or lower modelled results.

3.2 WATERSHED DELINEATION

To undertake spatial slope stability analysis in the western stretch of Kerio escarpment would require meticulous delineation along area of interest to be performed from regional digital elevation model, DEM. Watershed delineation was performed by a series of tasks on the regions DEM using ArcGIS 10.1 tool. In principle, the goal is to obtain the flow directions throughout the watershed, based on elevation data. With the flow direction information, the river network can be extracted and watershed of interest can be delineated.

The flow direction computations and filling of sinks need to be done in one step. In ArcGIS, flow direction is computed for every cell with the D8 method which finds the steepest direction to one of 8 neighbours of a cell (diagonal flow is allowed). Once we have the flow directions, we can find the cells that do not drain anywhere, which are sinks or holes in the watershed. For hydrological modelling purposes these are not acceptable, although there may be reasons why such features exist in a DEM. So the common procedure is to fill these depressions by adding elevation to the cells until they are at equal elevation with the surrounding area. Watershed delineation is done automatically by the following sequence of steps in ArcGIS watershed analysis (see Figure 3. 1).

In delineation of western stretch of Kerio escarpment, River Kerio was used as eastern boundary while a limiting distance of 20 km from 2400m contour was used as the western boundary while selecting sub-catchments in Nzoia basin to be merged into study area.

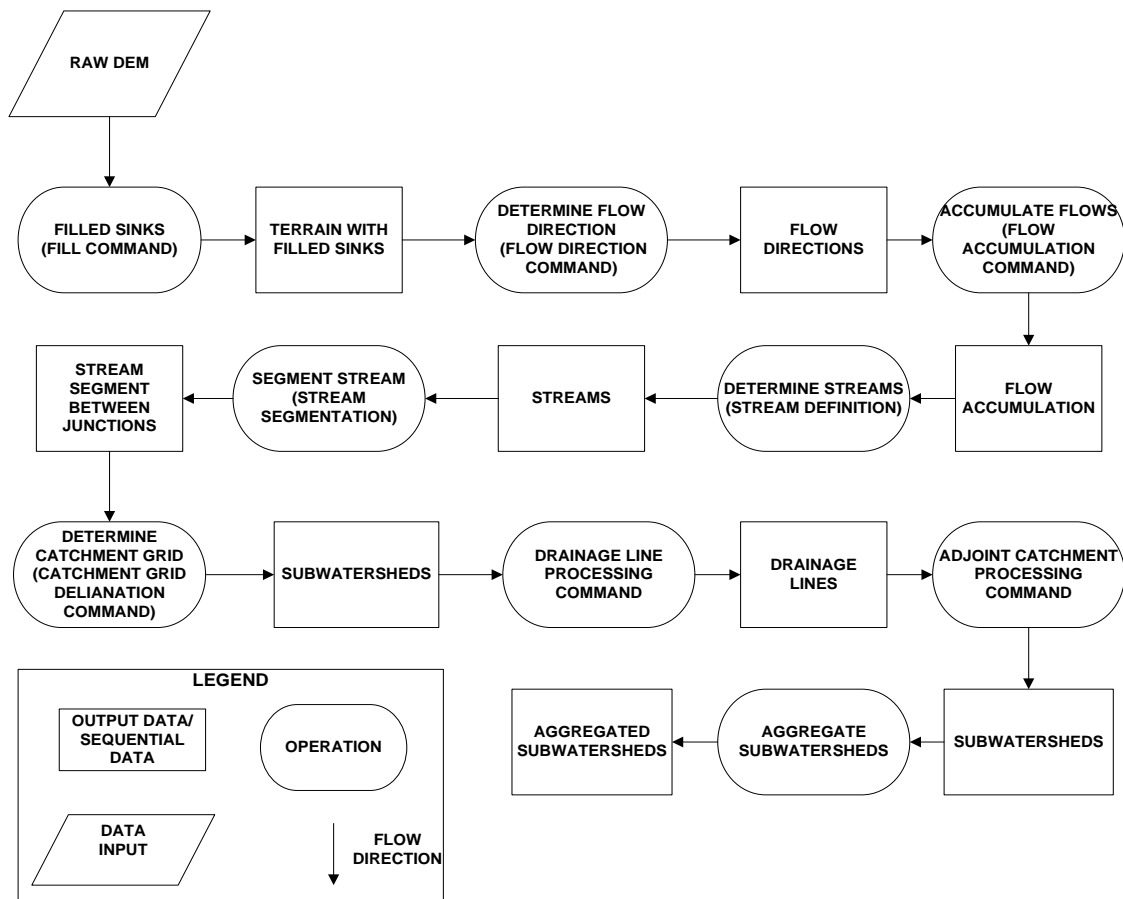


Figure 3. 1: Procedure for watershed delineation using ArcGIS tool.

3.3 STOCHASTIC GENERATION OF DAILY RAINFALL

3.3.1 Introduction

The natural systems are so complex that no exact laws have yet been developed that can explain completely and precisely the natural hydrological phenomena (Priyaranjan, 2012). Rainfall exhibits a strong variability in time and space and hence its stochastic modelling is not an easy task. Rainfall is the principal phenomenon driving many hydrological extremes such as floods, droughts, landslides, debris and mud-flows; its

analysis and modelling are typical problems in applied hydrometeorology. Therefore the amount and pattern of rainfall are the most important weather characteristics and hence forms the principal input to all hydrological and agronomic models (Hossain and Anam, 2012).

The development of a rainfall occurrence model is increasingly in demand, not only for data-generation purposes, but also to provide some useful information in various applications; including water resource management, the hydrological and agricultural sectors (Hossain and Anam, 2012). The information on weather's wet and dry behaviour also has vital importance to all allied fields like insurance, agriculture etc. Once the rainfall process is adequately and appropriately modelled, the model can then be used to aid in drought, soil erosion, landslides and flood predictions, impact of climate change studies, crop growth studies and other important fields (Barkotulla, 2010).

Identifying the appropriate model of daily rainfall occurrence, particularly on the distribution of dry/wet spells, is very important as almost all of the climate variables are dependent on the rainfall events. In this study, rainfall patterns and events depths were stochastically generated using Markov chains and event based formulated models. These models require rainfall and evapotranspiration data as inputs.

3.3.2 Rainfall Data

In the study area it was possible to collect rainfall data for 15 stations. The rainfall data was obtained from the Kenya Meteorological Department (KMD). A list of rainfall stations with their location coordinates are shown in Table 3. 1 and their spatial distribution are shown in Figure 3. 1. According to KMD, meteorological stations have been named by a station code (i.e. HYDROID) and the data was in the form of daily rainfall amount.

3.3.2.1 Estimating missing precipitation data

Inverse Distance Weighting (IDW) will be used to fill gaps in the rainfall data. IDW is an interpolation technique in which interpolated estimates were made based on values at nearby locations weighted only by distance from the interpolation location. IDW does not make assumptions about spatial relationships except the basic assumption that nearby points ought to be more closely related than distant points to the value at the interpolate location (Naoum and Tsanis, 2004).

In this method, weights for each sample are inversely proportionate to its distance from the point being estimated (Lam, 1983).

$$P_x = \frac{\sum_{i=1}^N \frac{1}{d_i^2} P_i}{\sum_{i=1}^N \frac{1}{d_i^2}} \quad (3.1)$$

Where,

P_x = estimate of rainfall for the ungauged station,

P_i = rainfall values of rain gauges used for estimation

d_i = distance from each location the point being estimated and

N = No. of surrounding stations.

Table 3. 1: Location coordinates of rainfall stations

S/N	STATION NAME	HYDROID	LATITUDE (Degrees)	LONGITUDE (Degrees)
1	Tambach -labot	8835035	1.066667	35.41667
2	Chebororwa FTC	8935002	0.983333	35.55
3	Tambach –gov school	8935047	0.937	35.5252
4	-	8935220	0.983333	35.56667
5	Tambach -chebiemi	8935014	0.92	35.5217
6	Marakwet africa	8935104	0.866667	35.5
7	Moiben kenley	8935108	0.8	35.43333
8	Moiben karuna farm	8935106	0.716667	35.51667
9	Elgeyo - forest	8935222	0.7	35.5
10	Tambach DO	8935134	0.65	35.51667
11	-	8935184	0.466667	35.55

12	Kaptagat forest	8935010	0.433333	35.5
13	Kaptagat Nvita estate	8935175	0.416667	35.48333
14	Tambach chepkorio	8935131	0.366667	35.55
15	Eldoret skyline	8935121	0.166667	35.55

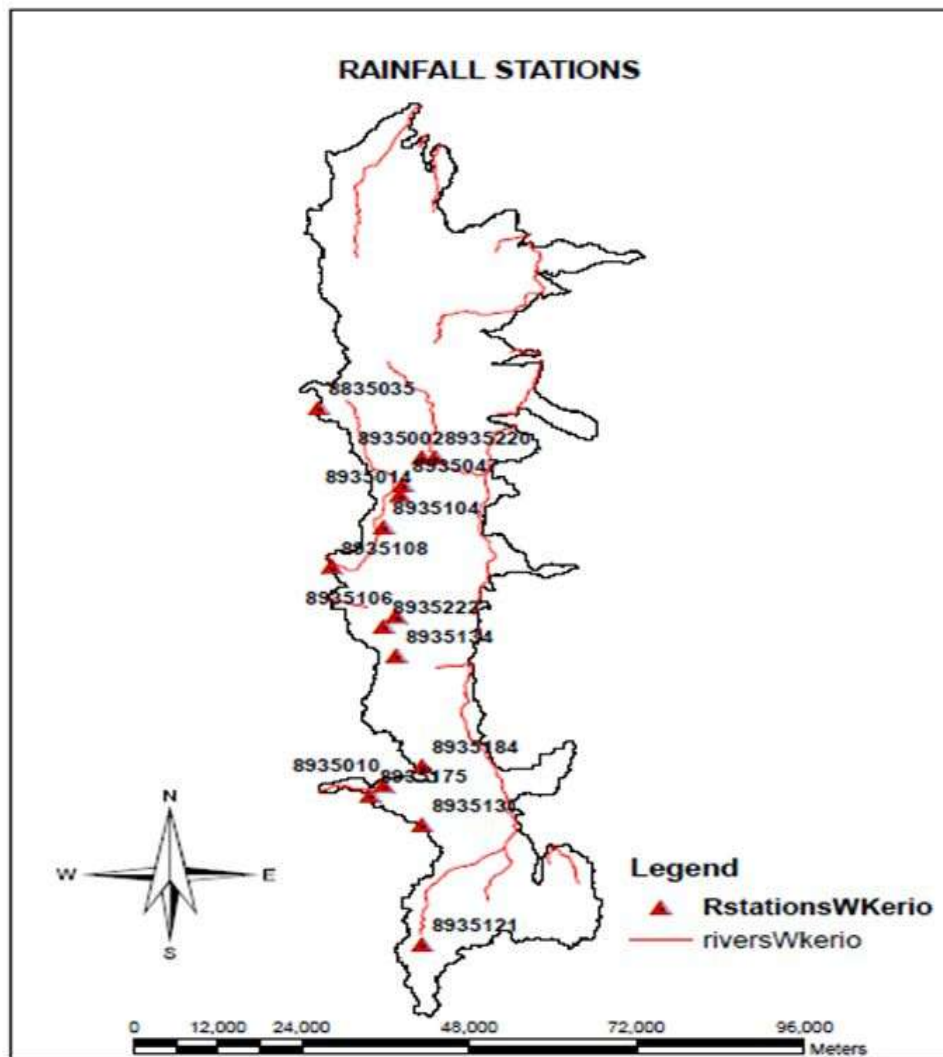


Figure 3. 2: Distribution of rainfall stations along western stretch of Kerio escarpment

3.3.2.2 Estimating spatial rainfall

One important aspect of hydrologic modelling is the estimation of the total precipitation and its distribution within a watershed. There are many various suitable methods of determining areal rainfall which include; Arithmetic Average Method, Thiessen Polygon Method and Isohyetal method. Thiessen polygon method is easily applicable where average precipitation is to be computed for a certain region, and the

method was adopted in this study since the rainfall stations are fairly distributed along the study area and their annual rainfall amounts were not varying much. The data used in the analysis were from stations close to or within the Kerio escarpment (station not further than 20km from 2400m contour) and whose mean annual rainfall amounts were nearly equal (varies between 1100mm to 1400mm).

Thiessen polygon method involves determining the area of influence for each rainfall station, rather than assuming a straight-line variation. The procedure is as follows;

- a) Locate all rainfall stations on a base map and record the rainfall amount.
- b) Connect each station by straight lines with the several nearest stations to form a series of polygons.
- c) Erect perpendicular bisectors on each of these lines and extend them to the intersect with other bisectors, thus forming a series of irregular polygons

In this study, ArcGIS 10.1 was used in deriving the Thiessen Polygons. Every polygon (sub region) belongs to one of the rain gauges. The spatial average precipitation in each region assumed to be identical with precipitation value of the region's rain gauge.

The Thiessen polygon formula (see equation 3.2) is applied in computing the areal rainfall:

$$\bar{p} = \frac{\sum_{i=1}^n A_i p_i}{\sum_{i=1}^n A_i} \quad (3.2)$$

Where;

\bar{p} = Spatial average of precipitation (Areal rainfall)

A_i = Area of the part of the sub-catchment belongs to the rain gauge i

p_i = Rain gauge precipitation value at rain gauge i

n = Total number of rain gauges

$$A = \sum_{i=1}^n A_i = \text{Total area of the sub-catchment}$$

3.3.2.3 Fitting characteristics of spatial rainfall to distributions

Various characteristics describing a rainfall occurrence will have to be fitted to the distribution which best describes each of them. The characteristics to be fitted to various distributions are; rainfall events per season, daily rainfall depths, inter-event time and rainfall duration.

1. Events per season

Poisson probability density function adequately describes the distribution of the number of events per season. Poisson PDF is given as follows (Bogardi and Rumambo, 1988),

$$f_N(n) = \frac{e^{-\lambda} \lambda^n}{n!}, n = 0, 1, 2, 3.. \quad (3.3)$$

The arithmetic mean appears to provide a stable estimate of the parameter λ .

2. Duration of rainfall events

Geometric density function provides excellent fits for the events durations. Geometric PDF is given as (Bogardi and Rumambo, 1988),

$$f_N(j) = pq^{j-1} \quad (3.4)$$

Where;

j = duration of the events in days,

$p = \frac{1}{\bar{j}}$, where \bar{j} is the value of mean event duration and

$$q = 1 - p$$

3. Rainfall depth per event

Two parameter gamma distribution provides a best fit to rainfall depths distribution per event especially because of its long tail (Barkotulla, 2010). The gamma distribution is given as;

$$f(x; \beta, \alpha) = \frac{x^{\alpha-1} e^{-x/\beta}}{\beta^\alpha \Gamma(\alpha)}; \text{ If } x > 0 \text{ and } \alpha > 0 \text{ and } \beta > 0 \quad (3.5)$$

Where;

$\Gamma(\alpha)$ is the gamma function,

α and β are denote the shape and scale parameters respectively.

α and β are specific parameters for each month and are estimated, on a monthly base.

4. Inter-event time (dry days duration)

The distribution of inter-event time also follows a geometric distribution, (see section 3.2.2 2)

3.3.3 Potential Evapo-Transpiration data

Evaporation data was obtained from Eldoret Experimental Farm and ranged from 1960-2009. The potential evapo-transpiration was then calculated using ETo calculator. The calculated values of potential evapo-transpiration do not vary significantly throughout the year and so the mean annual value was calculated (5.0mm/day) and applied over the analysis period.

3.3.4 Markov Chains Application in Stochastic Rainfall Generation

Markov chain is generally recognized as a simple and effective description of the rainfall occurrence. The first order Markov chain model was used to simulate the sequence of rainfall occurrence using the method of transitional probability matrices, while daily rainfall amount was generated using a gamma distribution. The model parameters were estimated from historical rainfall records. The shape and scale parameters in gamma distribution were estimated by moment method and hence it

became possible to find the parameter values at the study area and then to generate synthetic sequences according to the gamma distribution. The parameters necessary for the whole generation include the means, variance or standard deviation and conditional probabilities of wet and dry days. Results obtained showed that the model could be used to generate rainfall data satisfactorily (Barkotulla, 2010).

The rainfall data is analyzed to establish the Markovian dependency. If it is assumed that first-order Markov process is exhibited, the transitional probability matrix, $[M 1]$, can be represented by

$$[M 1] = \begin{bmatrix} pp & 1 - pp \\ 1 - qq & qq \end{bmatrix}$$

Where pp refers to the conditional probability of any day being wet given that the day before was also wet, while qq represents the probability that a wet day follows a dry day. For completely random (independent) rainfall events, the transitional probability matrix changes to $[M 2]$:

$$[M 2] = \begin{bmatrix} p & 1 - p \\ 1 - q & q \end{bmatrix}$$

Where, p is the probability of a wet day and q is the probability of a dry day.

The equivalence of matrices $[M 1]$ and $[M 2]$ will determine whether the rainfall events are random, exhibit Markov dependency or other non-Markovian processes. Ordinary chi-square or matrix algebra can also be used to establish the equivalence and If the χ square statistic is less than 3.84 at 5% level of significance, then $[M 1]$ and $[M 2]$ are equivalent, and the rainfall events (occurrence of dry and wet days) follow Markov processes (Ochola and Kerkides, 2003).

The Markov chain models have two advantages (Fraedrich and Leslei, 1987);

- A. The forecasts are available immediately after the observations are done because they use as predictors only the local information on the weather and
- B. They need minimal computation after the climatological data have been processed.

Rain is generated first because it is required for the generation of the other variables in the landslide prediction model. Two aspects are considered: the occurrence of the rain event (if a day is wet or dry) and the amount of rainfall for the wet days.

3.3.4.1. Rain occurrence

Occurrence of rainfall is described by a two state Markov chain (day is wet or dry) of first order, that is the probability of rain on a given day depends on whether or not rain occurred on the previous day and the approach has been used successfully and studied extensively to generate rainfall (Barkotulla, 2010).

Let $X_0, X_1, X_2, \dots, X_n$, be random variables distributed identically and taking only two values, namely 0 and 1, with probability one, i.e.,

$$X_n = \begin{cases} 0 & \text{if the } n\text{th day is dry} \\ 1 & \text{if the } n\text{th day is wet} \end{cases}$$

Firstly, it may be assume that,

$$P(X_{n+1} = x_{n+1} \mid X_n = x_n, X_{n-1} = x_{n-1}, \dots, X_0 = x_0) = P(X_{n+1} = x_{n+1} \mid X_n = x_n)$$

where $x_0, x_1, \dots, x_{n+1} \in \{0, 1\}$.

It is assumed that probability of wetness of any day depends only on whether the previous day was wet or dry. Given the event on previous day, the probability of wetness is assumed independent of further preceding days. So, the stochastic process $\{X_n, n = 0, 1, 2, \dots\}$ is a Markov chain.

Consider the transition matrix as

$$\begin{bmatrix} P_{00} & P_{01} \\ P_{10} & P_{11} \end{bmatrix}$$

Where, $P_{ij} = P(X_1 = j \mid X_0 = i)$ $i, j = 0, 1$.

Note $P_{00} + P_{01} = 1$ and $P_{10} + P_{11} = 1$

The transition probabilities are considered on a monthly base and then the model requires 24 parameters for the rain event generation i.e. 12 for P_{01} and 12 for P_{11} (Barkotulla, 2010). For this study, 4 parameters are required since our interest is only the two months of April and May as these are months that the region receives heavy rainfall and also most of historical landslides occurred during this period of the year. These probabilities are calculated on all the available recordings in the data set as:

$$P_{01} = N_{01}/N_0 \text{ and}$$

$$P_{11} = N_{11}/N_1$$

Where;

N_{01} number of wet days in the month after a dry day;

N_0 total number of dry days in the data set, for the month;

N_{11} number of wet days in the month after a wet day;

N_1 total number of wet days in the data set, for the month.

3.3.4.2. Algorithm for Stochastic rainfall generation process using on Markov model

The procedure adopted for determining the occurrence of a wet day and corresponding rainfall depth was as follows (Barkotulla, 2010);

- a. Derive the counts of N_1 , N_0 , N_{01} and N_{11} using INSTAT + model and use them to derive values in $[M1]$ and $[M2]$.

- b. Rainfall data is assessed for Markovian dependency using chi-square. If the χ square statistic is less than 3.84 at 5% level of significance, then $[M1]$ and $[M2]$ are equivalent, and the rainfall events (occurrence of dry and wet days) is random and do not follow Markov processes.
- c. Fit daily rainfall amount (depths) to a Gamma distribution.
- d. Random numbers are generated from a uniform distribution between 0 and 1, and assigned to each day.
- e. The generated random numbers are then compared with the value of the transition probabilities P_{01} or P_{11} ; and if the preceding day is dry and the random number is smaller than P_{01} , then the current day is a wet day. Alternatively, if the preceding day is dry and the random number is greater than P_{01} , then the current day is dry. The decision process is similar if the preceding day is wet.
- f. Once the occurrence of a wet day has been established, the amount of rainfall on that day is determined by generating a new random numbers from a uniform distribution and assigning them to wet days.
- g. The inverse cumulative distribution function is solved to determine daily rainfall, i.e. the random number is taken as the cumulative frequency value and the corresponding daily rainfall is determined numerically.

3.3.5 Event Based Synthetic Rainfall Generation Method

3.3.5.1. Introduction

A rainfall event may be defined as an interrupted sequence of rain days and a dry event is a sequence of dry days as observed in a given rain gauge. A limit corresponding to the expected regions daily evaporation rate, is thus taken as the lowest physical limit

for considering rainfall that may produce utilizable surface water resources (Bogardi and Rumambo, 1988). Figure 3. 3 illustrate various definitions in rainfall pattern.

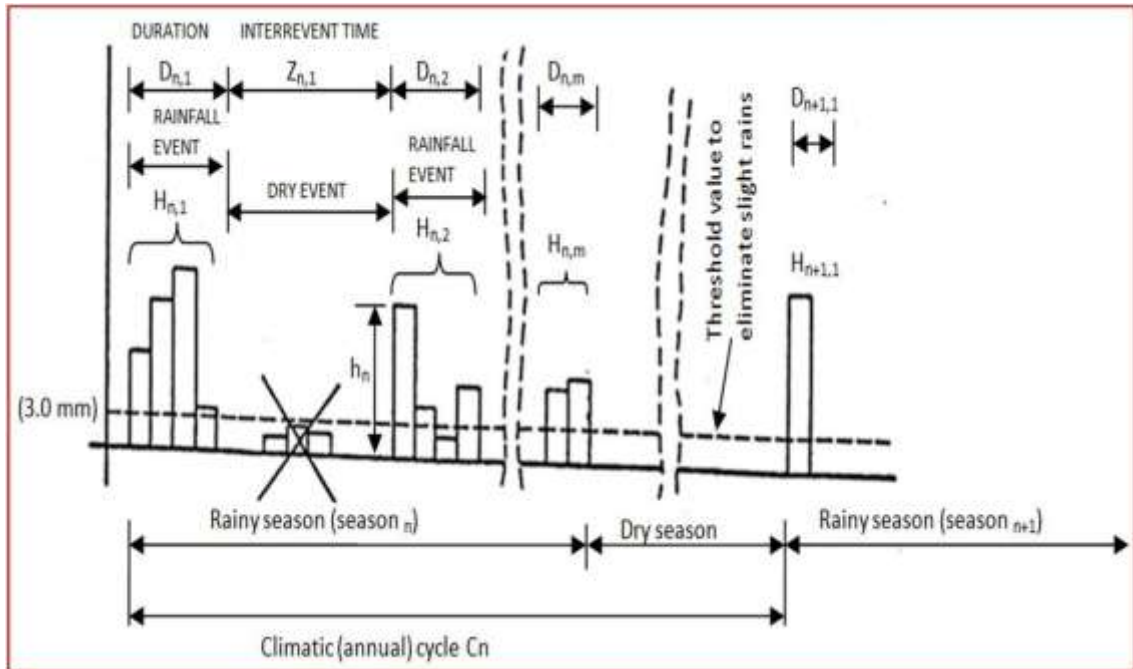


Figure 3. 3: Definitions for event based analysis

(source: Bogardi and Rumambo, 1988)

The rainfall event m in a given rainy season n will be characterized by its duration $D_{n,m}$ symbolizing the number of subsequent rainy days and the total accumulated rainfall depths of $H_{n,m}$ of $D_{n,m}$ rainy days in mm. Inter-revent time $Z_{n,m}$ represents the number of days without rainfall between two subsequent events. $R_{n,m}$, the rainfall event m of the n th rainy season is defined as a vector featuring depth, duration and inter-revent time;

$$R_{n,m} = (H_{n,m}, D_{n,m}, Z_{n,m})$$

The length of the rainy season L_n is defined as the time span between the start of the first and the end of the last event of the given season; while the annual (climatic) cycle is determined as the time lapsed between the onset of two subsequent rainy seasons.

$$L_n = \sum_{m=1}^{M_n} D_{n,m} + \sum_{m=1}^{M_n-1} Z_{n,m}$$

L_n = length of rainy season in days, and M_n = number of events/season.

3.3.5.2. Algorithm for Stochastic generation of rainfall using event based method

The procedure adopted for determining the occurrence of a wet or dry day and the corresponding rainfall depth for wet days is as follows (Bogardi and Rumambo, 1988);

- a) Fit various rainfall characteristic to distributions best describing them.
- b) Select the number of climatic cycles, N , to be generated. For this study one climatic cycle would be adopted since our interest was only rainfall simulation for months of April and May.
- c) Draw N uniformly distributed random numbers from Poisson- distributed rainfall event population. The random number is taken as the cumulative frequency value in the Poisson CDF and the corresponding number of rainfall events is determined numerically by solving the inverse cumulative distribution function for number of rainfall events.

$$M_n, n = 1, \dots, N$$

- d) Draw $\sum_{n=1}^N M_n$ uniformly distributed random numbers from Geometrically- distributed rainfall events population. The random number is taken as the cumulative frequency values in the geometric CDF and the corresponding duration of rainfall events is determined numerically by solving the inverse cumulative distribution function for number of rainfall duration. Assign these values to the rainfall events to obtain events duration, $D_{n,m}$.

$$D_{n,m}, n = 1, \dots, N, m = 1, \dots, M_n$$

e) Draw $\sum_{n=1}^N M_n$ uniformly distributed random numbers from Gamma- distributed rainfall depths population. The random number is taken as the cumulative frequency values in the Gamma CDF and the corresponding depth of rainfall events is determined numerically by solving the inverse cumulative distribution function for number of rainfall depths. Assign these values to the rainfall events to obtain events depths, $H_{n,m}$.

f) Draw $\sum_{n=1}^N (M_n - 1)$ uniformly distributed random numbers from geometrically-distributed population to represent interevent time, $Z_{n,m}$. The random number is taken as the cumulative frequency values in the geometric CDF and the corresponding interevent time is determined numerically by solving the inverse cumulative distribution function. Assign these values to the periods of no rainfall days.

$$Z_{n,m} \quad n=1, \dots, N, \quad m=1, \dots, (M_n - 1)$$

g) As a byproduct of the previous steps, the length of the rainy season, L_n can be derived as;

$$L_n = \sum_{m=1}^{M_n} D_{n,m} + \sum_{m=1}^{M_n-1} Z_{n,m}$$

The steps (a) to (g) define the synthetic rainfall events, and their positions within the individual rainy seasons.

The flow chart of Event based stochastic rainfall generation process is shown in Figure 3. 14.

3.4 PHYSICAL PROPERTIES OF SOIL

Information on soil physical properties is required by hydrological and slope stability models and this information are derived from the principles of soil mechanics as discussed below.

3.4.1 Soil as a Three Phase System

A soil mass consists of solid soil particles, air and water situated in the voids between the particles. If a soil volume V is considered (see Figure 3. 4), it consists of the volume of soil particles or solids V_s and the void volume V_v .

The void volume may be partly filled with a volume of air V_a and a volume of water V_w . In formula form:

$$V = V_s + V_v ; V_v = V_a + V_w \quad (3.6)$$

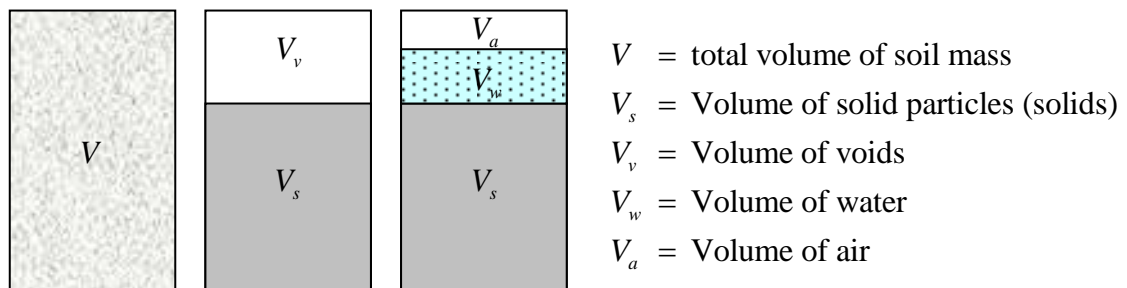


Figure 3. 4: The three phases of a natural soil mass.

3.4.2 Porosity, Volumetric Water Content and Degree of Saturation

An important quantity of soil is the porosity. It is the ratio of the pore volume and total volume.

$$\eta = \frac{V_v}{V} \quad (3.7)$$

The porosity for most soils varies between 0.35 and 0.45 (35 % and 45 %). Loose soils have a large porosity and dense soils have a low porosity.

Another quantity to describe the pore volume is the void ratio e , defined by:

$$e = \frac{V_v}{V_s} \quad (3.8)$$

Normally e falls in the range 0.5 to 0.8.

Since $V = V_s + V_v$ it easily can be confirmed that the following relations between η and e are valid:

$$e = \frac{\eta}{1-\eta} ; \eta = \frac{e}{1+e} ; 1-\eta = \frac{1}{1+e} \quad (3.9)$$

The void ratio is used widely to describe the *relative density* RD of a soil. It is defined by:

$$RD = \frac{e_{\max} - e}{e_{\max} - e_{\min}} \quad (3.10)$$

Where e_{\max} is the maximum void ratio of the soil in its loosest state and e_{\min} is the minimum void ratio of the soil in its densest state. Both void ratios can be determined in the laboratory.

To describe the amount of water in the soil, the *volumetric water content* θ can be used which is the ratio of the volume of water V_w and total volume V :

$$\theta = \frac{V_w}{V} \quad (3.11)$$

The volumetric water content varies from 0 under dry conditions to η in case the soil is completely saturated.

Another quantity to describe the water content is the *degree of saturation*, defined by:

$$S = \frac{V_w}{V_v} \quad (3.12)$$

The degree of saturation ranges from 0 to 1 for completely dry and completely saturated conditions, respectively.

It easily can be confirmed that the following relation between θ and S holds:

$$\theta = S\eta \quad (3.13)$$

For saturated conditions: $V_w = V_v$; it then can be derived:

$$S = 1 \rightarrow \theta = \theta_{sat} = \eta \quad (3.14)$$

Where the subscript "sat" indicates the saturated condition.

The normalised volumetric water content Θ is defined by:

$$\Theta = \frac{\theta - \theta_{res}}{\theta_{sat} - \theta_{res}} \quad (3.15)$$

Where; θ_{res} is the residual volumetric water content.

3.4.3 Density, Specific Gravity and Unit Weight

For the description of the density and unit weight of the soil the ratios such as η , e and S are required as well as the densities of the composing materials. The *density* ρ of a material is the mass per unit of volume. Approximate values for the density of water ρ_w and the density of soil solids ρ_s are:

$$\rho_w \approx 1000 \text{ kg/m}^3 ; \rho_s \approx 2650 \text{ kg/m}^3 \quad (3.16)$$

The unit weight or specific weight γ is the weight of the material per unit of volume.

Since weight is mass times the gravitational acceleration g , for water and soil solids it can be found $g \approx 10 \text{ N/kg}$

$$\gamma_w = \rho_w g \approx 10 \text{ kN/m}^3 ; \gamma_s = \rho_s g \approx 26.5 \text{ kN/m}^3 \quad (3.17)$$

The *specific gravity* SG of a material is the density or weight relative to that of water.

The specific gravity of the soil solids is:

$$SG_s = \frac{\rho_s}{\rho_w} = \frac{\gamma_s}{\gamma_w} \approx 2.65 \quad (3.18)$$

The total weight W of a volume V of soil is an important quantity. It is the sum of the weights of the solids, water and air. Neglecting the weight of the air it can be derived:

$$W = W_s + W_w + W_a = W_s + W_w = \gamma_s V_s + \gamma_w V_w \quad (3.19)$$

With $V_s = V - V_v = (1 - \eta)V$ [equations (3.11) and (3.13)] it follows:

$$W = [\gamma_s(1-\eta) + \gamma_w\theta]V = [\gamma_s(1-\eta) + \gamma_w S\eta]V \quad (3.20)$$

For the unit weight γ of the soil the following expressions can be found:

$$\gamma = \frac{W}{V} \rightarrow \gamma = \gamma_s(1-\eta) + \gamma_w\theta = \gamma_w(SG_s(1-\eta) + \theta) = \gamma_w\left(\frac{SG_s}{1+e} + \theta\right) \quad (3.21)$$

With $\theta = S\eta$ it can be written:

$$\gamma = \frac{W}{V} \rightarrow \gamma = \gamma_s(1-\eta) + \gamma_w S\eta = \gamma_w[SG_s(1-\eta) + S\eta] = \gamma_w\left(\frac{SG_s + Se}{1+e}\right) \quad (3.22)$$

The dry unit weight of the soil γ_d can be obtained from Equations (3.21) and (3.22)

using $\theta = S = 0$:

$$\gamma_d = \gamma_s(1-\eta) = \gamma_w SG_s(1-\eta) = \frac{SG_s\gamma_w}{1+e} \quad (3.23)$$

With an average value of the porosity of 40% the value of the dry unit weight γ_d approximately is:

$$\gamma_d \approx 10 \times 2.65(1-0.4) \approx 16 \text{ kN/m}^3 \quad (3.24)$$

Similarly for the fully saturated unit weight γ_{sat} using $\theta = \eta$ and $S = 1$ it can be obtained:

$$\gamma_{sat} = \gamma_s(1-\eta) + \gamma_w\eta = \gamma_w(GS_s(1-\eta) + \eta) = \frac{(GS_s + e)\gamma_w}{1+e} \quad (3.25)$$

An approximation for the numerical value of γ_{sat} is:

$$\gamma_{sat} \approx 10 \times [2.65(1-0.4) + 0.4] \approx 20 \text{ kN/m}^3 \quad (3.26)$$

3.4.4 Gravimetric water content

The gravimetric water content w is the ratio of the weight of water W_w and the weight of the solids W_s in a total volume V :

$$w = \frac{W_w}{W_s} \rightarrow w = \frac{\gamma_w V_w}{\gamma_s V_s} = \frac{\gamma_w}{\gamma_s} \frac{\eta}{1-\eta} S = \frac{\eta}{1-\eta} \frac{S}{SG_s} \quad (3.27)$$

With η replaced by e the gravimetric water content becomes:

$$w = \frac{W_w}{W_s} \rightarrow w = \frac{\gamma_w V_w}{\gamma_s V_s} = \frac{\gamma_w}{\gamma_s} e S = \frac{e S}{SG_s} \quad (3.28)$$

3.4.5 Soil Water Conservation Curve (SWCC)

Soil water characteristic curve, SWCC for a soil is defined as the relationship between water content and suction for the soil (Williams, 1982). The water content defines the amount of water contained within the pores of the soil. The suction may be either the matric suction (also known as capillary pressure) of the soil (i.e. $u_a - u_w$, where u_a is the pore-air pressure and u_w is the pore-water pressure) or total suction (i.e. matric plus osmotic suction). At high suctions (i.e. greater than about 1500 KPa), matric and total suction can generally be assumed to be equivalent (Fredlund et al, 1994).

Figure 3. 5 shows a typical plot of a soil water characteristic curves.

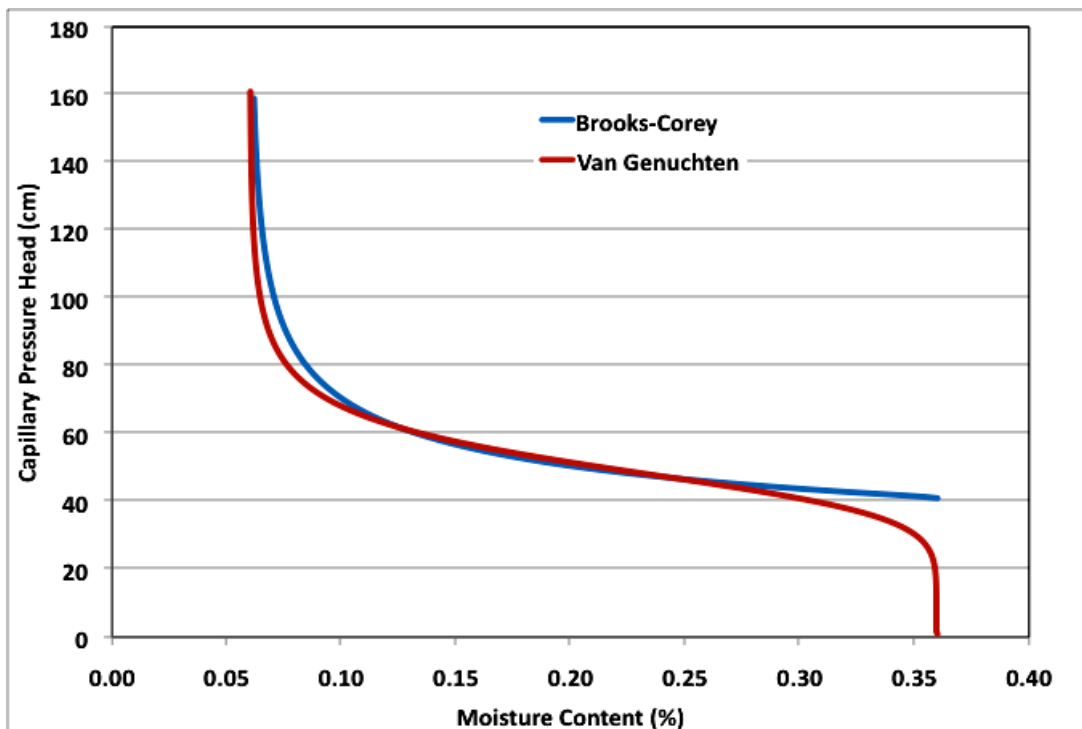


Figure 3. 5: Comparison plot of SWCC models

(Source: www.ce.utexas.edu/prof/mckinney/ce374l/ce374l.html)

The air entry value of the soil (i.e. bubbling pressure) is the matric suction where air starts to enter the largest pores in the soil. The residual water content is the water content where a large suction change is required to remove additional water from the soil (Fredlund et al, 1994). Croney and Coleman, (1961) established that the total suction corresponding to zero water content was essentially the same for all types of soils and had a value slightly below 10^6 kPa. This value has been experimentally supported for a variety of soils. This value is also supported by thermodynamics considerations (Richards, 1965), implying that there is a maximum total suction value corresponding to a zero relative humidity in any porous medium.

3.4.5.1. Calculating water contents and water pressure head using SWCC models

1. Van Genuchten model;

This model works well for most soils (Van Genuchten, 1980). The relationship between volumetric water content and matric suction in this model is;

$$\Theta = \frac{\theta_t - \theta_r}{\theta_s - \theta_r} = \left[\frac{1}{1 + (\alpha\psi)^n} \right]^m$$

and on rearranging,

$$(u_a - u_w) = \frac{\left[\frac{1}{\left(\frac{\theta_t - \theta_r}{\theta_s - \theta_r} \right)^{\frac{n}{n-1}} - 1} \right]^{\frac{1}{n}}}{\alpha} \quad (3.29)$$

Where;

Θ = normalized volumetric water content

θ_t = the volumetric water content at any matric suction,

θ_s = the saturated volumetric water content,

θ_r = the residual volumetric water content,

$n = \lambda + 1$; λ is the pore-size distribution factor.

$(u_a - u_w)$ = soil suction head

$\alpha = \frac{1}{(u_a - u_w)_b}$; $(u_a - u_w)_b$ is the bubbling pressure (the air entry value of the soil)

$$m = \left(\frac{n-1}{n} \right)$$

2. Brooks and Corey model

This model is good for coarse soils with narrow pore size distribution factor (Brooks and Corey, 1964). The relationship between volumetric water content and matric suction in this model is as follows;

$$\Theta = \frac{\theta_t - \theta_r}{\theta_s - \theta_r} = \left(\frac{(u_a - u_w)_b}{(u_a - u_w)} \right)^\lambda$$

and on rearranging,

$$(u_a - u_w) = \left(\frac{(u_a - u_w)_b}{\left(\frac{\theta_t - \theta_r}{\theta_s - \theta_r} \right)^{\frac{1}{\lambda}}} \right) \quad (3.30)$$

Where;

λ = the pore-size distribution factor.

3.4.5.2. Comparison of SWCC models

Mavimbela and van Rensburg (2012) established that Brooks and Corey model shows some deviation near or at the air entry point given its assumption to impose a zero slope at this suction from saturation, while Van Genuchten model fits well to sandy textured soils.

Figure 3. 5 is a comparison plot of suction head verses volumetric moisture content generated for van Genuchten and Brooks & Corey SWCC models. From the plot, the two models tend to give approximately same relationship of pressure head and soil moisture contents up to the near air entry point when Brooks and Corey model imposes zero slope while van Genuchten model tended to zero. In this study Van Genuchten model was adopted for any calculation involving SWCC models.

3.5 HYDRUS 1D MODEL

The HYDRUS program numerically solves the Richards's equation (see equation 3.31) using Galerkin-type linear finite element schemes for variably saturated water flow and advection-dispersion type equations for heat and solute transport.

$$\frac{\partial \theta}{\partial t} = \frac{\partial}{\partial z} \left[K(\theta) \left(\frac{\partial h}{\partial z} + 1 \right) \right] \quad (3.31)$$

Where;

K is the hydraulic conductivity,

h is the pressure head,

z is the elevation above a vertical datum,

θ is the water content, and

t is time.

3.5.1 Uniform Water Flow

One-dimensional uniform (equilibrium) water movement in a partially saturated rigid porous medium is described by a mixed form of the Richards equation using the assumptions that the air phase plays an insignificant role in the liquid flow process and that water flow due to thermal gradients can be neglected (Šimůnek et al 2009):

$$\frac{\partial \theta}{\partial t} = \frac{\partial}{\partial z} \left[K \left(\frac{\partial h}{\partial z} + \cos \alpha \right) \right] - S \quad (3.32)$$

Where h is the water pressure head [L], θ is the volumetric water content [L^3L^{-3}], t is time [T], z is the spatial coordinate [L] (positive upward), S is the sink term [$L^3L^{-3}T^{-1}$] defined as the volume of water removed from a unit volume of soil per unit time due to plant water uptake (Feddes et al., 1978), α is the angle between the flow direction and the vertical axis (i.e., $\alpha = 0^0$ for vertical flow, 90^0 for horizontal flow, and $0^0 < \alpha < 90^0$ for inclined flow), and K is the unsaturated hydraulic conductivity function [LT^{-1}] given by;

$$K(h, z) = K_s(z)K_r(h, z) \quad (3.33)$$

Where; K_r is the relative hydraulic conductivity [-] and K_s the saturated hydraulic conductivity [LT^{-1}].

3.5.2 Numerical Solution of Variably Saturated Flow Equation in HYDRUS 1D

3.5.2.1. Space and Time Discretization

The soil profile is first discretized into $N-1$ adjoining elements, with the ends of the elements located at the nodal points, and N being the number of nodes (see Figure 3. 6).

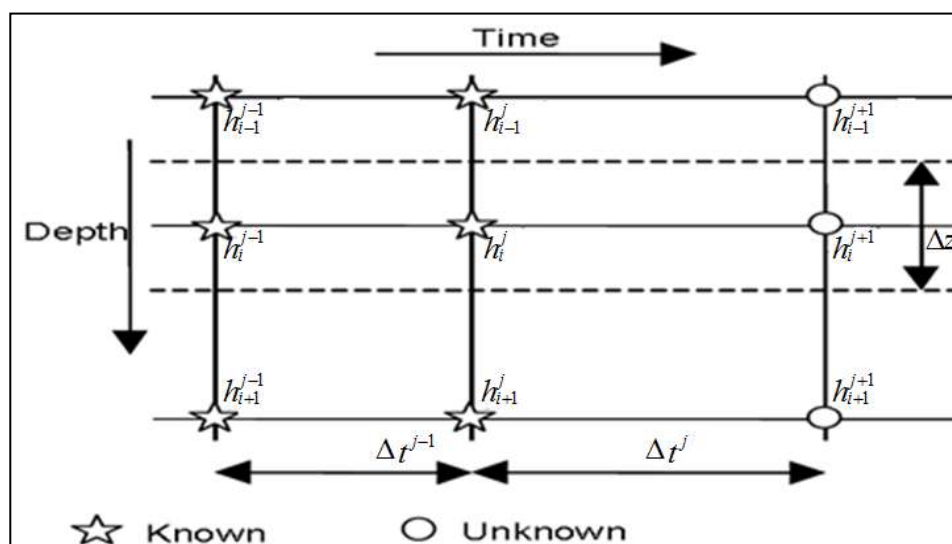


Figure 3. 6: spatial and temporal discretization used in solving Richards's equation
(Source: Gurrapu S., 2005)

The same spatial discretization is used for water flow, solute transport and heat movement. A mass-lumped linear finite elements scheme was used for discretization of the mixed form of the Richards' equation (3.32).

The mass-lumped scheme results in an equivalent and somewhat standard finite difference scheme [e.g., Vogel et al., 1996].

$$\frac{\theta_i^{j+1,k+1} - \theta_i^j}{\Delta t} = \frac{1}{\Delta z} \left(K_{i+1/2}^{j+1,k} \frac{h_{i+1}^{j+1,k+1} - h_i^{j+1,k+1}}{\Delta z_i} - K_{i-1/2}^{j+1,k} \frac{h_i^{j+1,k+1} - h_{i-1}^{j+1,k+1}}{\Delta z_{i-1}} \right) + \frac{K_{i+1/2}^{j+1,k} - K_{i-1/2}^{j+1,k}}{\Delta z} \cos \alpha - S_i^j \quad (3.34)$$

Where;

$$\Delta t = t^{j+1} - t^j$$

$$\Delta z = \frac{z_{i+1} - z_{i-1}}{2} \quad \Delta z_i = z_{i+1} - z_i \quad \Delta z_{i-1} = z_i - z_{i-1}$$

$$K_{i+1/2}^{j+1,k} = \frac{K_{i+1}^{j+1,k} - K_i^{j+1,k}}{2} \quad K_{i-1/2}^{j+1,k} = \frac{K_i^{j+1,k} - K_{i-1}^{j+1,k}}{2}$$

in which subscripts $i-1$, i , and $i+1$ indicate the position in the finite difference mesh; superscripts k and $k+1$ denote the previous and current iteration levels, respectively; and superscripts j and $j+1$ represent the previous and current time levels, respectively. Equation (3.34) is based on a fully implicit discretization of the time derivative, and will be solved with a Picard iterative solution scheme. Notice also that the sink term, S , is evaluated at the previous time level. The mass-conservative method proposed by Celia et al. [1990], in which $\theta^{j+1, k+1}$ is expanded in a truncated Taylor series with respect to h about the expansion point $h^{j+1, k}$, is used in the time difference scheme of equation (3.34):

3.5.2.2. Computation of Nodal Fluxes, q

Components of the Darcian flux are computed at each time level during the simulation only when the water flow and solute (or heat) transport equations are solved

simultaneously. When the flow equation is being solved alone, the flux components are calculated only at selected print times. The z -components of the nodal fluxes are computed for each node n according to;

$$q_i^{j+1} = \frac{-K_{i+1/2}^{j+1} \left(\frac{h_{i+1}^{j+1} - h_i^{j+1}}{\Delta z_i} + 1 \right) \Delta z_{i-1} - K_{i-1/2}^{j+1} \left(\frac{h_i^{j+1} - h_{i-1}^{j+1}}{\Delta z_{i-1}} + 1 \right) \Delta z_i}{\Delta z_{i-1} + \Delta z_i}$$

$$q_N^{j+1} = -K_{N-1/2}^{j+1} \left(\frac{h_N^{j+1} - h_{N-1}^{j+1}}{\Delta z_{N-1}} + 1 \right) - \frac{\Delta z_{N-1}}{2} \left(\frac{\theta_N^{j+1} - \theta_N^j}{\Delta t} + S_N^j \right) \quad (3.35)$$

3.5.3 Model Parameters, Inputs and Outputs

3.5.3.1 model parameters

Before application of HYDRUS 1D model in hydrological modelling, some parameters have to be specified and include; Soil hydraulic model (modified van Genuchten, brooks and Corey), Water flow boundary conditions, Time variable boundary conditions, Geometry information, Time information, Print information and Iteration criteria.

HYDRUS 1D model allows users to select six types of models for the soil hydraulic properties i.e. the van Genuchten-Mualem model, the van Genuchten-Mualem model with an air-entry value of -2 cm, modified van Genuchten type equations, Brooks and Corey model, the lognormal model, and a dual-porosity model (Šimůnek et al 2009). Van Genuchten model with no hysteresis was adopted in this study. In the Soil Catalogue of the Pre-Processing Menu (Water Flow Submenu), HYDRUS model allows selection of various soil hydraulic parameters. The model takes parameters from Carsel and Parrish (1988) for the van Genuchten model and from Rawls et al. (1982) for the Brooks-Corey model.

HYDRUS model allows users to specify the type of upper and lower boundary conditions to be used. For this study upper boundary condition was chosen as

atmospheric boundary condition with surface run off while lower boundary conditions was chosen as Constant flux ($q = 0$). The initial condition was specified either in terms of the water content and an assumed value of 0.2 was set in the Profile Summary tab of Pre-Processing Menu.

In graphical editor tab a soil layer can be described into several nodes and for this study a soil layer was described into one hundred and one equidistant nodes and the soil moisture simulation were monitored using nodes 11, 46, 86 and 101. Nodes 11, 46 and 86 would represent the central nodes of saturated, transmission and wetting zones of precipitation infiltration soil profile (see Figure 3. 7) and the modelled water content in these nodes would represent average water content in each of the respective zones.

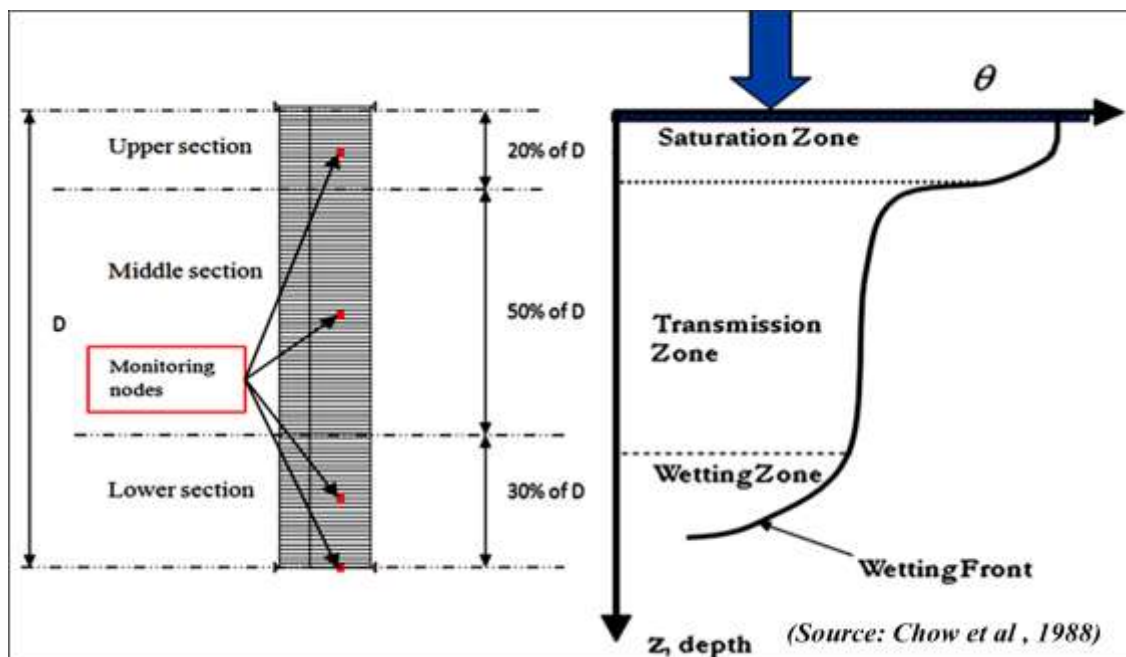


Figure 3. 7: Description of soil layer in Hydrus 1D model and an illustration of infiltration/percolation front.

The monitoring nodes in HYDRUS -1D model was formulated as shown in Figure 3. 7. The upper section which is highly affected by weather conditions was represented by about 20% of soil layer thickness while the lower section of the soil that majorly represent water accumulation was represented by 30% of soil thickness. The middle

section (transmission zone) of soil layer which consist of drainage and accumulation of infiltrated rain water takes 50% the thickness of soil.

3.5.3.2 model inputs

HYDRUS model also require input of time variable data. These data includes; Time for which a data record is provided [T], Precipitation rate [LT^{-1}] (in absolute value), Potential evapotranspiration rate [LT^{-1}] (in absolute value), and absolute value of the minimum allowed pressure head at the soil surface [L]. HYDRUS model requires that the minimum allowed pressure head at the soil surface be selected such so that the corresponding water content is at least 0.005 higher than the residual water content. This value was calculated using equation (3.29) and inputted into the model. The precipitation rate data was obtained through transformation of daily rainfall data into hourly rates using gamma distribution (see section 3.6.3) while the average hourly value of potential evapotranspiration data was used as potential evapotranspiration rate [LT^{-1}].

3.5.3.3 model outputs

In the Observation Points tab of post processing menu, graphical representation of modelled water content, pressure head, temperature and/or solution and adsorbed concentrations at specified observation nodes can be viewed. Water fluxes are printed instead of temperatures when “Print Fluxes instead of Temperatures for Observation Nodes” is checked in the Print Information dialog.

3.6 SLOPE STABILITY ASSESSMENT USING INFINITE SLOPE MODEL

3.6.1 Infinite Slopes and Mode of Failure

Infinite slope is a slope that extends for a relatively long distance and has a consistent subsurface profile. These slopes mainly fail through translational slip whereby the slip surface is parallel to the soil surface. Translational slides occur in areas where hard

stratum underlies the soil layer. Slope shear failure occurs when the shear strength of a soil layer on a hill slope becomes smaller than the shear stress acting on the soil, resulting in plan a movement of the affected soil layer along the slip surface.

The infinite slope model assumes that the soil depth is shallow compared to the hillslope length (infinitely smaller), therefore the boundary exerts little influence on slope failure. The slope factor of safety F_s can be defined as the ratio between the soil strength S and shear stress T . The factor of safety can be mapped in space and if it is smaller than 1 (i.e. $F_s < 1$), then it will indicate likely failure. The most sensitive variables in the model are soil depth and the saturated layer thickness, or the soil wetness index.

The role of water in slope failures is very important since slope saturation of adds to the soil weight. Positive pore water pressure (due to infiltration from surface, exfiltration from bedrock, preferential flow, also dynamic loadings) decreases the factor of safety. On the other hand, negative pore pressures (suction) in unsaturated soils, adds to the apparent cohesion of soils and increases the factor of safety.

3.6.2 Determination of Root Cohesion Strength Using Wu Method

3.6.2.1. Introduction to Root apparent cohesion determination

Roots of vegetation are known to stabilize, or, improve the bearing in forest soils (Wasterlund, 1989) and slopes (Waldron and Dakessian, 1982). Investigations conducted by Willatt and Sulistyaningsih (1990) on loamy soil showed increases in both bearing capacity and shear vane resistance in the presence of roots, whilst Goss (1987) reported an increase in the soil bulk density in similar studies. According to Wasterlund (1989), the increase in soil strength caused by the presence of tree roots may range between 50 and 70%. The intermingled roots of plants tend to bind the soil together in a monolithic mass and contribute to strength by providing an additional

apparent cohesion, C_r . As a result of their random orientation, roots have a negligible influence on the frictional component of soil strength. Thus, in a root-permeated soil the Mohr- Coulomb failure criterion is modified to include effective root cohesion, C_r'

$$S = C_s' + C_r' + (\sigma - u) \tan \phi' \quad (3.36)$$

Where; S is the shear strength of the soil-root composite, C_s' is effective soil cohesion, σ is normal stress, u is pore-water pressure and ϕ' is the effective angle of internal friction. The magnitude of C_r' varies with the distribution of the roots within the soil and with the tensile strength of individual roots (De Beats et al, 2008).

3.6.2.2. Root area ratio calculations

Root Area Ratio (RAR) is required in order to estimate root contribution to soil strength, and Gray and Leiser (1982) defined RAR as the fraction of the soil cross-sectional area occupied by roots per unit area. Investigation by Schmidt et al., (2001) in mixed natural forests of the Oregon coast range established that the mean RAR ranged between 0.1 and 1% in 1.2 m deep pits dug midway between neighbouring trees, whereas Abernethy and Rutherford (2001) found values between 0.001 and 0.756% in *Eucalyptus camaldulensis* Labill and *Melaleuca ericifolia* Smith growing along riverbanks in Australia and can be said therefore that the values of RAR are highly variable. RAR is given by (De Beats et al, 2008);

$$RAR = \frac{\sum_i^n n_i a_i}{A} \quad (3.37)$$

Where;

a_i is the mean root cross sectional area (m^2)

A is the reference area (m^2) of soil occupied by roots

n_i is the number of roots in a diameter class

3.6.2.3. Shear strength of root reinforced soil

The model of Wu et al. (1979) was used to estimate the increase in soil shear strength due to the presence of roots, because this model allows for simple and quick calculation of soil reinforcement by roots using tensile strength and root distribution information. Wu model assumes that all roots grow vertically and act as loaded piles, so tension is transferred to them as the soil is sheared. According to Abernethy and Rutherford (2001), plant roots tend to bind the soil together in a monolithic mass and contribute to the strength by providing an apparent additional cohesion. If the soil is rooted, the increased soil shear strength can be expressed as an additional cohesion (De Beats et al, 2008) i.e.,

$$S_r = S + C_r \quad (3.38)$$

Where S_r is the shear strength (KPa) of the soil reinforced by roots, S is soil shear strength (KPa) and C_r is the increase in shear strength due to the presence of roots (KPa).

When shear forces occur, the root fiber deforms. This deformation causes the fiber to stretch, provided there is sufficient interface friction, confining stress and anchorage length to lock the fiber in place and to prevent slippage or pullout. Gray and Sotir (1996) noted that the fiber elongation mobilizes the tensile resistance in the fiber. The tension developed in the roots is resolved with a tangential component resisting shear and a normal component increasing the confining pressure on the shear plane. According to Simon et al (2006), Wu model assumes that all roots attain ultimate tensile strength simultaneously during soil shearing. The shear strength increase from a full mobilization of root tensile strength and is given by (De Beats et al, 2008):

$$C_r = \sigma_R (\cos \alpha \tan \varphi + \sin \alpha) \quad (3.39)$$

Where ; α is the angle of shear distortion in the shear zone, φ is the soil friction angle ($^\circ$) and σ_R is the total mobilized tensile stress of root fibres per unit area of soil. Wu et al. (1979) found that the value of the bracket term in equation (3.39) is relatively insensitive to normal variation in α and φ and has a value ranging from 1.0 to 1.3. In most studies this term is set to an average value of 1.2 (De Beats et al, 2008).

$$C_r = 1.04 \frac{\sum \sigma_i n_i a_i}{A} \quad (3.40)$$

Where σ_i is root tensile strength (MPa), n_i is the number of roots in a diameter class, i is root diameter class, a_i is the root cross-sectional area (m^2) and A is the reference area of soil occupied by roots (m^2).

The total amount of root cohesive strength within a soil column is dependent on the number, size, and tensile strengths of the roots within a specific soil mass (Pollen and Simon, 2005; Schmidt et al., 2001). The tensile strength of an individual root (σ_{ri}) can be defined by,

$$\sigma_{ri} = \left(\frac{T_{ri}}{\pi \left(\frac{d_{ri}}{2} \right)^2} \right) \quad (3.41)$$

Where T_{ri} is the tensile force of root i at failure and d_{ri} is the diameter of root i at the failure point (De Beats et al, 2008).

3.6.2.4. Root apparent Cohesion Calculations

In this study root cohesion strength contribution was calculated using the following equation (Pollen and Simon, 2005 and De Beats, 2008);

$$C_r = \sigma_T * RAR * (\cos \alpha \tan \varphi + \sin \alpha) \quad (3.42)$$

Where;

C_r = root cohesion strength.

σ_T = Mean root tensile strength across the landslide failure plane.

RAR = root area ratio

φ = angle of friction.

α = the angle of shear distortion in the shear zone.

3.6.2.5. *RAR distribution with depth*

Roots decline in number as depth increases, and at approximately 1.5 to 2 meters, the number of root present in soil mass is approximately zero. Hales et al (2008) and Mattia et al (2005) found exponential decay in the number of roots from the soil surface. This fact will have to be considered while determining contribution of roots to increase in soil cohesion strength. The distribution that can well describe this fact of roots number variation with depth is exponential distribution below;

$$p(d, \lambda) = \exp(-\lambda d) \quad (3.43)$$

Where,

λ = constant

d = depth of soil

3.6.3 Rainfall Occurrence

The rainfall data obtained from meteorological department were in daily rainfall form, but for landslide modelling, a way has to be formulated to transform these daily amount data into hourly incremental amount for better prediction of landslides. During this transformation the reality in the ground must to be maintained. This can be achieved by fitting hourly rainfall occurrence to a distribution. Rainfall occurrence charts required for this analysis was not available in any of the meteorological stations found within my study area, and so rainfall occurrence charts for Moi University station (see *Appendix G*), was adopted in this study since the plots of average monthly

rainfall for the Moi University station and those of rainfall stations found in the study (see Figure 3. 8), indicates that they receive nearly the same rainfall patterns. It was established that gamma distribution in equation (3.44) fit well to the Moi University hourly rainfall data and was used in this study.

$$f(x, \beta, \alpha) = \frac{x^{\alpha-1} e^{-x/\beta}}{\beta^\alpha \Gamma(\alpha)} \quad (3.44)$$

Where,

$$\alpha = 4$$

$$\beta = 0.2$$

x Ranges from 0 to 4

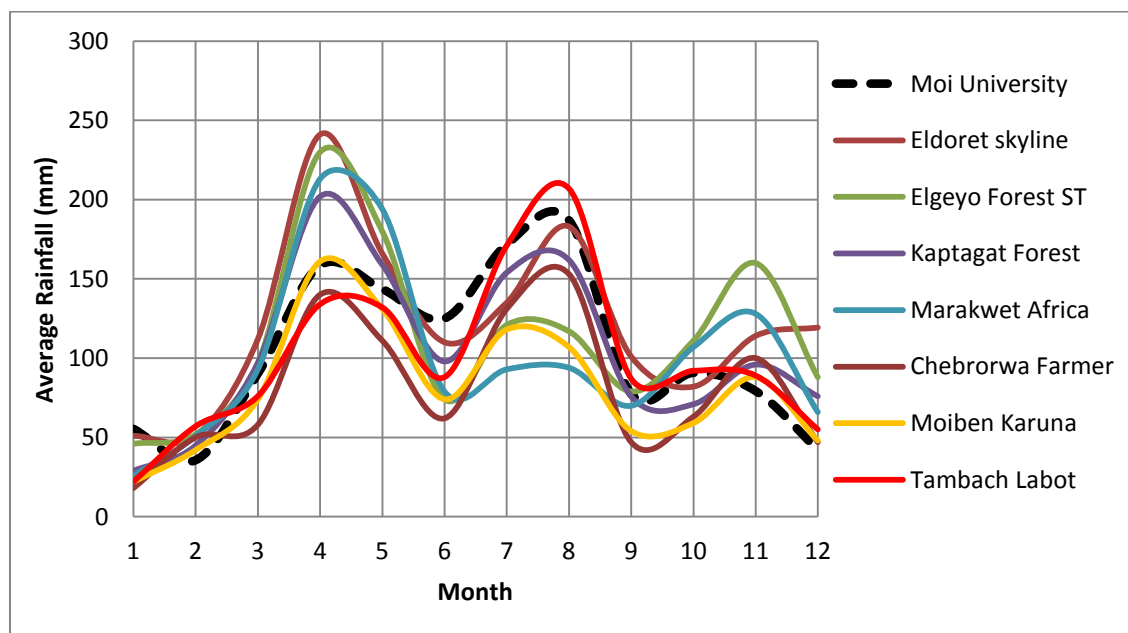


Figure 3. 8: Comparative assessment of mean monthly rainfall data for various stations

3.6.4 Matric Suction and Suction Stress in Absence of a Water Table

The generalized effective stress that unifies both saturated and unsaturated conditions proposed by Lu and Likos (2004, 2006) is:

$$\sigma' = (\sigma - u_a) - \sigma^s \quad (3.45)$$

Where;

u_a is the pore air pressure, and

σ^s is defined as the suction stress characteristic curve of the soil with a general functional form of (Lu and Likos 2006):

$$\begin{aligned} \sigma^s &= -(u_a - u_w) & u_a - u_w &\leq 0 \\ \sigma^s &= f(u_a - u_w) & u_a - u_w &> 0 \end{aligned} \quad (3.46)$$

Where;

u_w is the pore water pressure,

3.6.4.1. Deriving the matric suction, ($u_a - u_w$), profile

From the Darcy's law for 1-D steady seepage,

$$q = -K \frac{\partial A}{\partial z} \quad (3.47)$$

Where;

q is the flow rate (per unit area),

K is permeability,

A is the total head, and

z is a depth coordinate equal to zero at the water table/bedrock.

If equation (3.47) gives negative q it implies infiltration or steady seepage towards the water table, and positive q implies evaporation or steady seepage away from the water table.

The total head consists of pressure and elevation components i.e.,

$$A = \psi + z$$

Where;

$$\psi \text{ is the pressure head, and is given by } \psi = \frac{-(u_a - u_w)}{\gamma_w}$$

z is the elevation head

From van Genuchten (1980) SWCC, matric suction as a function of water content is given by;

$$(u_a - u_w)_{z=0} = \frac{\left[\frac{1}{\left(\frac{\theta_t - \theta_r}{\theta_s - \theta_r} \right)^{\frac{n}{n-1}}} - 1 \right]^{\frac{1}{n}}}{\alpha} \quad (3.48)$$

Where;

θ_t = the volumetric water content at a point in soil layer,

θ_s = the saturated volumetric water content,

θ_r = the residual volumetric water content,

$n = \lambda + 1$;

λ is the pore-size distribution factor.

$(u_a - u_w)$ = soil matric suction

$$\alpha = \frac{1}{\psi_b}$$

ψ_b is the bubbling pressure head (the air entry value of the soil)

A simple expression for the permeability of an unsaturated soil as a function of its matric suction and saturated hydraulic conductivity K_s ; has been proposed by Gardner (1958),

$$K = K_s e^{-\alpha(u_a - u_w)} \quad (3.49)$$

Where;

α is the inverse of the air entry pressure (in KPa-1) and typically lies in the range $0.001 < \alpha < 0.5$ kPa-1. The air entry pressure is the matric suction value that must be exceeded before air recedes into the soil pores.

Let $\beta = \gamma_w \alpha$

Where;

γ_w is the unit weight of water.

Equation (3.47) may thus be written as follows;

$$q = -K_s e^{\beta\psi} \left(\frac{d\psi}{dz} + 1 \right) = -K_s e^{\beta\psi} \left(\frac{d\psi + dz}{dz} \right) \quad (3.50)$$

$$-\frac{q}{K_s} dz = e^{\beta\psi} d\psi + e^{\beta\psi} dz$$

$$-\left(\frac{q}{K_s} + e^{\beta\psi} \right) dz = e^{\beta\psi} d\psi$$

$$dz = -\frac{e^{\beta\psi} d\psi}{\frac{q}{K_s} + e^{\beta\psi}}$$

On rearranging further gives;

$$dz = -\frac{1}{\beta} \frac{d \left(\frac{q}{K_s} + e^{\beta\psi} \right)}{\frac{q}{K_s} + e^{\beta\psi}} \quad (3.51)$$

And integrating equation 3.51 and inserting the boundary condition that at the water table or bedrock top, matric suction is $\psi(z=0) = \psi(\theta)$ and limiting the value to a maximum of 100kPa (atmospheric pressure); will lead to the solution for the matric suction as a function of z , $\psi(\theta)$ and q ; and the material parameters K_s , α and γ_w for steady 1-d flow.

$$\int_0^z dz = -\frac{1}{\beta} \int_{\psi(z=0)}^{\psi(z)} \frac{d \left(\frac{q}{K_s} + e^{\beta\psi} \right)}{\frac{q}{K_s} + e^{\beta\psi}}; \text{ on integrating and rearranging gives,}$$

$e^{\beta\psi(z)} = e^{-\beta z} \left(\frac{q}{K_s} + e^{\beta\psi(z=0)} \right) - \frac{q}{K_s}$; making $\psi(z)$ the subject gives;

$$\psi(z) = \frac{\ln \left[e^{-\beta z} \left(\frac{q}{K_s} + e^{\beta\psi(z=0)} \right) - \frac{q}{K_s} \right]}{\beta} \quad (3.52)$$

In terms of $(u_a - u_w)$ and parameter α ;

$$(u_a - u_w)_z = - \frac{\ln \left[e^{-\gamma_w \alpha z} \left(\frac{q}{K_s} + e^{-\alpha(u_a - u_w)_{z=0}} \right) - \frac{q}{K_s} \right]}{\alpha} \quad (3.53)$$

Where;

$$(u_a - u_w)_{z=0} = \frac{\left[\frac{1}{\left(\frac{\theta_{z=0} - \theta_r}{\theta_s - \theta_r} \right)^{\frac{n}{n-1}}} - 1 \right]^{\frac{1}{n}}}{\alpha}$$

3.6.4.2. Derivation of matric suction stress, σ^s , profile

Suction stress can be expressed in terms of normalized volumetric water content or degree of saturation (Lu and Likos, 2004) as:

$$\sigma^s = - \frac{\theta_t - \theta_r}{\theta_s - \theta_r} (u_a - u_w) = - \frac{S_t - S_r}{S_s - S_r} (u_a - u_w) \quad (3.54)$$

If the SWCC model by Van Genuchten (1980) is used, the normalized degree of saturation can be expressed as:

$$\frac{S_t - S_r}{S_s - S_r} = \left(\frac{1}{1 + \{\alpha(u_a - u_w)\}^n} \right)^{\frac{(n-1)}{n}} \quad (3.55)$$

Where;

S is the degree of saturation,

γ_w is the unit weight of water,

n is parameter related to the rate of change of the de-saturation zone of the SWCC.

S_r is the residual degree of saturation, and

α is a suction value corresponding to the inflection point on the SWCC, which has physical meaning in that it bears a relationship to the air entry value. The parameter has units of soil suction or the inverse of soil suction.

Matric suction at any point z , is given by equation (3.53) i.e.;

$$(u_a - u_w)_z = - \frac{\ln \left[e^{-\gamma_w \alpha z} \left(\frac{q}{K_s} + e^{-\alpha(u_a - u_w)_{z=0}} \right) - \frac{q}{K_s} \right]}{\alpha} \quad (3.56)$$

Substituting for equation (3.55) and (3.56) in (3.54) and rearranging further gives;

$$\sigma^s = - \frac{\ln \left[e^{-\gamma_w \alpha z} \left(\frac{q}{K_s} + e^{-\alpha(u_a - u_w)_{z=0}} \right) - \frac{q}{K_s} \right]}{\alpha} \cdot \left(\frac{1}{1 + \{ \alpha(u_a - u_w)_z \}^n} \right)^{\frac{(n-1)}{n}}$$

$$\sigma^s = - \frac{\ln \left[e^{-\gamma_w \alpha z} \left(\frac{q}{K_s} + e^{-\alpha(u_a - u_w)_{z=0}} \right) - \frac{q}{K_s} \right]}{\alpha \left(1 + \{ \alpha(u_a - u_w)_z \}^n \right)^{\frac{(n-1)}{n}}} \quad (3.57)$$

Where;

$$(u_a - u_w)_z = - \frac{\ln \left[e^{-\gamma_w \alpha z} \left(\frac{q}{K_s} + e^{-\alpha(u_a - u_w)_{z=0}} \right) - \frac{q}{K_s} \right]}{\alpha}$$

The notations n and α are empirical fitting parameters of unsaturated soil properties.

The flow chart of matric suction stress modelling process is shown in Figure 3. 15.

3.6.5. Formulation of Generalized Infinite Slope Stability Function

Figure 3. 9 shows forces acting in a saturated slope and from infinite slope model.

$$z_c = \frac{c}{\cos \alpha [\gamma_{sat} (\tan \alpha - \tan \varphi) + \gamma_w \tan \varphi]} \quad (3.60)$$

For partially saturated soils, there exists suction stress that increases the soil effective shear resistance of slope materials and therefore infinite slope stability equation has to be modified to take into consideration of this phenomenon during slope stability assessment. The generalized effective stress in soil that unifies both saturated and unsaturated conditions recently proposed by Lu and Likos (2004, 2006), i.e. equation (3.45) is:

$$\sigma'_z = (\sigma_z - u_a) - \sigma_f^s \quad (3.61)$$

To derive the factor of safety under any saturated conditions, the generalized effective stress equation (3.61) above is used to replace the effective normal stress of infinite slope stability equation (3.58) above (Duncan and Wright, 2005), resulting in the formation of equation describing stability of slope under any saturated condition of soil;

$$F_s = \frac{C + (\gamma Z - \gamma_w Z_w + \sigma^s) \tan \varphi}{\gamma Z \cos \beta \sin \beta} \quad (3.62)$$

Where;

σ'_z = effective normal stress

σ_z = total normal stress

Z = depths of partially saturated soil wetting fronts

γ = unit weight of soils

C = combination of soil cohesion strength, C_s and root cohesion strength, C_r

σ_f^s = matric suctions stress at failure plane determined by Equation (3.57).

The flow chart of formulating infinite slope stability model is shown in Figure 3. 19

3.7 SLOPE STABILITY ASSESSMENT AND HAZARD MAPPING

Instability of slopes is a function of many parameters which include rainfall, nature of topography, soil type and type of land use in the region; and is assessed by calculating factor of safety, F_s . For spatial slope stability mapping in ILWIS GIS tool, modified infinite slope model is used, and this tool requires setting up of various spatial data and other inputs that will constitute the input as temporal values, polygon or raster layers for use by the mapping function and for display in ILWIS GIS tool.

3.7.1 ILWIS GIS Tool Data inputs

The spatial raster and point maps required in mapping by ILWIS GIS tool include; DEM map (for 3D maps generation), Soils cohesion strength map, Roots cohesion strength contribution map, Slope map, Soils angle of friction map, soil depth map, soil hydraulic conductivity map, Root Area Ratio (RAR) map, Root tensile strength (RTS) map, soil porosity map, residual soil moisture content map and Landslide inventory map (point map) for validation (see Figure 3. 17 for the flow chart).

3.7.1.1 DEM and Slope map

Topography is represented by a digital elevation model (DEM). A DEM was obtained in Shuttle Radar Topography Mission (SRTM DEM) of 90m resolution from <http://srtm.csi.cgiar.org/SELECTION/inputCoordinate.asp>. A digital elevation model (DEM) is used to derive information on elevation, slope aspect, slope angle, watersheds, and cut/fill volumes. Slope angle is one of the key factors in contributing towards slope instability and ArcGIS 10.1 was used to derive the slope map from filled DEM. The slope map shown in Figure 3. 10 represents the spatial distribution of slope values in the study area and was varying from 0 degrees to 61 degrees.

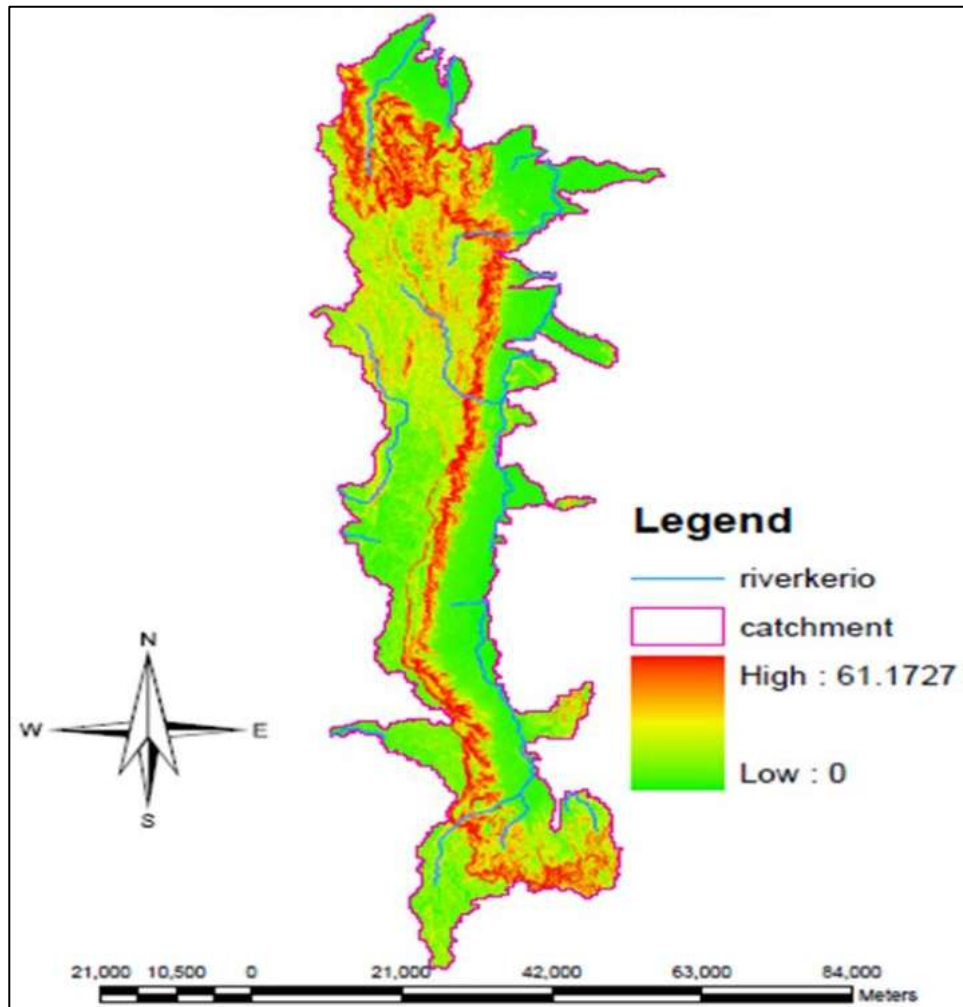


Figure 3. 10: Slope map in degrees for the study area

3.7.1.2 Land use

Land use is one of the important parameter in the landslide modelling. Soil physical properties might be different for a same soil type because of the land use. The information of land use was derived from land use map of Kenya (1980) and was delineated using ArcGIS 10.1. From the map; we established that the dominant land use along the escarpment was bush land and agriculture. The classifications in the delineated land use map were: Bushland (dense and sparse), Agriculture (dense and sparse), Forest, Woodland and Plantation (see Figure 3. 11)

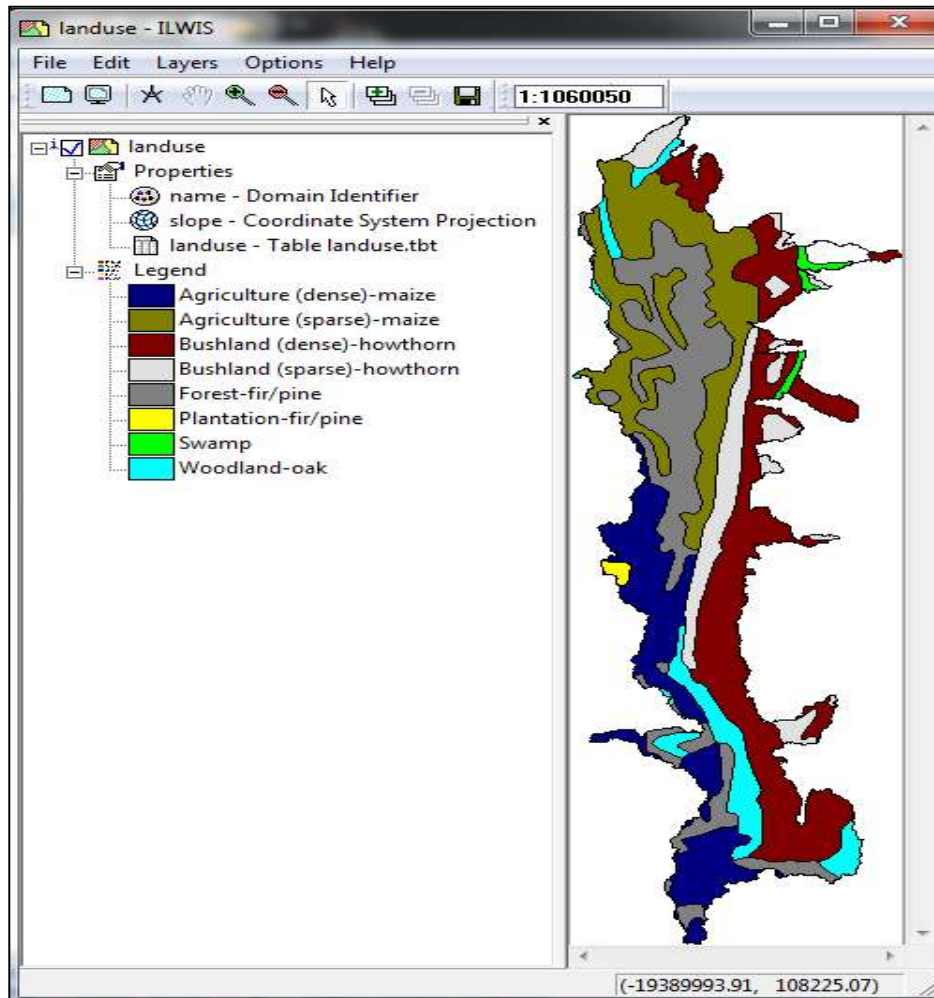


Figure 3. 11: Land use map for the study area

3.7.1.3 Root apparent Cohesion calculation

As described in section 3.6.2.4, root cohesion strength contributions were calculated in this study using equation (3.42).

Studies have been done on the variation of RAR with depth for various vegetation covers. De Baets et al (2008) did study on RAR for 25 typical Mediterranean plant species and the results are as shown in Figure 3. 12 (a), (b) and (c). He found out that, Mediterranean plant roots occupy less than 1% of the area under the crown of the plants. RAR for the topsoil ranges over one order of magnitude, from 0.08% for the grass *Piptatherum miliaceum* to 0.8% for the tree *Tamarix canariensis*.

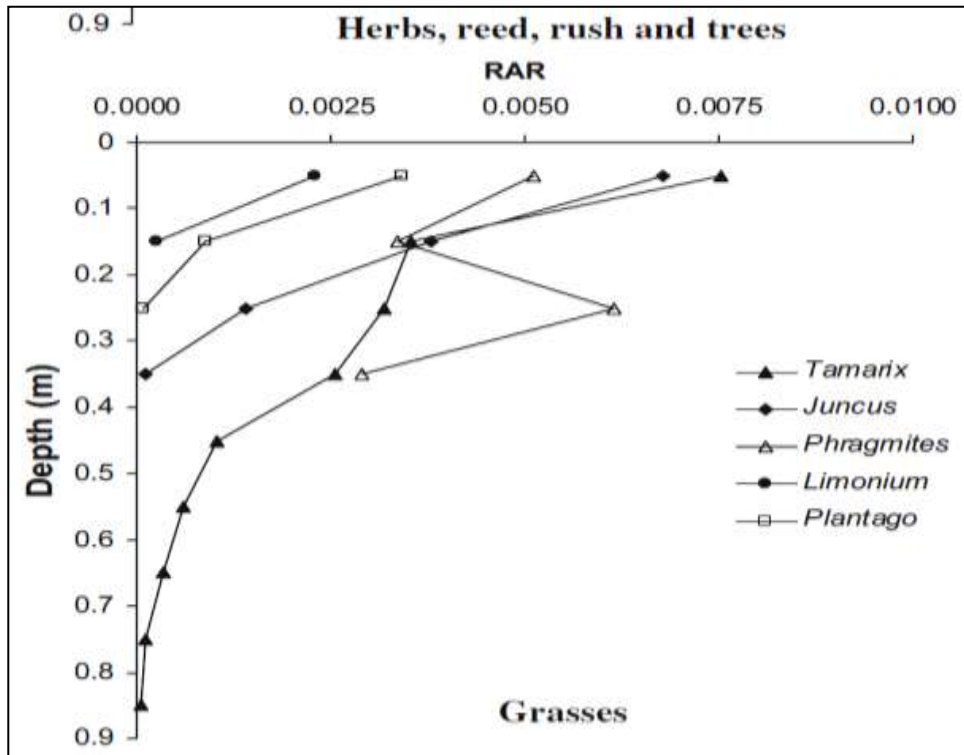


Figure 3. 12 (a): RAR variation with soil depth for trees, herbs and reed

(Source: S. De Baets et al, 2008)

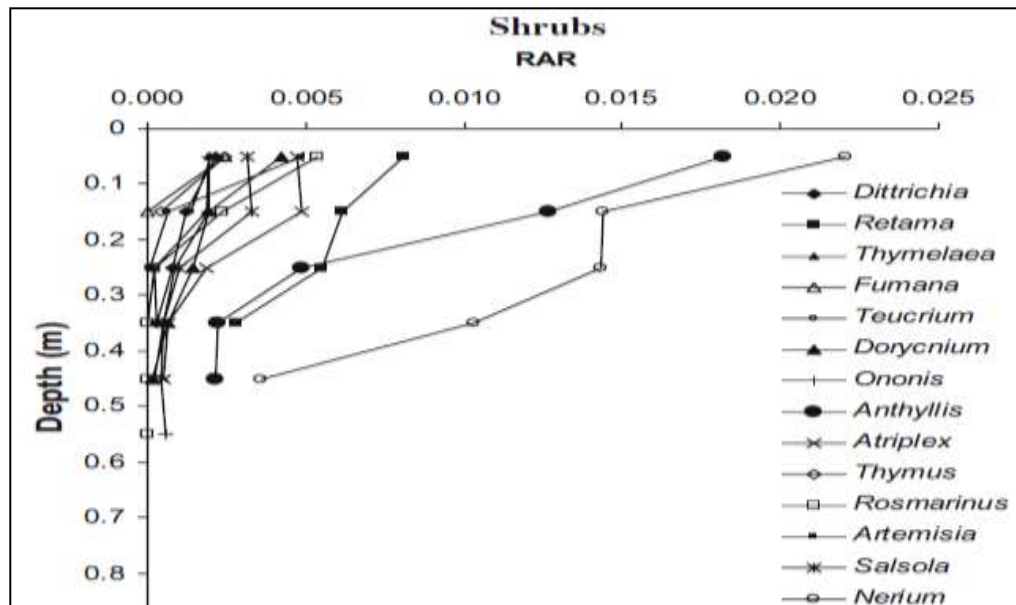


Figure 3. 12 (b): RAR variation with soil depth for shrubs

(Source: S. De Baets et al, 2008)

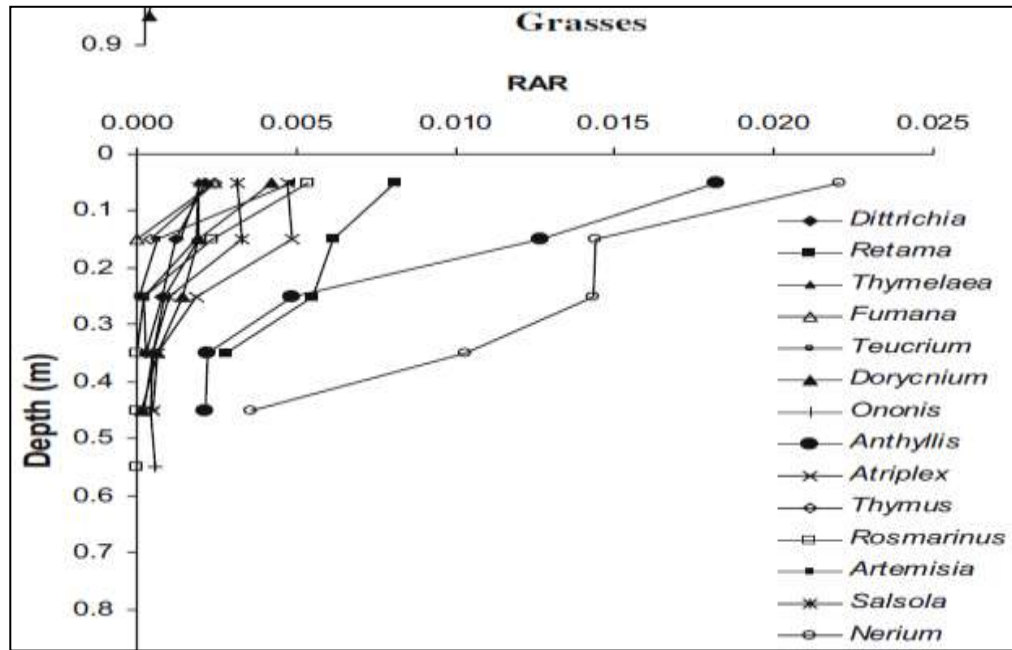


Figure 3. 12 (c): RAR variation with soil depth for Grasses

(Source: S. De Baets et al, 2008)

From Figure 3. 12 (a), (b) and (c); RAR variation with soil depth tend to follow exponential distribution as described in section 3.6.2.5.

The lambda constant, λ in equation (3.43) will vary depending on the maximum rooting depth of plants and the value adopted are as shown in the Table 3. 2;

Table 3. 2: Lambda constant for calculating RAR distribution with depth

Maximum rooting depth (M)	Constant λ
$\leq 1\text{m}$	10
$1 \leq \text{depth} \leq 1.5\text{m}$	5
$\geq 1.5\text{ m}$	2

Appendix E shows the root strengths of grasses, shrub and tree species (Norris J.E. et al 2008).

Most tensile testing was carried out on roots with diameters ranging from 0.5 – 15 mm. Plant parameters used in this study were chosen based on the Figure 3. 12 (a-c) for RAR values, and Appendix E for root strength values. Table 3. 3 shows the assumed and

adopted parameters to enable estimation of roots cohesion strength contribution (see equation 3.42) for each and every land use type. Some of the columns in Table 3. 3 were rasterized to form maximum rooting depth map, root tensile strength map and root area ratio, RAR maps for use by mapping function in ILWIS GIS tool.

Table 3. 3: Plant properties used in calculating root cohesion strength

Land use type	Dominant plant in the area	Maximum rooting depth for April (M)	Maximum rooting depth for August (M)	Roots tensile strength, σ_T (MPa)	Root Area Ratio (RAR)
Bush land (dense)	Hawthorn	0.8	0.8	8	0.0015
Bush land (sparse)	Hawthorn	0.8	0.8	8	0.0015
Wood land	Oak	1	1	13	0.005
Agriculture (dense)	Maize	0	0.4	5	0.001
Agriculture (sparse)	Maize	0	0.4	5	0.001
Plantation	Fir/ pine	1.5	1.5	28	0.0075
Forest	Fir/ pine	1.5	1.5	28	0.0075
Swamp	-	0	0	0	0

3.7.1.4 Soil properties

The soil map of Kenya (1980) shows distribution of soils across the country and it gives out information on soil depth, soil type, soil description and type of soil clay mixture. The soil map for the study area was clipped using ArcGIS tool and the other properties of soils that were required for this study but were lacking in the map, i.e. hydraulic conductivity, angle of friction, saturated unit weight, cohesion strength and porosity, were approximated from existing literature. The soil types identified and adopted for this study with their properties are as shown in Table 3. 4 below.

Table 3. 4: Soil properties table

Soil Parameter	Units	Soil type			
		Clay loam	Clay loam	Loam	Sandy loam
Soil description in soil map	-	Very clayey	Clayey	Loamy	Sandy
Angle of friction	(Degrees)	20	22	28	32
Hydraulic conductivity	(mm/hr)	2.6	2.6	10.4	44.2
Saturated unit weight	(KN/M ³)	19.73	19.73	19.41	19.73
porosity	-	0.41	0.41	0.43	0.41
Soil cohesion strength	(KN/M ²)	18	16	14	11
Void ratio	-	0.695	0.695	0.754	0.695

(Source: Pavement manual, 2007).

3.7.1.5 Soil depth

It is difficult to get soil depth information at every location exactly. In ArcGIS, Point interpolation performs interpolation on randomly distributed points and return into regularly distributed value using Kriging, spline, Trend and Inverse Distance Weighting (IDW) methods.

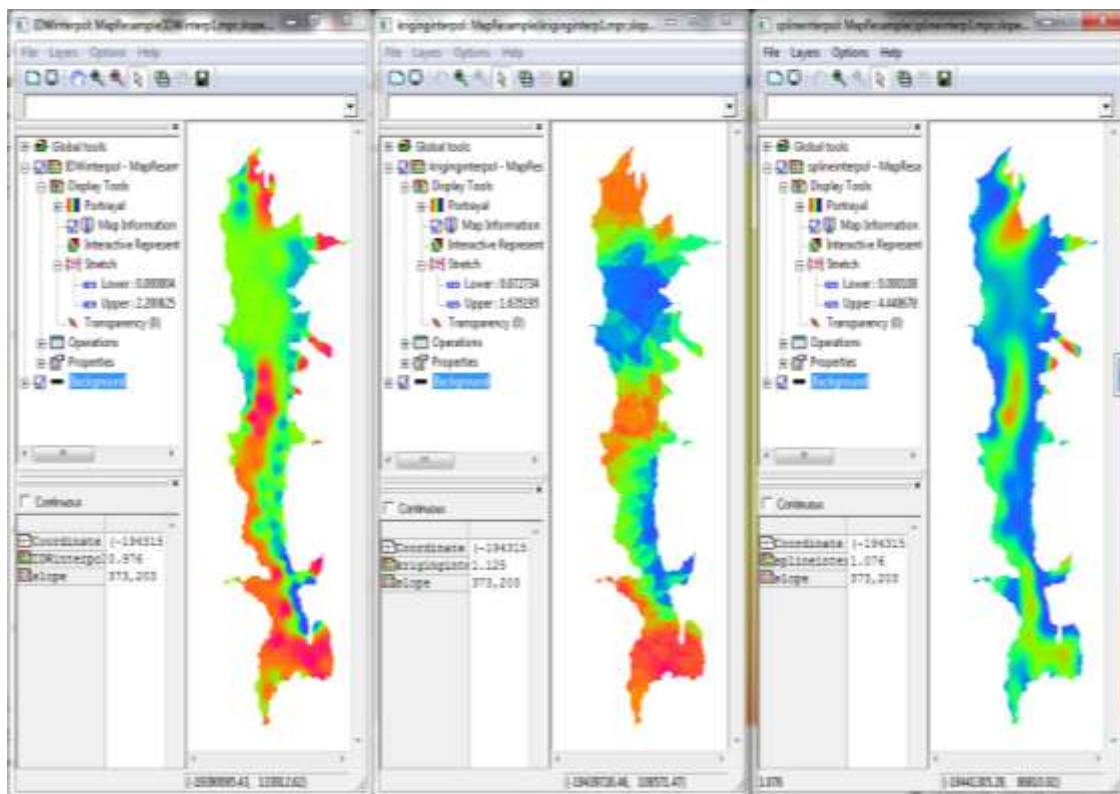


Figure 3. 13: Point interpolation results

The Inverse Distance Weighted (IDW), Trend and Spline methods are referred to as deterministic interpolation methods because they assign values to locations based on the surrounding measured values and on specified mathematical formulas that determine the smoothness of the resulting surface (ESRI, 2008). A second family of interpolation methods consists of geostatistical methods, such as kriging, that are based on statistical models that include autocorrelation (the statistical relationship among the measured points). Because of this, not only do geostatistical techniques have the capability of producing a prediction surface, but they also provide some measure of the certainty or accuracy of the predictions (ESRI, 2008). A point map was generated from the study area's soil depth polygon map using ILWIS GIS and then exported to ArcGIS tool for interpolation process. Kriging, spline and Inverse Distance Weighting (IDW) methods output maps were compared and the best results were then used in modelling. Figure 3. 13 shows results of the three interpolation methods.

IDW interpolation method produced soil depth map with maximum of 2.21m, Kriging interpolation method output map had a maximum depth of 1.65m while Spline interpolation method output map had a maximum of 4.44m. From soil map of Kenya the maximum depth for the study was 2.2m, tallying with the results from IDW method and thus this method's interpolation output map was adopted for modelling.

3.7.1.6 Classification of soil type and depth

Based on clipped soil map for the study area, soils were then classified as; clay loam, loam and sandy loam while the soil depths were classified as shown in Table 3. 5 below. The classification was adopted for soil moisture and water flow flux analysis.

Table 3. 5: Soil depth classification

Depth variation	Classified depth
Below 1 meters	1 meters
Depths between 1 and 1.5 meters	1.5 meter
Over 1.5 meters	2 meters

3.7.1.7 Matric suction parameters

Various researches that have been done established the ranges of parameters required for suction stress calculations (see equation 3.57) are shown in Table 3. 6.

Table 3. 6: Typical ranges of unsaturated soil parameters for various soils

Soil type	n	α (Kpa ⁻¹)	S_r (%)	k_s (m/s)
Sand	4 – 8.5	0.1 – 0.5	5 - 10	$10^{-2} - 10^{-5}$
Silt	2 – 4	0.01 – 0.1	8 - 15	$10^{-5} - 10^{-9}$
Clay	1.1 – 2.5	0.001 – 0.01	10 - 20	$10^{-9} - 10^{-13}$

(Source: Griffiths and Lu, 2005)

For this study, the adopted suction stress parameters are as shown in Table 3. 7;

Table 3. 7: Matric suction stress parameters

Soil type	n	θ_s	θ_r	α (KPa-1)	K_s (mm/hr)
Clay loam	2.2	0.41	0.095	0.01	2.6
Loam	3	0.43	0.078	0.05	10.4
Sandy loam	5	0.41	0.065	0.1	44.2

3.7.2 Formulation of ILWIS GIS Mapping Function

Mapping in ILWIS GIS requires formulation of mapping function, and was formulated using the generalized equation (3.63) The formulated function in ILWIS GIS model takes into consideration the spatial variability in land use, topographic variation, soil types and soil depths. Also the function is able to differentiate between the possible soil saturated conditions i.e.

1. Condition that soil is fully saturated
2. Condition that soil is partially saturated and
3. Condition that soil has composite saturation.

The temporal soil moisture conditions were obtained from HYDRUS 1D model for the instant of time that mapping is intended. For this study, (1) the observed rainfall for the

months of April and May was applied to HYDRUS 1D to simulate temporal soils parameters during calibration and (2) the stochastically generated rainfall for April and May rainfall was applied to HYDRUS 1D to simulate temporal soils parameters during scenario analysis. These parameters were then used in generation of slope stability (hazard) maps for any hour of the analysis period but mostly on the day when Ms-Excel infinite slope model display lower F_s value. To understand effects of rainfall on slope stability, more than one hazard maps were generated in the analysis period (April and May) for either observed or modelled rainfall pattern, and then comparison were undertaken to establish rate of increase or decrease of susceptible areas using the histograms that are automatically generated in ILWIS model.

3.7.2.1 Application of infinite slope equations in mapping equation

Infinite slope equation was applied depending on the nature of soil saturation, i.e.

1. Soil layer is fully saturated

For the case when whole of soil is fully saturated, then the factor of safety is calculated from the following equation since any point in a soil layer would have zero matric suction;

$$F_s = \frac{\tau_r}{\tau} = \frac{c_t + (\gamma_{sat} - \gamma_w) z_t \cos^2 \beta \tan \phi}{\gamma_{sat} z_t \cos \beta \sin \beta} \quad (3.64)$$

Where;

Z_t = depths of soil layer,

c_t = combination of soil cohesion strength, C_s and root cohesion strength, C_r

γ_{sat} = saturated unit weight of soil

γ_w = unit weight of water

ϕ = angle of friction

β = slope obliquity

2. Soil layer has composite saturation

Composite saturation arises from the fact that the layer of soil would not get saturated at the same instant of time. When it rains, it is usually the top section of soils layer that gets saturated before the lower section of soil layer.

Therefore the equation that would take into consideration the whole of composite scenario was formulated as;

$$F_s = \frac{c_t + \left[(\gamma_{sat}Z_1 + \gamma_2Z_2 + \gamma_3Z_3 - \gamma_w Z_w) \cos^2 \beta + \sigma_f^s \right] \tan \phi}{(\gamma_{sat}Z_1 + \gamma_2Z_2 + \gamma_3Z_3) \cos \beta \sin \beta} \quad (3.65)$$

Where;

Z_1 , Z_2 and Z_3 = thickness of sections adopted in a soil layer,

σ_f^s = suction stress at the failure plane (i.e. top of bedrock), if the lower section of soil layer is unsaturated else zero.

c_t = combination of soil cohesion strength, C_s and root cohesion strength, C_r

γ_{sat} = saturated unit weight of soil

γ_2 and γ_3 = partially saturated unit weight of sections of soil layer

γ_w = unit weight of water

Z_w = depth of water table

ϕ = angle of friction

β = slope obliquity

3. Soil layer is fully partially saturated

For the scenario that the soil layer does not have a section that is fully saturated, then ILWIS GIS model would calculate F_s using the equation below;

$$F_s = \frac{c_t + \left[(\gamma_1 Z_1 + \gamma_2 Z_2 + \gamma_3 Z_3) \cos^2 \beta + \sigma_f^s \right] \tan \phi}{(\gamma_1 Z_1 + \gamma_2 Z_2 + \gamma_3 Z_3) \cos \beta \sin \beta} \quad (3.66)$$

Where;

Z_1 , Z_2 and Z_3 = thickness of sections adopted in a soil layer,

c_t = combination of soil cohesion strength, C_s and root cohesion strength, C_r

σ_f^s = suctions stress at the failure plane (bedrock top)

γ_1 = partially saturated unit weight of top section of soil layer

γ_2 = partially saturated unit weight of middle section of soil layer

γ_3 = partially saturated unit weight of lower section of soil layer

ϕ = angle of friction

β = slope obliquity

3.7.2.2 Water table

The upper surface of ground water is the water table. Below this surface, all the pore spaces and cracks in sediments and rocks are completely filled (saturated) with water. These saturated layers, known as the saturated zone (or the phreatic zone), are where ground water occurs (http://www.indywatersolutions.com/index_files/Page911.htm).

In formulation of mapping equation care was taken to ensure that any development of water table during analysis period in the soil shall be taken into consideration by the model. To ensure this, water table in any of the soil section is defined as situation occurring in soil when water flow flux, q is equal to zero and soil moisture content is equal to soil porosity, η . Soil layer is fully saturated only when all monitoring nodes have q equal zero and soil moisture equals porosity. Water table reaches mid section only if the same condition applies also applies to the mid and lower soil sections'

monitoring nodes, else water table reaches only lower section of the soil layer if conditions applies only to lower section's monitoring node.

3.7.2.3 Formulated ILWIS GIS mapping functions

The core mapping functions that were implemented in ILWIS GIS model based on conditions that have been described in section 3.7.2.1 and 3.7.2.2 are;

- 1) Root cohesion strength function (C_r), as shown in *appendix A (i)*
- 2) Factor of safety (Mapping) function (F_s), as shown in *appendix A (ii)*.

The temporal (dynamic) parameters required by the mapping functions to run are as shown in the *appendix A (iii)* and were obtained from HYDRUS 1D model, and were converted and arranged into ILWIS GIS input sequence using formulated Ms-EXCEL model. Apart from temporal parameters, other non dynamic parameters required for mapping were obtained from soil and land use map, and were converted into raster maps. These maps are listed in *appendix A (iv)*.

3.8 FORMULATION OF LANDSLIDE PREDICTION MODEL (LPM)

Integration of models and equations relating to rainfall generation (Markov and Event based model), soil moisture redistribution (HYDRUS 1D model) and slope stability assessment (infinite slope model) resulted in the formation of Landslide Prediction Model (LPM). Some assumptions have been made while LPM was being formulated and integrated, and these assumptions would affect the modelled results in one way or the other. The assumptions made are;

- i. Time for the start of rainfall in any rainy day is assumed to be the same.
- ii. Initial water content in all soils was assumed as $0.2 \text{ M}^3/\text{M}^3$ on 1st April.
- iii. Rainfall depth per event follows the Gamma distribution; equation (3.44)
- iv. Water table is a function of soil moisture and water flow flux.

- v. The soil moisture in soil is monitored using three nodes in the central points of the assumed three sections of a soil layer (see Figure 3. 7)

The integration of events, models and equations into LPM for use in the predicting slope instability as a consequence of rainfall occurrence is discussed as follows;

- a) Historical and Areal rainfalls are analyzed by method of counting to establish their descriptive characteristics (i.e. number and duration of events, duration of inter-events and rainsum of events). The rainsum of rainfall events that previously caused historical landslides would act as the threshold of rainfall amount to input into LPM for scenario analysis in landslide vulnerability assessment.
- b) Descriptive characteristics of historical and areal rainfall data are fitted into distributions PDF, best describing them. Number of events is fitted to Poisson distribution as in equation (3.3), duration of events is fitted to Geometric distribution as in equation (3.4), duration of inter-events is fitted to Geometric distribution as in equation (3.4) and daily rainfall depths is fitted to Gamma distribution as in equation (3.5). The cumulative PDF of each fit is also derived.
- c) Stochastic rainfall generating models are formulated using algorithm in section 3.3.4.2 for Markov models or algorithm in section 3.3.5.2 for event based model. Since rainfall occurrence is a stochastic event, models will have to be run several times to establish a variety of possible rainfall patterns meeting landslide triggering threshold in the study area. The generated rainfall is analyzed for variation with historical rainfall having amount nearly equal to the generated rainfall using ANOVA (single factor) and Student t-test. If limits of these tests are violated, then the generated rainfall is ignored and new set generated. Also the derived rainfall patterns are analyzed to establish their

descriptive characteristics. Rainfall pattern with higher amount or longer than threshold/mean length of events would be considered for analysis. Figure 3. 14 is the flow chart illustrating event based stochastic rainfall generation method.

- d) The evapotranspiration data is using ETo calculator model to establish mean daily evapotranspiration which is then be assigned to each day. The evapotranspiration value would act as the limiting (threshold) for daily rainfall amount to be considered as event in any of the models in LPM since any rainfall amount less than this value will be evaporated back to atmosphere without causing changes to the soil moisture.
- e) Redistribution of soil moisture and water flow flux is undertaken in HYDRUS 1D model (Richards's equation). The model is configured to simulate moisture conditions of a soil layer using four monitoring nodes (see Figure 3. 7).
- f) The positive or negative pore water pressure affect slope soil normal stress either by increasing or decreasing it and therefore methods of accurately determining its value should be applied. The MSA model will strive to undertake this by first determining the magnitude of Matric suction at the failure plane using equation (3.53). Equation (3.57) is then applied to determine suction stress at the same plane and Figure 3. 15 is the flow chart of formulating MSA model.
- g) Infinite slope model is applied in assessing the stability of slopes at any time. The slope failure occurs when the soils are fully saturated to the critical depth or when soil shear stress exceeds soil shear strength. Equation (3.60) and is applied in determining the critical depth for parallel seepage flow conditions. Modified infinite slope model function is formulated in ILWIS GIS (for use in assessing spatial distribution of slope instability) and in Ms-EXCEL formulated

model (for use in sensitivity analysis, calibration and establishment of critical mapping day) using equation (3.62). The flow chart of formulating modified infinite slope model in Ms-EXCEL and in ILWIS GIS is Figure 3. 16. Some of the conditions that have to be taken into consideration by infinite slope model include;

- a. Situation when soils are fully saturated, and
- b. Condition when soil is partially saturated.

3.9 MODELS FORMUALTION ALGORITHMS

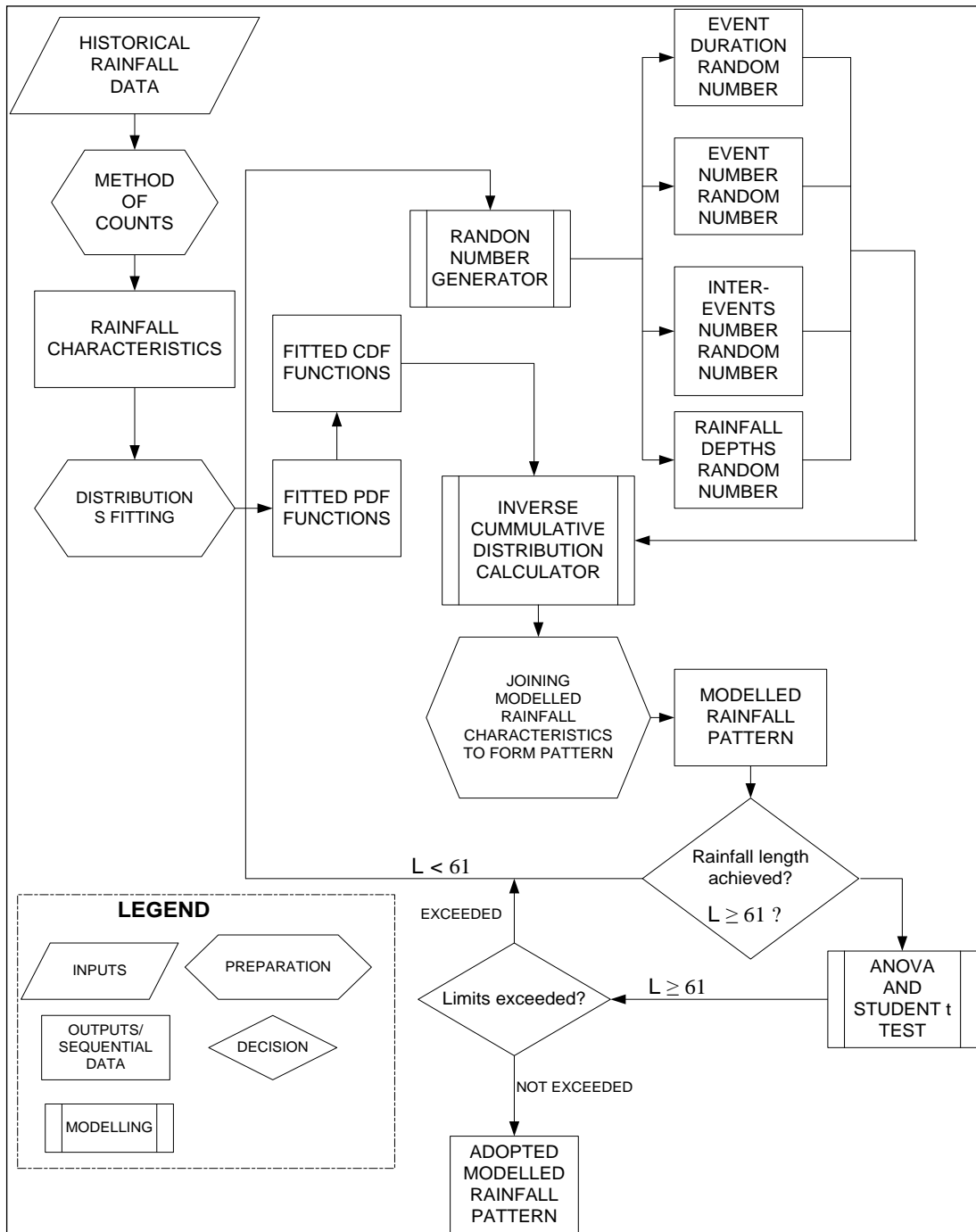


Figure 3. 14: flow chart for Event based stochastic rainfall generator

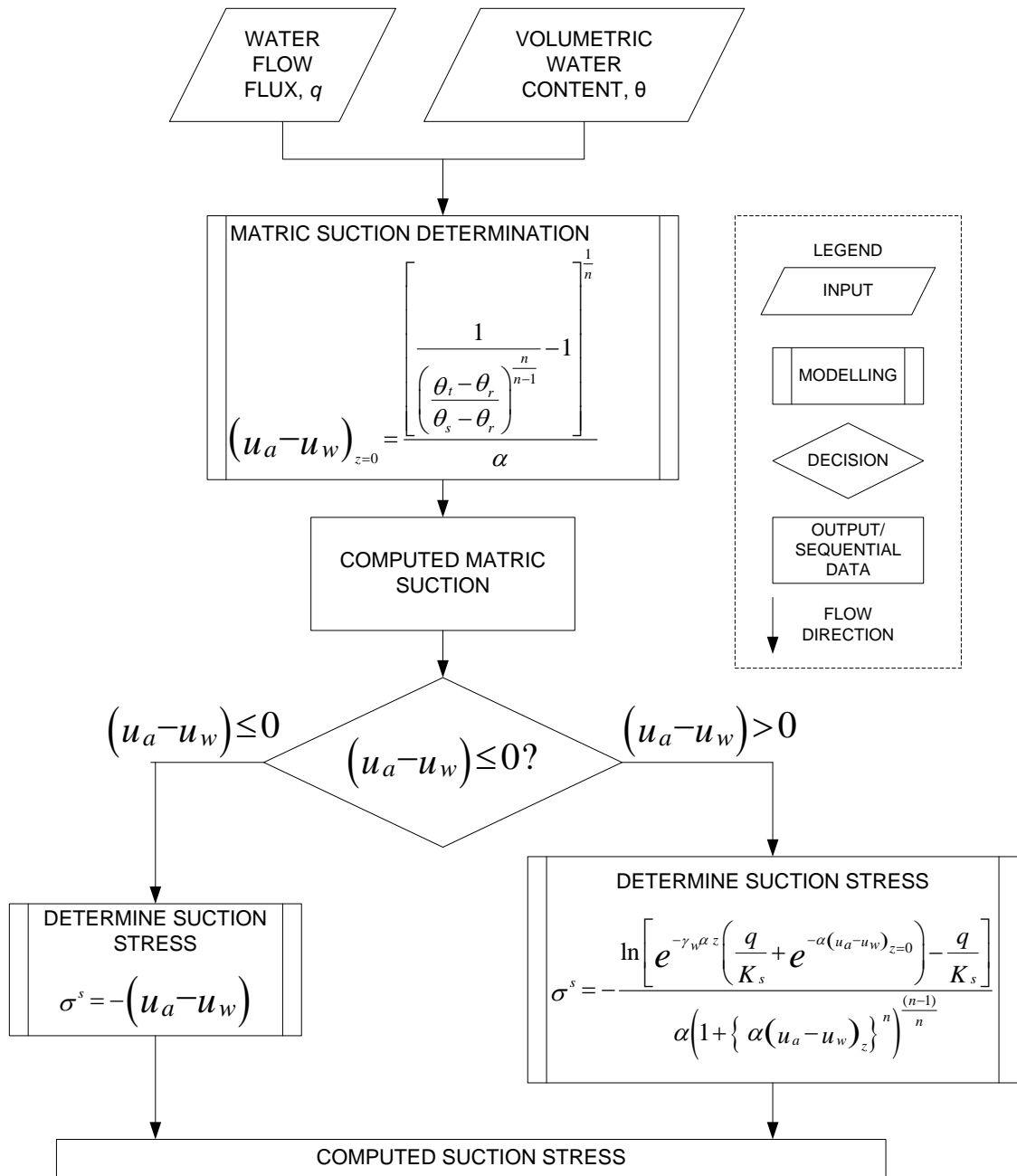


Figure 3. 15: Flow chart of Suction stress analysis (MSA) model

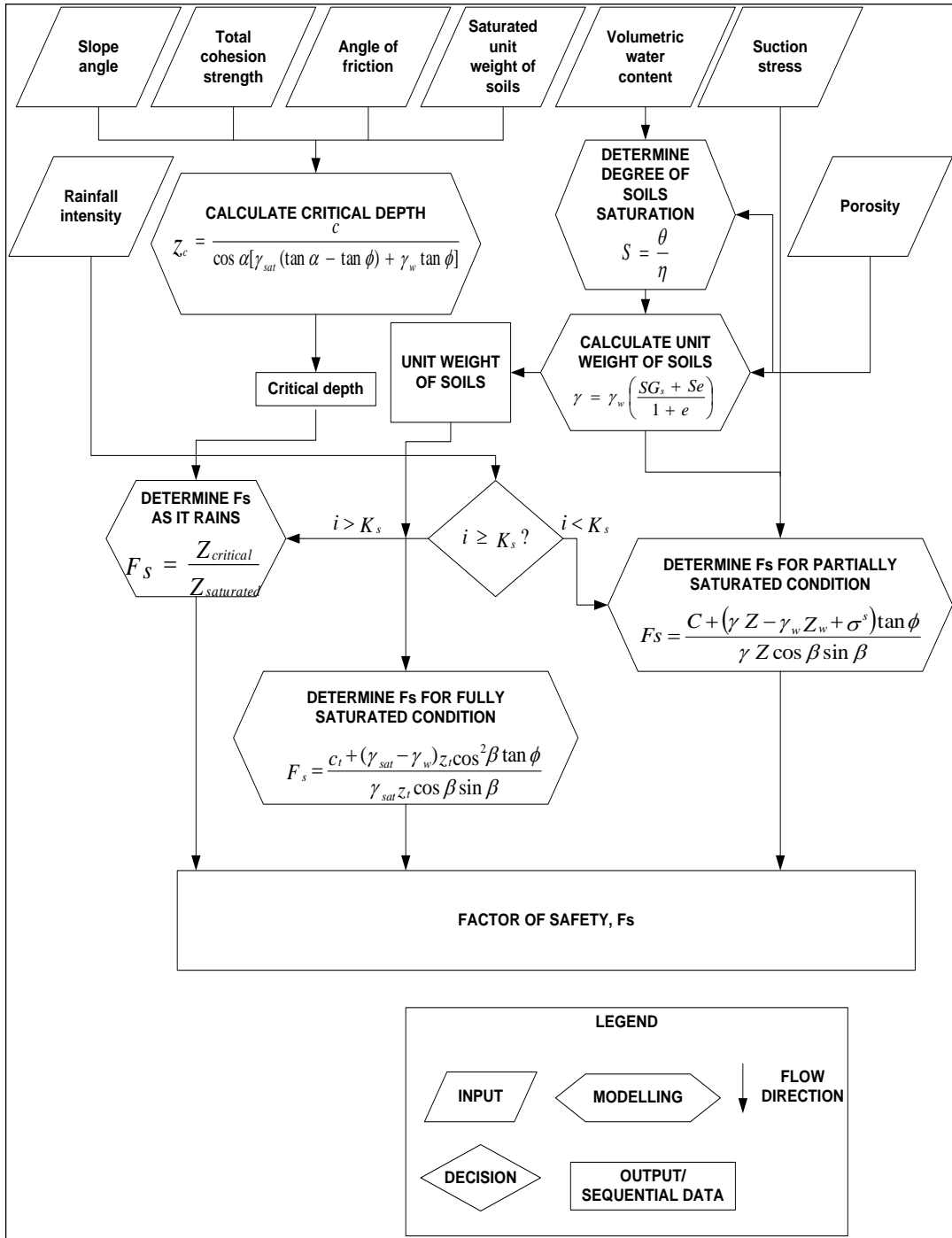


Figure 3. 16: Flow chart of modified infinite slope stability model

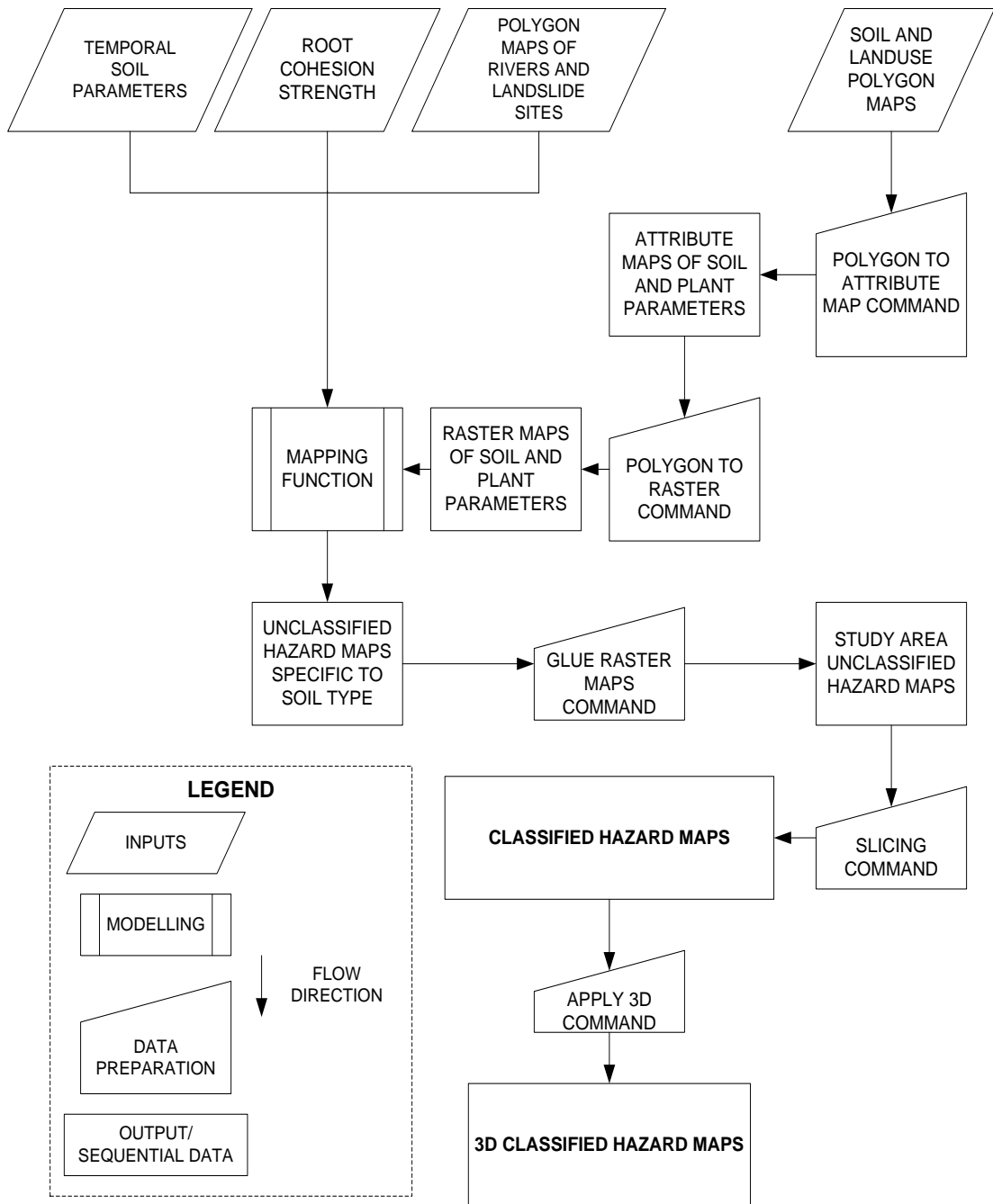


Figure 3. 17: Flow chart of spatial mapping in ILWIS GIS Tool

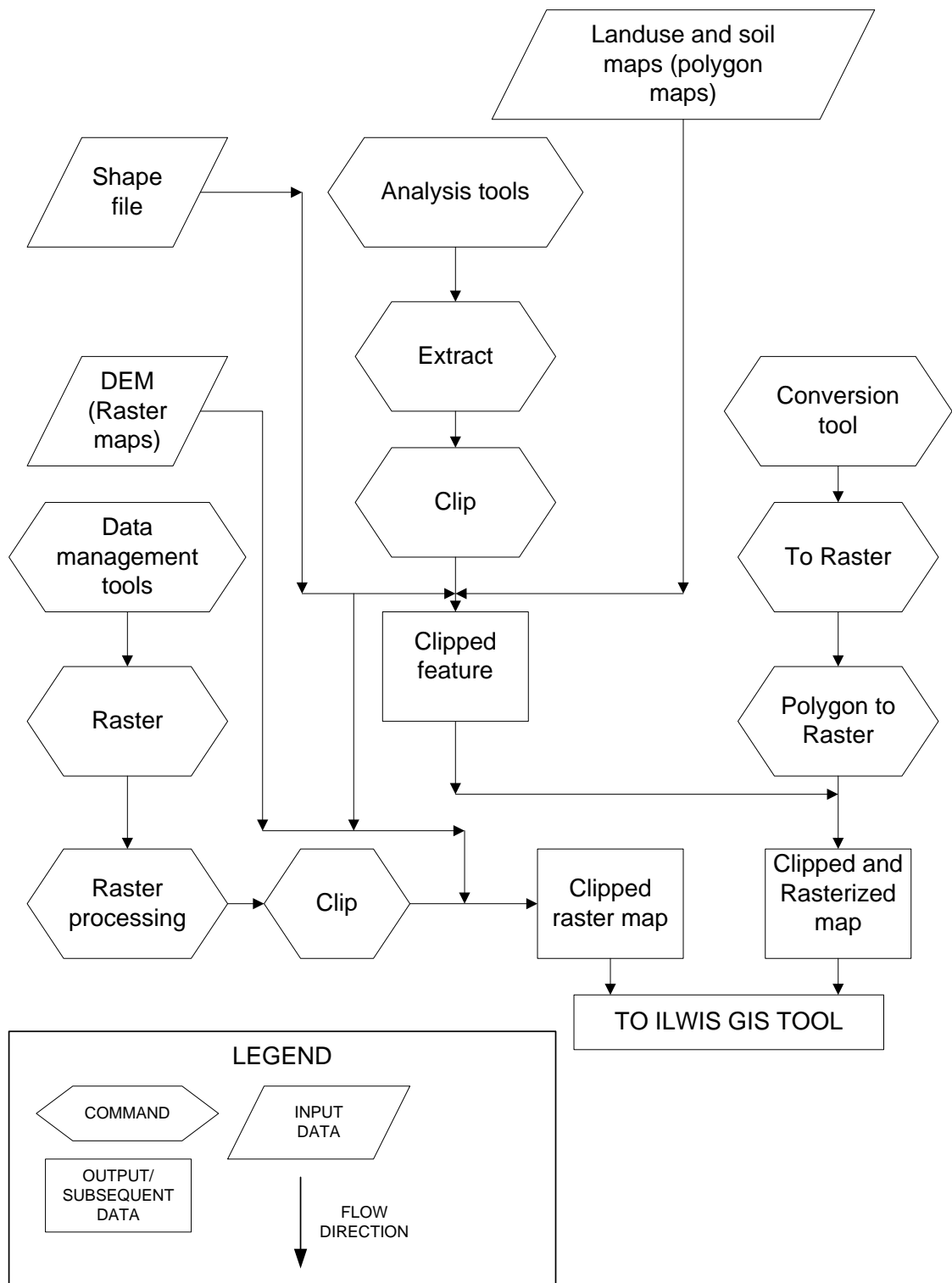


Figure 3. 18: Flow chart of extracting and clipping maps using GIS

3.10 MODELLING STEPS

1. Establish the thresholds for rainfall causing landslides by analyzing the rainfall that previously caused landslide to establish number and duration of spells, cumulative rainfall amount and duration of inter-events for months of April and May.
2. Establish the geotechnical properties of soil, land use, nature of topography and geographic coordinates for the previous landslide occurrence site.
3. Input the rainfall data that previously caused landslide into HYDRUS 1D model and running it to establish corresponding soil moisture content.
4. Input modelled soil moisture content from HYDRUS 1D, geotechnical and morphological properties of previous landslide site (Mokwo) into the Ms-EXCEL Landslide prediction model and running it to establish if it does indicate the failure of slope at that point of time when landslide occurred. If it does not, then the model is calibrated by inputting numerical constants.
5. A spatial mapping can then be implemented in ILWIS GIS software using calibrated mapping function and checking to establish if the coordinates of modelled unstable regions corresponds to those of historical landslide occurrence areas.
6. Having calibrated the Ms-Excel LPM in step (d) and ILWIS GIS mapping function in step (e), the methodology can then be used to evaluate the sensitivity of slope stability to land use changes and wet spell persistence as follows;
7. The sensitivity of slopes to land use changes, i.e. the land use in the area is assumed to have been completely shifted to forest (pine or fir plantation) or agriculture (maize farming) and using the areal rainfall to assess stability of

slope using steps 4 and 5 above and comparing percentages of unstable areas to establish which land use scenario causes more of unstable areas.

8. The sensitivity of slopes to wet spell variables can be achieved by generating various rainfall patterns with the rainsums equal or greater than those that previously caused landslide using rainfall generating models. The skewed and evenly distributed rainfall patterns are adopted for analysis and are inputted in HYDRUS 1D model and run to establish temporal properties of soils for use in spatial slope stability assessment using ILWIS GIS software. Spatial mapping is implemented in ILWIS GIS for the both rainfall distribution cases using the temporal soil properties values from the calibrated LPM and percentage of unstable area are compared to establish which rainfall pattern causes more of unstable areas.

The flow chart of Landslide Prediction Model (LPM) is shown in Figure 3. 19.

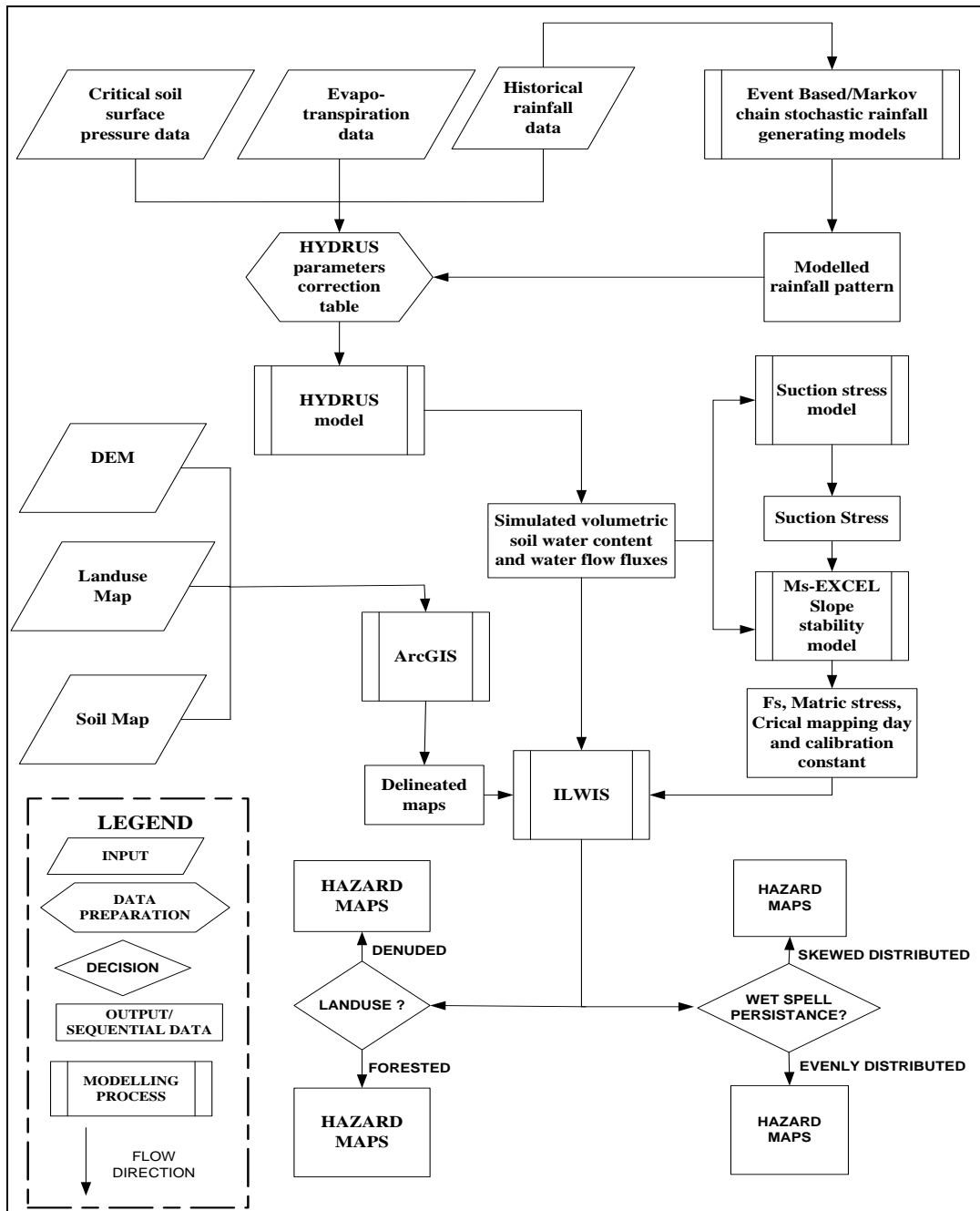


Figure 3. 19: Summary flow chart of Landslide Prediction Model, LPM

CHAPTER FOUR: RESULTS AND DISCUSSIONS

4.1 INTRODUCTION

This chapter presents analysis and interpretation of results for various variables that affect stability of slopes. The variables that were analyzed in this study include; rainfall (Areal rainfall derivation and stochastic rainfall generation), soil moisture (infiltration and percolation), suction stress, pore water pressure and slope stability (factor of safety analysis).

4.2 GENERATION AND ANALYSIS OF SPATIAL RAINFALL

4.2.1 Analysis of Rainfall Data

This involves the process of filling of gaps (see section 3.3.2) and generation of Areal rainfall (see section 3.3.4).

Before data from western stretch rainfall stations were used in derivation of Thiessen polygons and areal rainfall, they were analyzed to establish deviation in the mean annual rainfall totals. Table 4. 1 below shows the mean annual rainfall for the rainfall stations along the highlands of western stretch of Kerio escarpment and it was established that the mean annual rainfall varies from 1061mm for HYDROID 8935108 to 1484mm for HYDROID 8935184 with standard deviation of 106mm. This deviation is not so much coupled with fact HYDROID 8935108 is in proximity with other stations which resulted in being assigned smaller weight and thereby not affecting much the anticipated Areal rainfall. Therefore all rainfall data from 15 stations were used in derivation of Areal rainfall using Thiessen polygons method.

Table 4. 1: Mean annual rainfall for Thiessen polygons

S/n	Station name	Hydroid	Latitude (degrees)	Longitude (degrees)	Mean annual rainfall (mm)
1	Tambach - labot	8835035	1.066667	35.41667	1252.9
2	Chebororwa FTC	8935002	0.983333	35.55	1293.6
3	Tambach –gov school	8935047	0.937	35.5252	1245.4
4	-	8935220	0.983333	35.56667	1272.2
5	Tambach - chebiemi	8935014	0.92	35.5217	1259.1
6	Marakwet africa	8935104	0.866667	35.5	1119.9
7	Moiben kenley	8935108	0.8	35.43333	1061.8
8	Moiben karuna farm	8935106	0.716667	35.51667	1285.3
9	Elgeyo - forest	8935222	0.7	35.5	1270.5
10	Tambach DO	8935134	0.65	35.51667	1315.3
11	-	8935184	0.466667	35.55	1484.6
12	Kaptagat forest	8935010	0.433333	35.5	1256.3
13	Kaptagat Nvita estate	8935175	0.416667	35.48333	1449.2
14	Tambach chepkorio	8935131	0.366667	35.55	1413.3
15	Eldoret skyline	8935121	0.166667	35.55	1275.3

ArcGIS tool provides a method of deriving Thiessen polygons. The derived Thiessen polygons are as shown in Figure 4. 1 and the area of each polygon are shown in Table 4. 2. The Thiessen polygon method assumes that each precipitation gauge does not get the same weight. The influence of rainfall station on the study area is derived from station weight which is the ratio of station Thiessen polygon to the total area of study area. The weights are multiplied with the respective rainfall amount of the station using equation (3.2).

Table 4. 2: Rainfall station and their weights as used in areal rainfall generation

S/n	Hydroid	Station name	Annual mean (mm)	Polygon area (m ²)	Weights
1	8835035	Tambach - labot	1252.91	973663594.4	0.282
2	8935002	Chebororwa FTC	1293.576	109281817.3	0.032
3	8935047	Tambach – gov school	1245.377	49316368.47	0.007
4	8935220	-	1272.222	608369665.417	0.025
5	8935014	Tambach - chebiemi	1259.132	85516133.472	0.014
6	8935104	Marakwet africa	1119.853	161695088.4	0.047
7	8935108	Moiben kenley	1061.805	52770830.35	0.062
8	8935106	Moiben karuna farm	1285.34	212377086.743	0.015
9	8935222	Elgeyo - forest	1270.457	45380239.525	0.103
10	8935134	Tambach DO	1315.272	191700304.2	0.085
11	8935184	-	1484.581	268268836	0.056
12	8935010	Kaptagat forest	1256.341	22503133.22	0.007
13	8935175	Kaptagat Nvita estate	1449.221	23102379.97	0.078
14	8935131	Tambach chepkorio	1413.296	291824590	0.176
15	8935121	Eldoret skyline	1275.348	356031552.2	0.013
TOTAL				3451801620	1

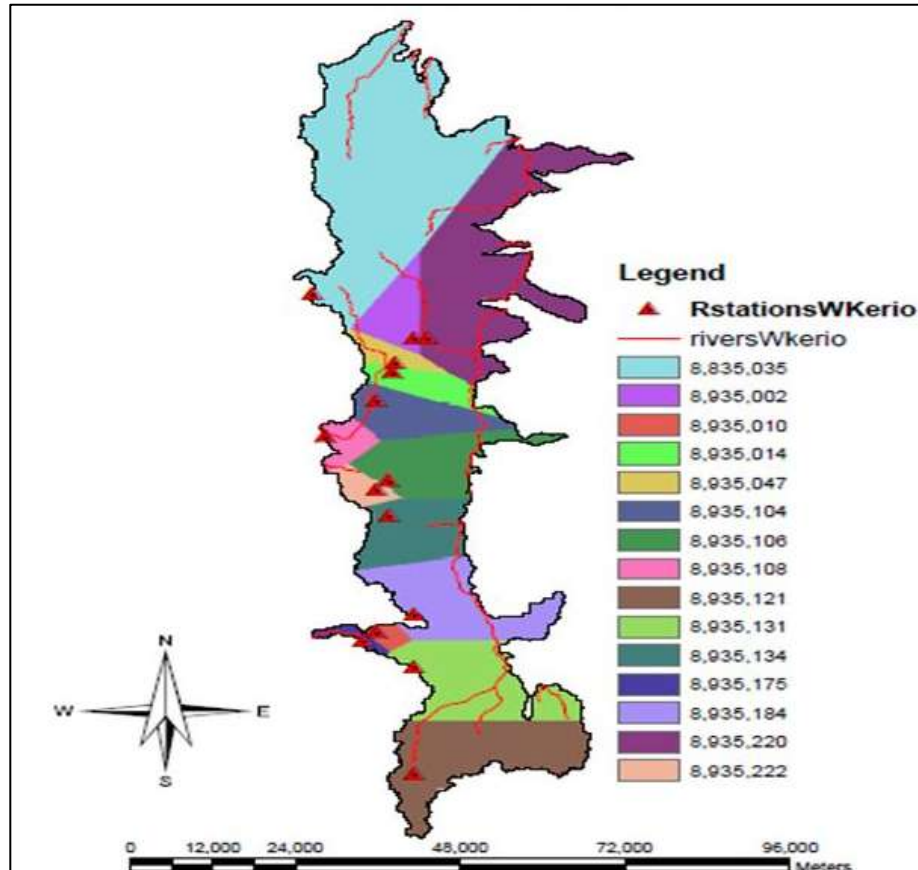


Figure 4. 1: Thiessen polygon for calculating areal rainfall

4.3 SIMULATING LANDSLIDE OCCURRENCE IN MOKWO AREA

The formulated model was used to simulate the occurrence of a landslide that occurred on 29th April 2007 at the escarpment near Mokwo. Figure 4. 2 shows location of Mokwo and Tot landslide occurrence sites in the study area.

Mokwo area has loam soil of an average thickness of about 1.5m and the major type of land use activity in the area is dense agriculture as per Kenya soil map and land use map respectively. The landslide occurrence site in the area is sloping at an angle of 40 degrees as per generated slope map. The rainfall data for HYDROID 8935184 rainfall station was used for simulation as was the nearest meteorological station to the landslide occurrence site and the results are as discussed below.

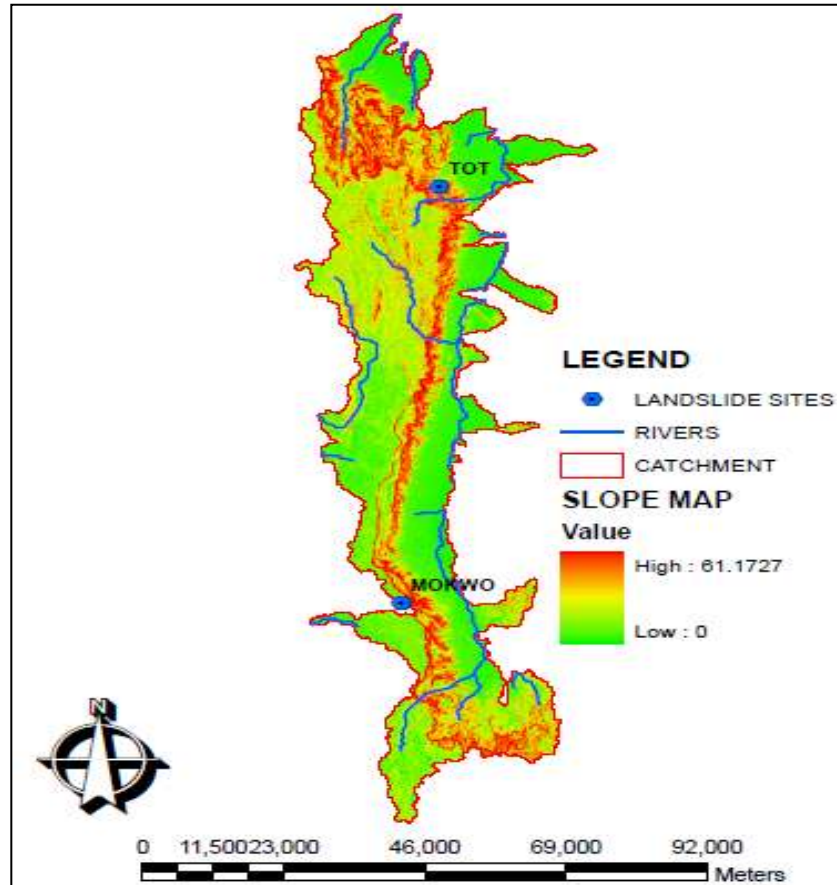


Figure 4. 2: Some of historical landslide occurrence sites in study area

4.3.1 Soil Moisture Redistribution and Water Flow Flux

The states of water flow flux, q and soil moisture content, θ at any time of analysis period were analyzed using HYDRUS -1D model. Redistribution of soil moisture depends majorly on hydraulic conductivity of soils. High hydraulic conductivity, K , in soils would results in higher rate of infiltration and percolation leading to development of water tables in soils and low surface runoffs, while low hydraulic conductivity of the soils would discourage infiltration of rain water into soil thus leading to high surface runoff. As the soil moisture redistribution is a function of soil type and depths, then the formulated infinite slope function for mapping, should take into consideration the spatial variability of these soil parameters.

April-May 2007 rainfall data for HYDROID 8935184 station was applied in HYDRUS 1D model. The results in Figure 4. 3 are the volumetric water content for loam soil layer with thickness of 1.5m.

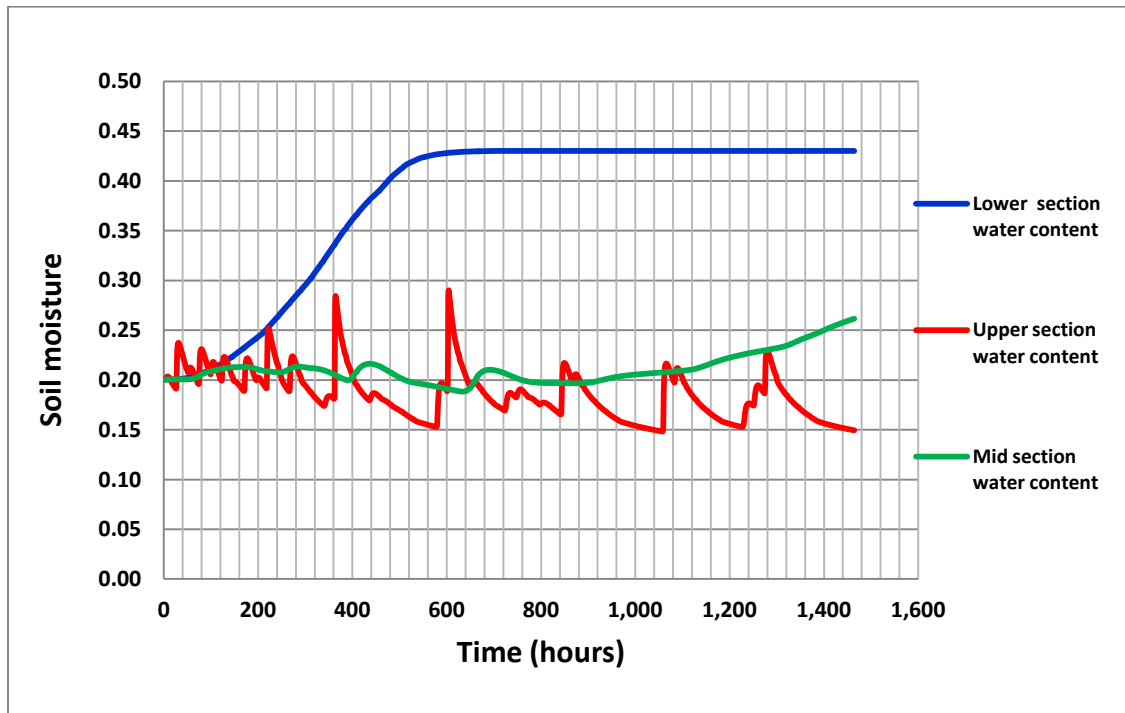


Figure 4. 3: Soil water redistribution curve for loam with soil thickness of 1.5 m

4.3.2 Suction Stress Analysis:

During periods of intense rainfall, positive pore water pressure tends to persist in soils and thus contributes to decrease in effective stress as it is compressive in nature and is illustrated by the equation (4.1) below thus inducing landslides;

$$\sigma'_n = \sigma_n - u_w \quad (4.1)$$

Where;

u_w is pore water pressure.

Negative pore water pressure is tensional in nature and exists in unsaturated soils and contributes to soil strength. Lu and Likos (2004, 2006), formulation was adopted in determining suction stress as a function of slope saturation by rain water. This formulation is used for determining suction stress in unsaturated soils on the condition

that water table is the lower boundary condition. Saturation levels in soils is highly variable and so to be able to determine suction stress for any soil saturation level, Lu and Likos (2004, 2006) formulation had to be modified to apply for general conditions (see equation 3.57).

Figure 4. 4 shows modelled suction stress results obtained from Ms-EXCEL infinite slope model for the nodes where soil moisture was being analyzed. In spatial mapping and factor of safety analysis only suction stress results for top of bedrock was used since failure plane in this study was assumed to coincide with the point of contact between soil layer and the hard stratum (rock).

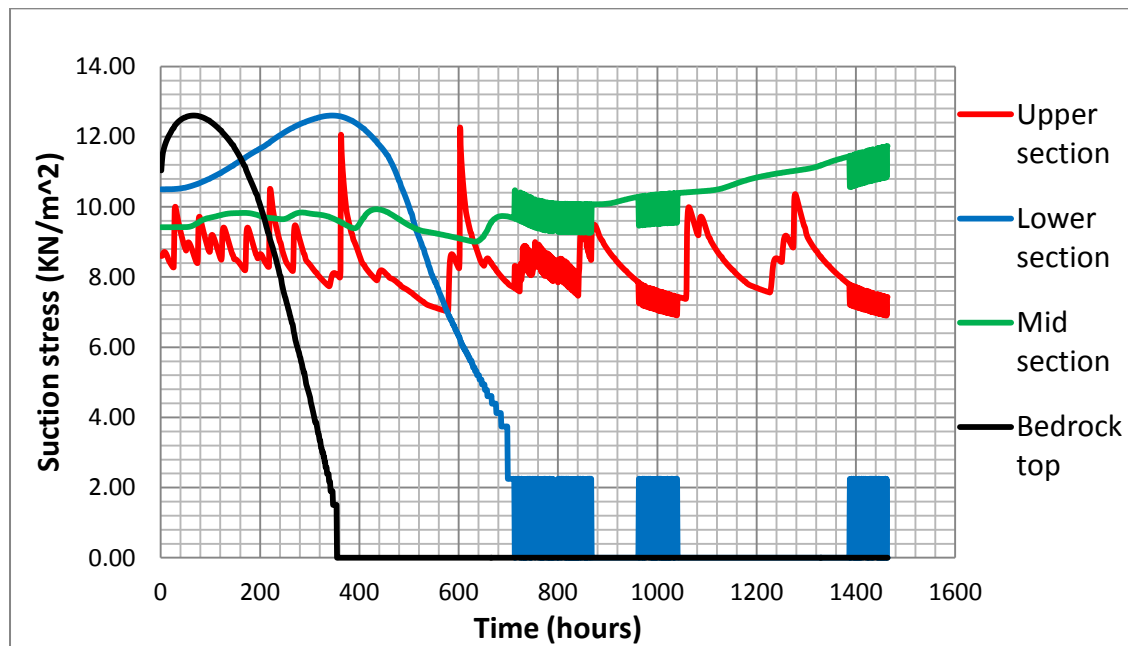


Figure 4. 4: Variation of suction stress for loam soil of depth 1.5m

4.3.3 Sensitivity Analysis and Model Correction

Variation of factor of safety with time during analysis period in this study was undertaken using formulated Ms-EXCEL infinite slope model and Figure 4. 5 shows the modelled results.

The modelled factor of safety results for 29th April (time around 700 hours) is overstated as it was above critical value of 1. This may have been caused by;

1. Overestimated angle of friction
2. Underestimated slope angle
3. Underestimated depth
4. Overestimated cohesion

This calls for correction of factor of safety in slope stability and spatial mapping models. Sensitivity analysis was conducted using HYDRUS model and Ms-EXCEL slope stability model to establish parameters influencing stability of slope. This was undertaken by varying either of parameters while holding the values of others constant until factor of safety for 29th April (700 hrs) indicates failure ($F_s < 1$), and Table 4. 3 shows some of sensitivity analysis results.

Table 4. 3: Sensitivity of model to parameter change

Parameter name	Parameter Value adopted	Increasing parameter value by 25%	Fs	Decreasing parameter value by 25%	Fs
Angle of friction	28	35	1.9	21	1.6
Soil cohesion	16	20	2.0	12	1.4
Soil depth	1.5	1.88	1.4	1.13	2.2
Slope angle	40	50	1.55	30	2.0

It was established that the slope failure could not occur after variation of slope angle and angle of friction within the possible ranges, though they had effect on slope stability, but for soil depth and cohesion strength, the failure occurred when variation reaches values of 3.5m and 6kPa respectively.

Since all the parameters had an effect on state of slope stability, we choose to calibrate the model by multiplying formulated factor of safety function with a constant that could force the model to indicate failure on 29th April and numerical constant 0.55 gave the anticipated results. Figure 4. 6 shows the calibrated results.

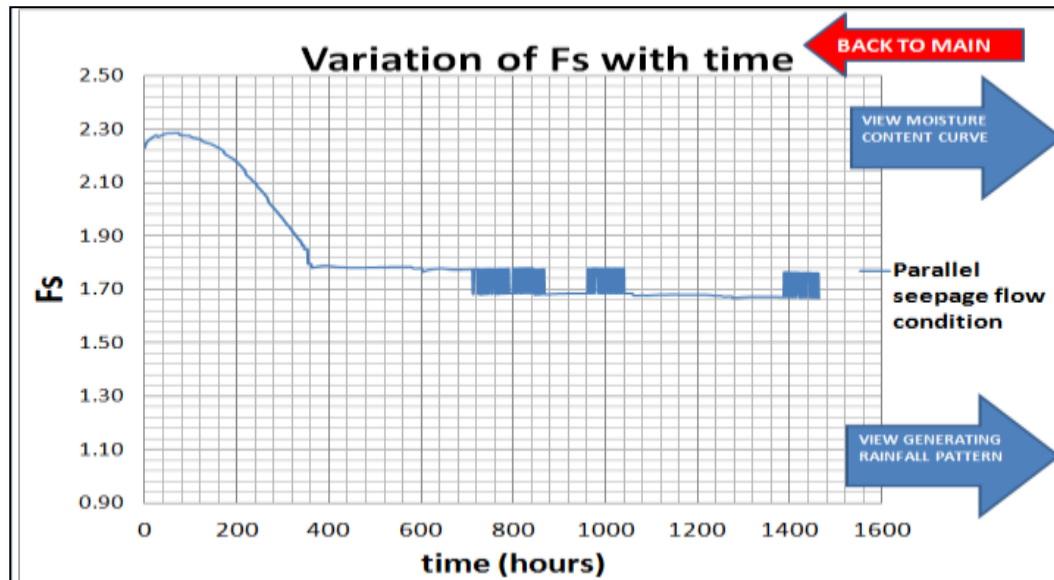


Figure 4. 5: Variation of F_s for loam soil of slope 40 degrees and depth of 1.5 m.

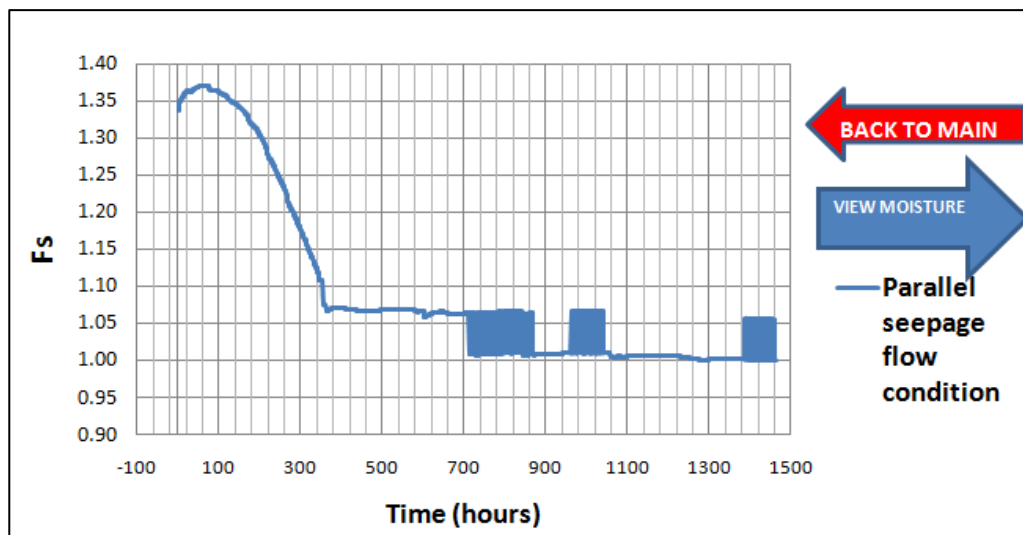


Figure 4. 6: Calibrated variation of F_s with time for soils in Mokwo area

4.3.4 Spatial Mapping Using ILWIS GIS MODEL

The calibrating factor of 0.55 in section 4.3.3 were then multiplied to the formulated mapping function and used in generation of the hazard maps. Figure 4.7 shows hazard map for the Mokwo area as on 29th April 2007.

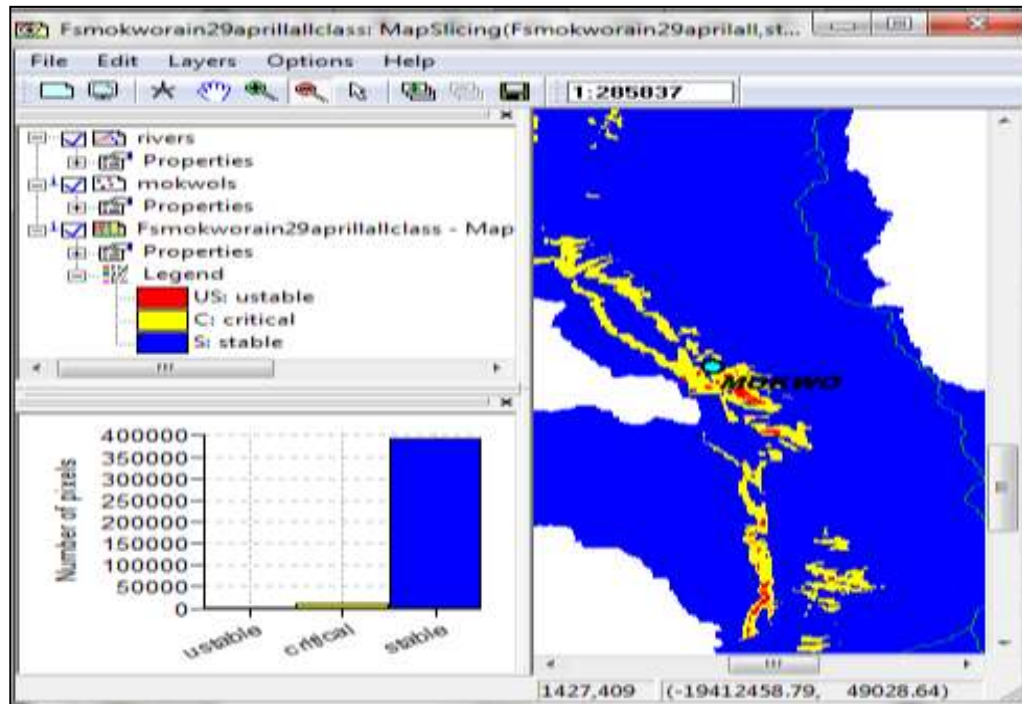


Figure 4.7: Hazard map for Mokwo area as on 29th April 2007.

4.3.5 Discussion

As discussed in section 2.2.4, rainfall has been considered to be the main cause of the majority of landslides. Landslides are triggered when either a critical pore water pressure threshold is being exceeded (Corominas and Moya, 1999) or as a result of the increased weight of the saturated soil (e.g. Van Asch and Sukmantalya, 1993). The mechanism that leads to slope failures is the matric suction (i.e. *negative pore water pressures*) that starts to decrease when water begins to infiltrate the unsaturated soil (Yeh et al., 2004). The loss of matric suction decreases the shear strength of the soil below the mobilized shear strength along the potential slip surface.

Figure 4. 3 shows that the top section of soil losses saturation faster than the other sections of a soil layer. This is because top sections are exposed directly to climatic factors such as wind and sun which activates higher rates of evapotranspiration. It was also established that during rainfall season, water would tend to build up at the lower section of soils layer since the bedrock do not allow further percolation of soil water.

Between 0-600hours for Figure 4. 3, no section of the soil is fully saturated, but beyond 700hrs, the lower section of the soil layer is saturated with water as can be attested with volumetric water content, θ of 0.43.

From Figure 4. 4, it is clear that for the same soil type, suction stress can be different in various depths. Also it was established that suction stress tends towards zero during moments of high saturation and suction stress only exists in soil section as long as soil it is unsaturated. The upper section of soil layer was sensitive to changes in spells contrasting the nearly constant values of zero in lower section's suction stress.

Between 0-500 hrs, the suction stress at the bedrock top of soil layer is declining. This is due to increasing saturation of soil at the section and beyond 500 hours, the bedrock top is fully saturated, implying that the suction stress is lost. The lower section is fully saturated at around 700 hours, but because of fewer divisions (3 sections applied in study; see Figure 3. 7) and definitions of water table (see section 3.7.2.2) used in this study, the curve is seen to be hopping at around 800, 1000 and 1400 hours. This occurs when a node of a fully saturated section of soil suddenly registers $q \neq 0$ or $\theta \neq \eta$.

The high F_s values in Figure 4. 5 are attributed to the adopted high values of soil parameter (cohesion and angle of friction) and underestimation of soil depth. It can be established from the Figure 4.7 that the calibrated model indicates that the area around Mokwo had places that were unstable and includes the site that experienced failure on

29th April 2007. Thus the formulated model can then be used to predict occurrence of landslide given that a rainfall pattern is known.

4.4 SCENARIO ANALYSIS FOR SLOPE STABILITY ASSESSMENT

Scenario analysis enables the answering of ‘what if’ questions in an integrated system of soil water movement and instability of slopes. The objective of simulating historical landslide first was to establish effectiveness of the formulated model in simulating dynamics of sub surface water movement *vis a vis* consequent slope instabilities. Two scenarios were analyzed in this study in order to understand landslides triggering conditions, and were;

- a) Evaluating effects of wet spell persistence on slope stability
- b) Evaluating sensitivity of slope stability to land use changes

Occurrence of a Landslide more often coincides at that point in time when there is high persistence of heavy wet spells and at a point in space where topography have been heavily modified by anthropogenic activities that are detrimental to future stability of slopes, (e.g. deforestation and practicing agriculture activities on sloppy piece of land).

4.4.1 Evaluating Effects of Wet Spell Persistence on Slope Stability

Rainfall occurrence is a stochastic event which may occur either as an evenly distributed or as skewed distributed over analysis period. Landslide occurrences do coincide with the period of high persistence of heavy wet spells (large rainsum wet spells). In this study, an attempt was made to simulate the effect of nature of rainfall amount distribution on the stability of slopes.

Rainfall patterns having nearly the same rainsums as the rains that caused historical landslides were generated from derived Areal rainfall data using either Markov or event based stochastic rainfall generating models. The generated rainfall patterns were

analyzed to establish their characteristics; i.e. number of rainy and dry days, rainsums and the occurrence distribution (skewed or evenly distributed across analysis period). Skewed and evenly distributed rainfall patterns were adopted for this analysis and was each inputted into HYDRUS 1D Model and run to establish temporal soil parameters for the analysis period. The derived temporal soil moisture parameters were then applied in ILWIS GIS software for generation of spatial slope instability map (hazard map) specific to randomly chosen days in analysis period.

4.4.1.1. Fitting rainfall characteristics to distributions functions

As described in section 3.2.2, rainfall characteristics have to be fitted to statistical distribution best describing them in order to allow for stochastic generation of rainfall patterns. The fitting parameters used in various distributions are as shown in Table 4. 4;

Table 4. 4: Distributions fitting parameters

DISTRIBUTION	CHARACTERISTIC	α	β	p	q	mean
Poisson distribution	Number of events					4
Gamma distribution	Rainfall depths	3.5	0.6			
Weibull distribution	Rainfall depths	2.4	2.5			
Geometric distribution	Inter-events			0.31	0.69	3.23
Geometric distribution	Events duration			0.18	0.82	5.48

The graphical results for distribution fitting are as shown in Figure 4.8 (1), (2), (3) (4) (5) (6) (7) and (8).

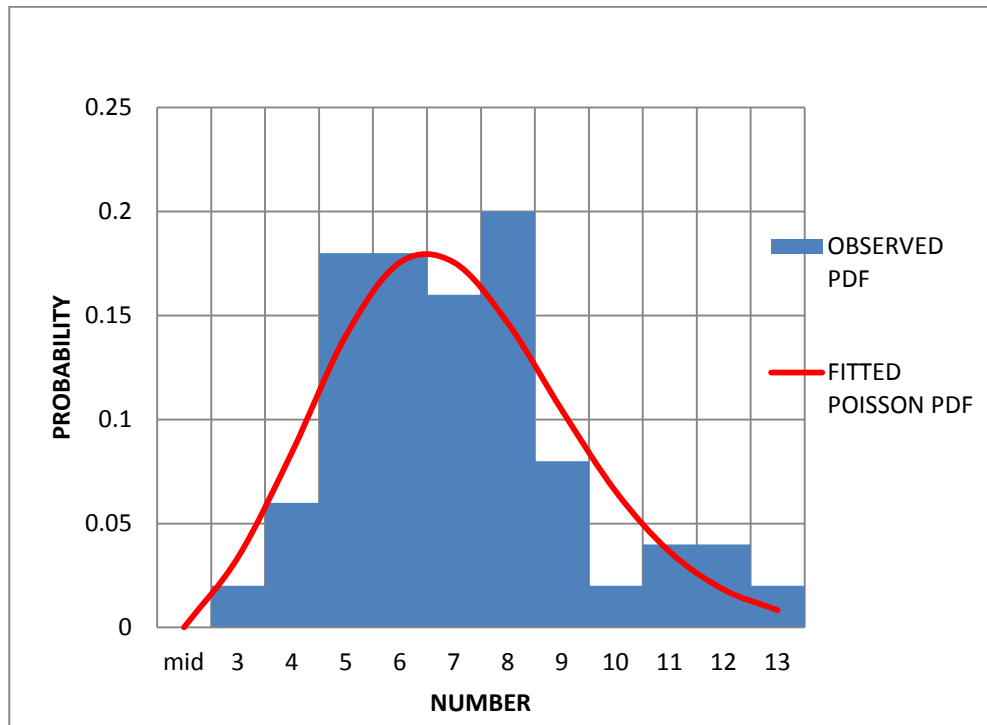


Figure 4.8 (1): Fitting events to Poisson PDF distribution

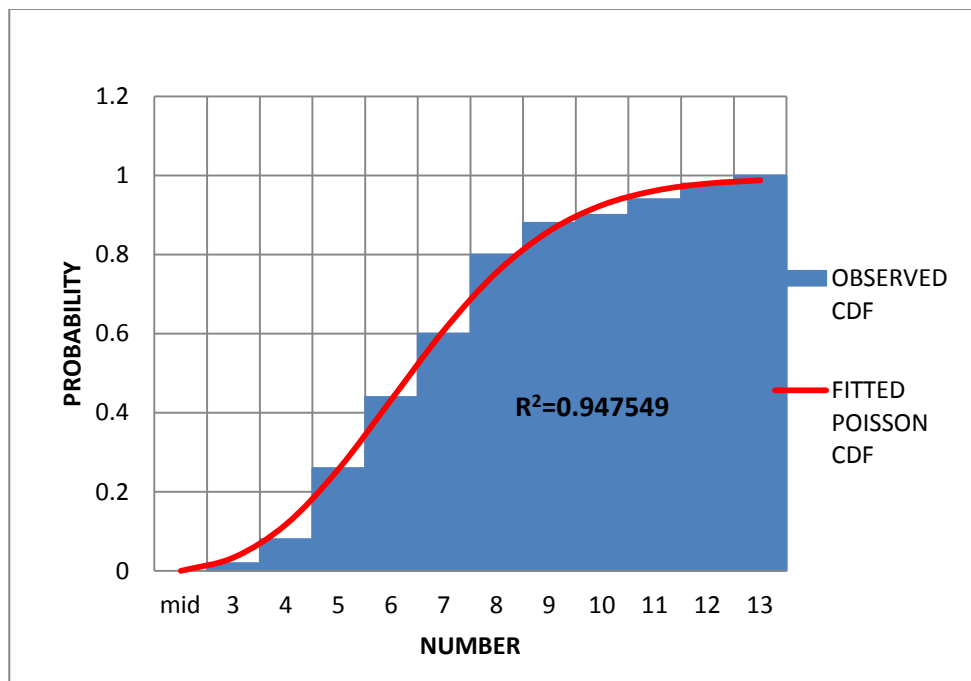


Figure 4.8 (2): Fitting events to Poisson CDF distribution

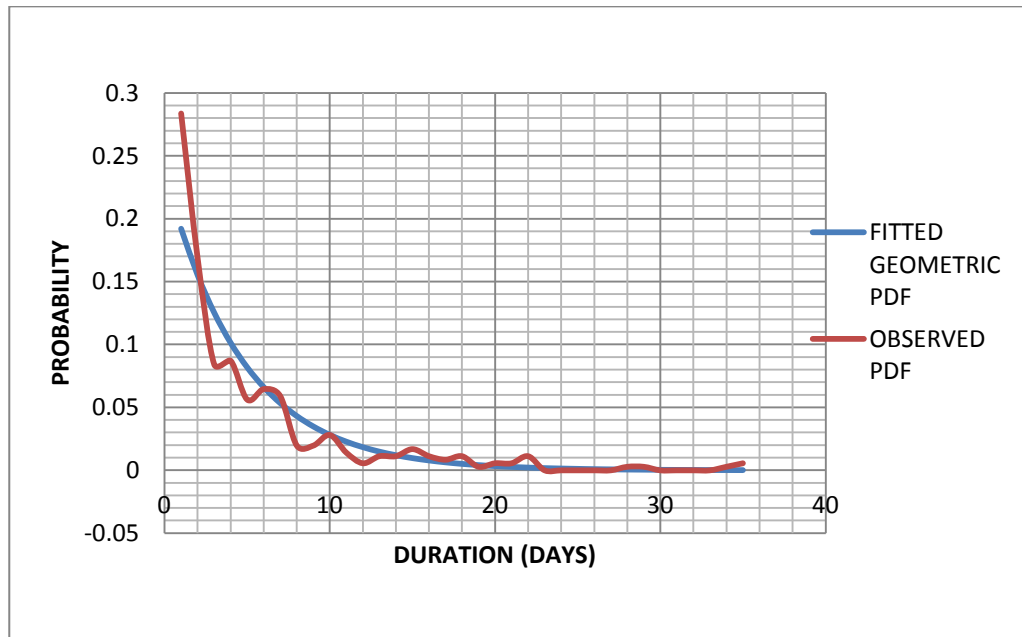


Figure 4.8(3): Fitting events duration to Geometric PDF distribution

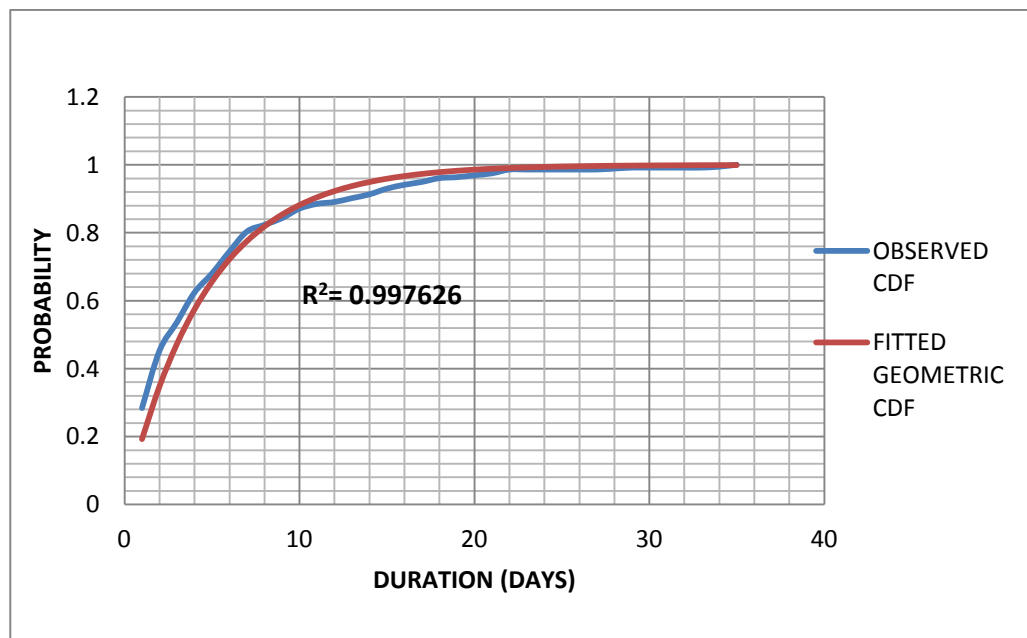


Figure 4.8(4): Fitting events duration to Geometric CDF distribution

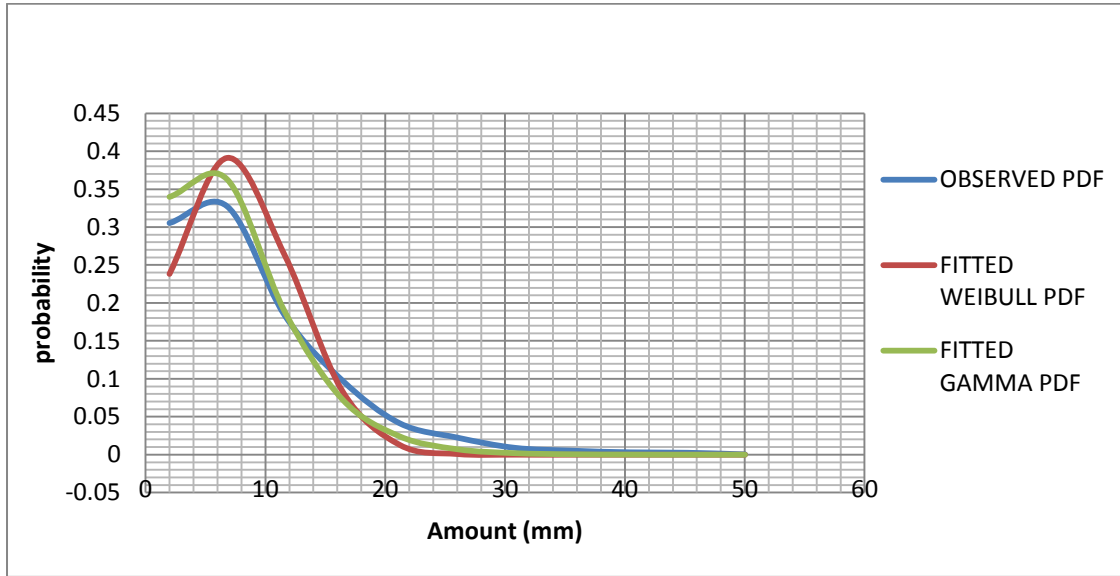


Figure 4.8(5): Fitting daily rainfall depths to Gamma PDF distribution

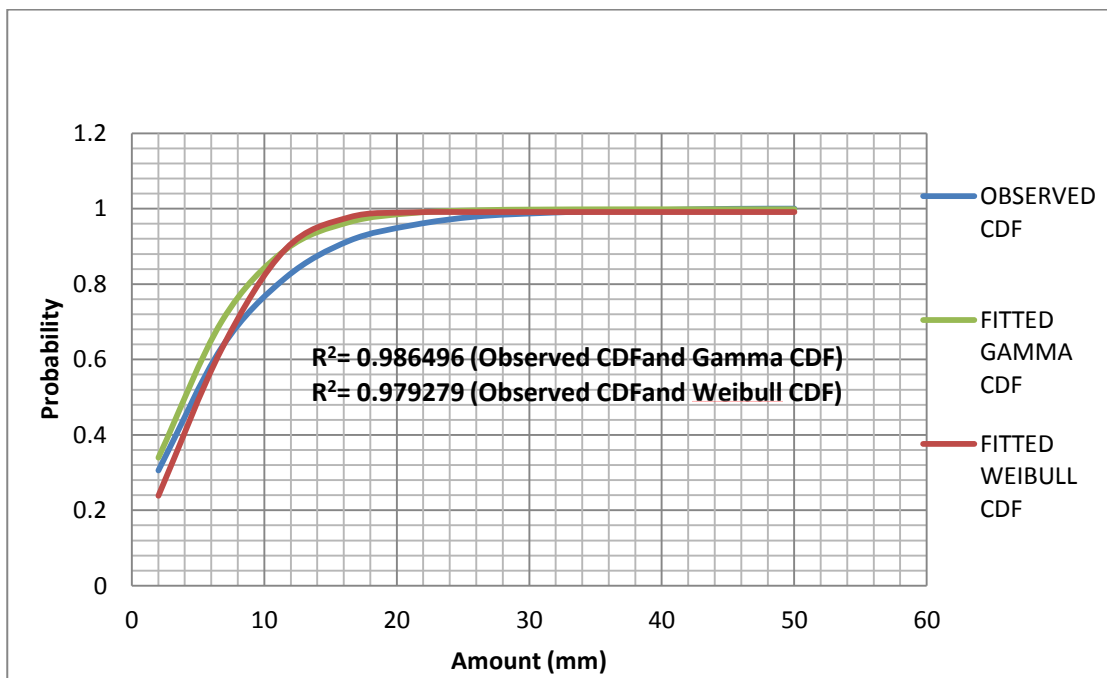


Figure 4.8(6): Fitting daily rainfall depths to Gamma CDF distribution

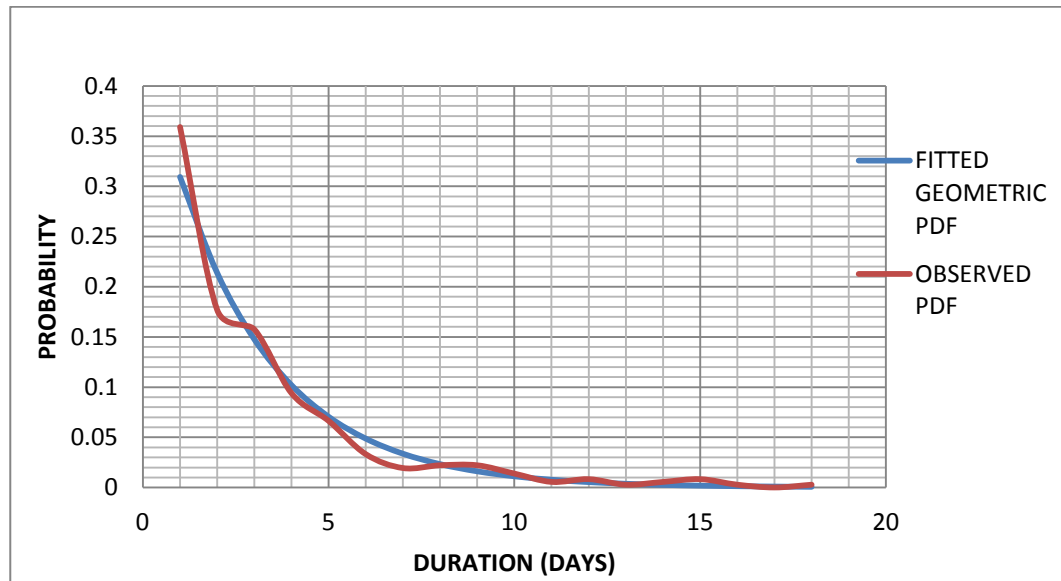


Figure 4.8(7): Fitting inter-events to Geometric PDF distribution

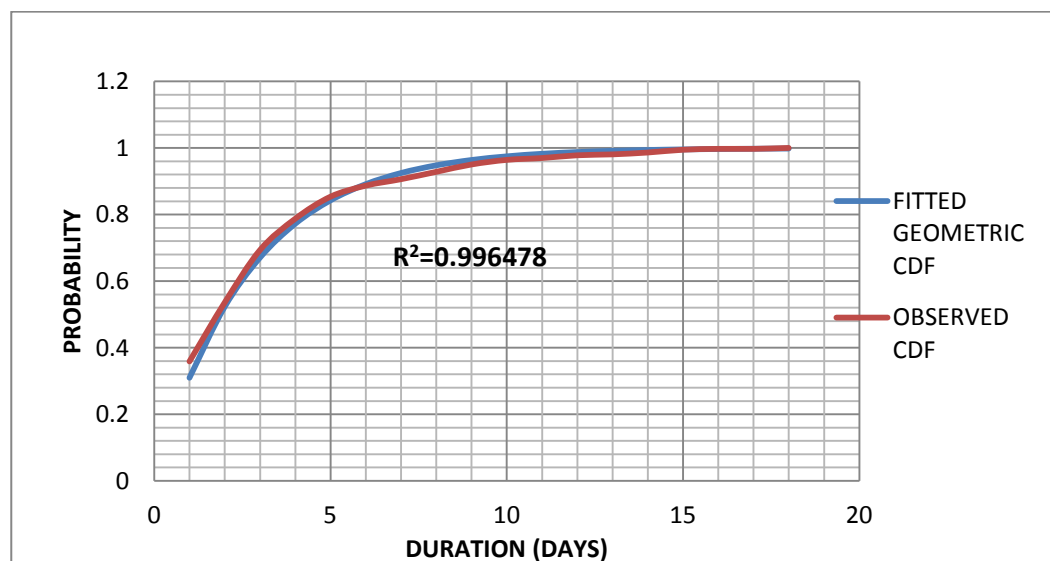


Figure 4.8(8): Fitting inter-events to Geometric CDF distribution

4.4.1.2 Stochastic generation of rainfall patterns

Using the algorithm in section 3.3.4(1) for event based model and section 3.3.2 (2) for Markov model, a rainfall pattern can be synthetically generated. The rainfall that previously caused landslide in the years 2007, 2010 and 2011 had a cumulative total of

between 420 and 460 mm for the months of April and May. Therefore in this scenario analysis, various generated rainfalls having rainsums greater than 420mm for the months of April and May will be considered for analysis. Figure 4. 9 and *Appendix F* shows plots and data of skewed and evenly distributed rains generated using Markov and Event based methods to be used in this study.

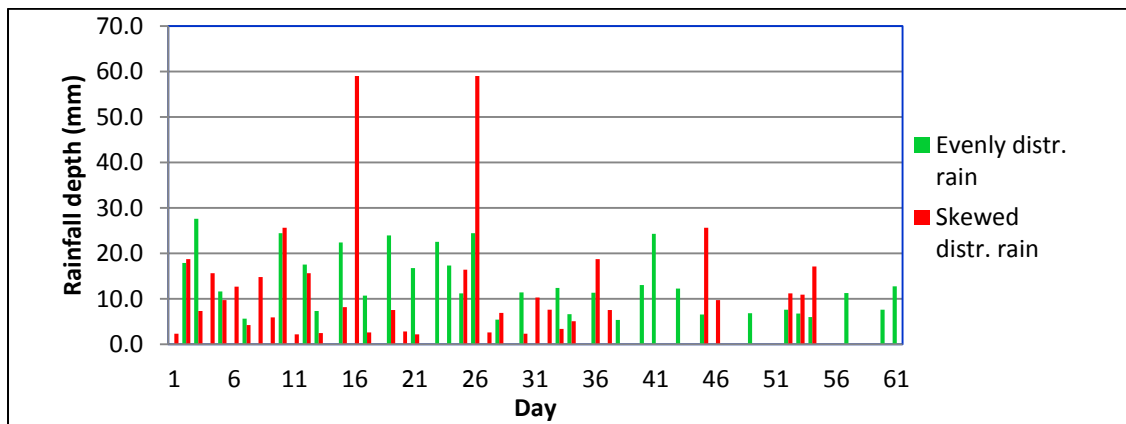


Figure 4. 9: Plots of generated skewed and evenly distributed rains

The rainfall generated was analyzed for variance with the historical rainfall of nearly the same amount using ANOVA one factor test and also using student t distribution (TTEST) to establish whether the generated rainfall and the historical rainfall are from the same population. For ANOVA test, the generated rainfall is rejected when F is greater than F critical (3.92) at 95% level of significance while for TTEST rejection occur if the t- calculated is greater than t- critical (2.45) at 95% level of significance.

4.4.1.3. Soil moisture analysis results

The modelled rainfall patterns were each applied to HYDRUS 1D model to simulate soil moisture condition and water flow flux. Some of the results for different types and depths of soils are as shown in Figure 4.10 (a-d);

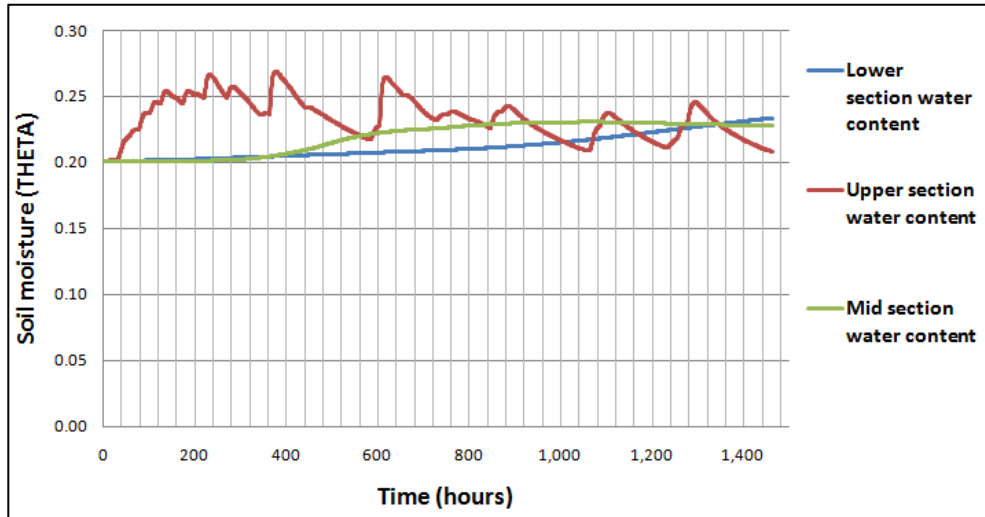


Figure 4.10 (a): Volumetric moisture content curves for clay loam with soil thickness of 1 m in analysis using skewed rainfall pattern.

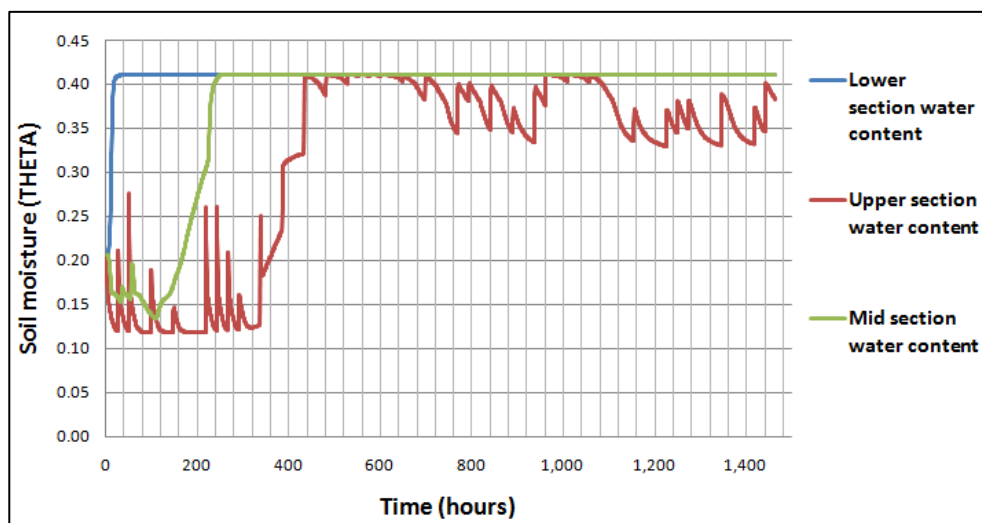


Figure 4.10(b): Volumetric moisture content curves for sandy loam with soil thickness of 1 m in analysis using skewed rainfall pattern.

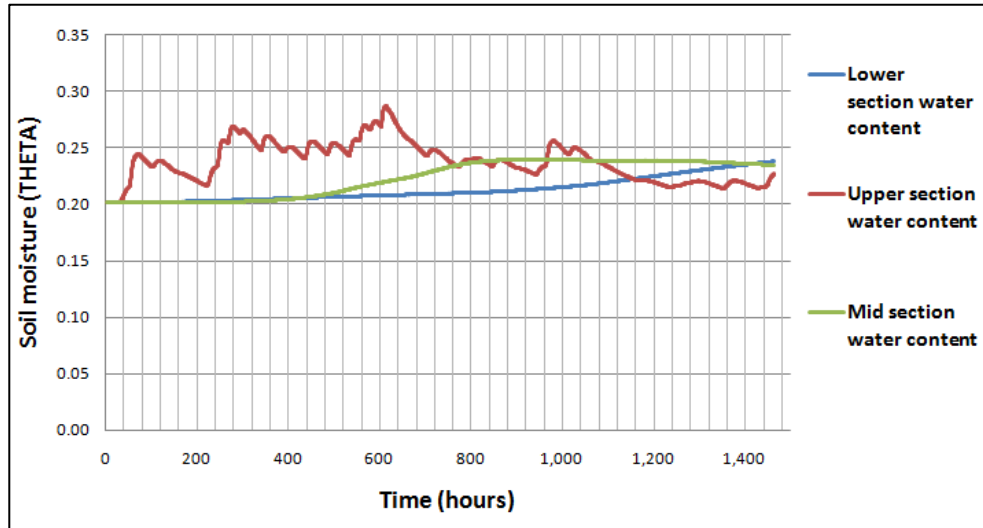


Figure 4.10(c): Volumetric moisture content curves for clay loam with soil thickness of 2 m in analysis using evenly rainfall pattern.

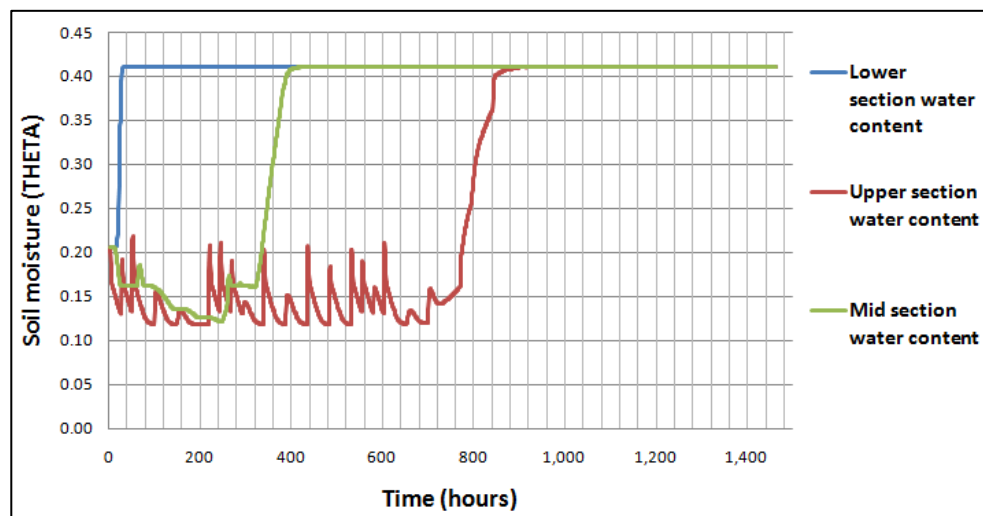


Figure 4.10(d): Volumetric moisture content curves for sandy loam with soil thickness of 2 m in analysis using evenly rainfall pattern.

4.4.1.4. *Matric suction stress analysis results*

Matric suction stress analysis was undertaken using modified Lu and Likos (2006) formulation and some of the analysis results for different soil types under different patterns of rains are as shown in Figure 4.11 (a-d).

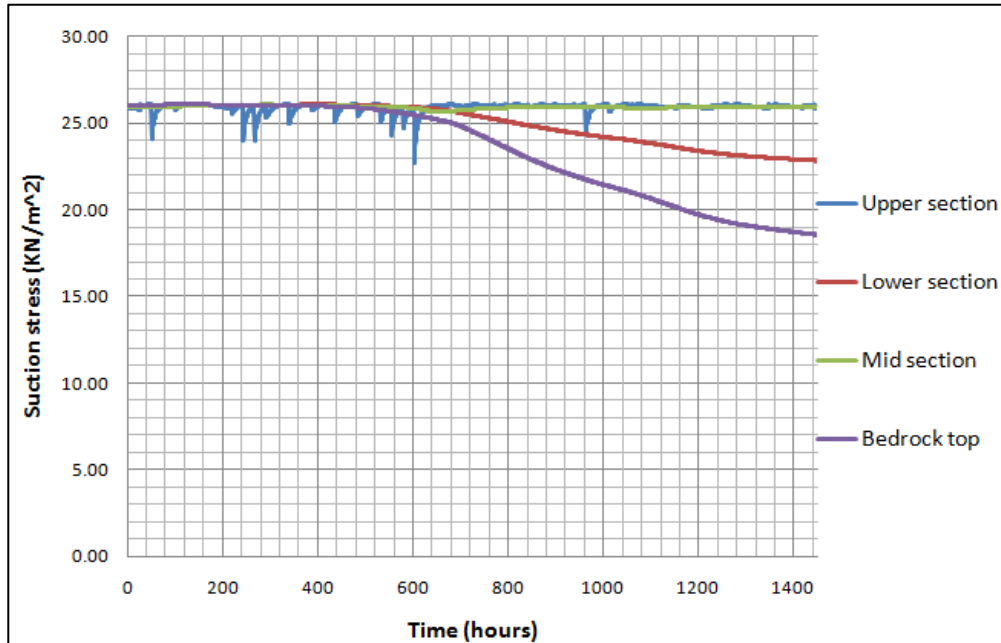


Figure 4.11 (a): Variation of Suction stress with time for clay loam soil with depth of 1m, under evenly distributed rainfall

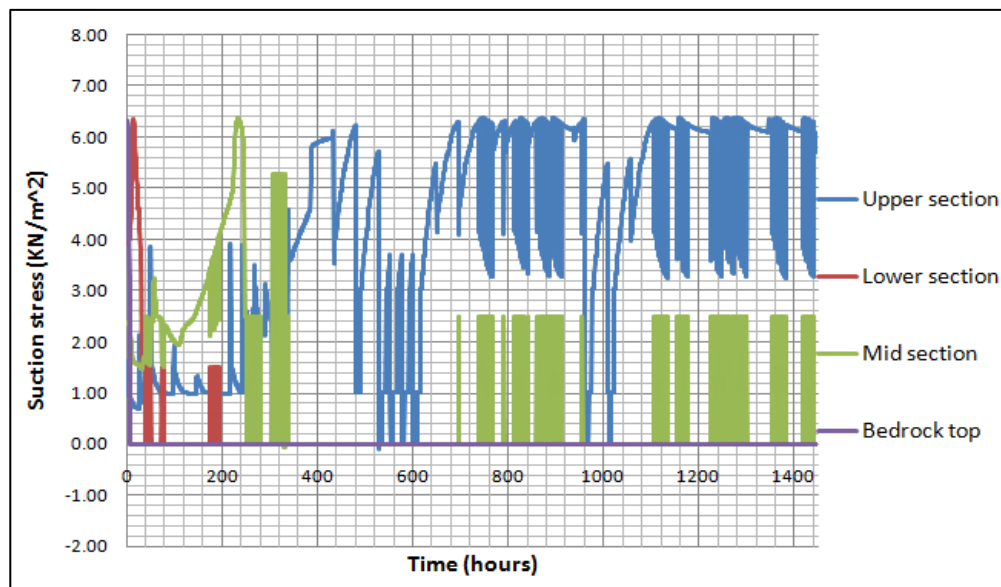


Figure 4.11(b): Variation of Suction stress with time for sandy loam soil with depth of 1m, under evenly distributed rainfall

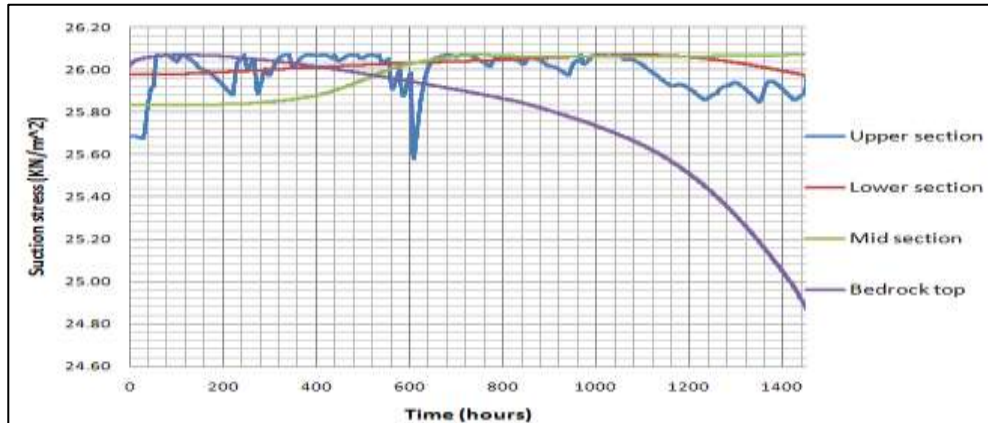


Figure 4.11(c): Variation of Suction stress with time for clay loam soil with depth of 2m, under evenly distributed rainfall

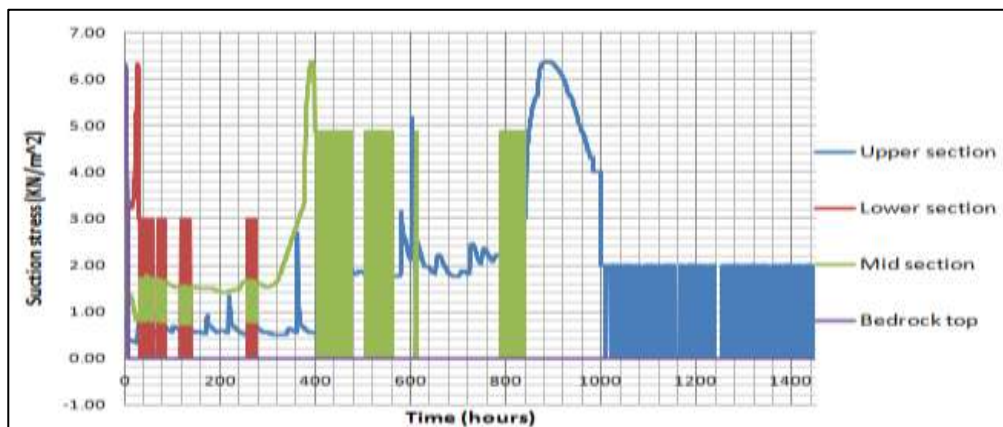


Figure 4.11(d): variation of Suction stress with time for sandy loam soil with depth of 2m, under skewed distributed rainfall

4.4.1.5. ILWIS GIS Statistical results for different wet spell persistence scenarios.

To understand effect of wet spell persistence on stability of slopes, hazard maps was generated for different days in the analysis period. The mapping days was randomly chosen such that every quartile of analysis period had representation and the days considered in analysis were; 13th April, 21st April, 6th May and 23rd may. The generated percentages of stable, critical and unstable area were then compared. The stability classification results are as shown in the Table 4. 5;

Table 4. 5: ILWIS GIS Statistical analysis for various stability classifications

	STABILITY RESULTS				
		Percentage area (%)		Area (m ²)	
date	stability class	evenly	skewed	evenly	skewed
13 th April	unstable	0.24	0.24	8028326.2	8002649.2
	critical	3.7	4	12372660.2	133871055.2
	stable	96.06	95.76	3213033709.9	3202916991.9
21 st April	unstable	0.86	0.84	28749624.4	28141936.5
	critical	4.74	4.73	158546603.6	158212803.3
	stable	94.4	94.43	3157494468.4	31584435956.5
6 th May	unstable	1.5	1.48	50309702.9	49642102.2
	critical	5.18	5.08	173113992.9	170049876.9
	stable	93.32	93.43	3121367000.6	3125098717.2
23 rd may	unstable	0.33	0.57	11546068.2	19685661.2
	critical	3.38	3.36	117300863.9	116530555.4
	stable	96.28	96.07	3338345782.0	3330976497.5

4.4.1.6. Discussion

Antecedent rainfall is defined as rain that falls in the days immediately preceding the landslide event (Rahardjo *et. al.*, 2001). Most of researches that have been done established that periods of rainfall with some associated threshold magnitudes that may induce landslide vary from less than 24 hours for shallow debris flows (Wieczorek, 1987) to a few months for deep seated slow moving landslides (Flentje, 1998).

In mapping results for 13th April, skewed rainfall pattern gave higher percentage of unstable areas as compared to evenly rainfall pattern (see Table 4. 5) and this stem from higher weekly antecedent cumulative rainfall to this day for this rainfall pattern as shown in

Table 4. 6. The same can be said for 6th May and 23rd May mapping results in which evenly rainfall pattern gave higher percentage of unstable areas because of higher weekly antecedent rainfall amount.

Table 4. 6: Cumulative antecedent rainfall for Skewed and evenly rainfall

Day	Weekly cumulative to date		Total cumulative to date	
	(mm)		(mm)	
	Even	Skewed	Evenly	Skewed
13 th April	59.2	90.7	112.0	137.1
21 st April	64.4	82.6	169.1	217.2
06 th May	30.4	28.7	308.4	351.7
23 rd May	21.2	22.1	391.1	416.6
31 st May	TOTAL		428.6	433.7

Also, from Table 4. 5 it was established that antecedent rainfall amount for long period of time greater than a week do not support the stability results obtained. This was attested from mapping results for 21st April and 6th May in which evenly distributed rainfall gave higher percentage of unstable areas compared to skewed rainfall though the later had the highest total cumulative antecedent rainfall (see Table 4. 6).

The results for 21st April indicate that evenly rainfall pattern gave higher percentage of unstable areas as opposed to skewed pattern which had higher weekly antecedent amount. To explain this scenario, soil infiltration capacity will have to be discussed.

The infiltration capacity is the maximum rate at which water can enter a particular soil. The infiltration capacity of the soil depends on its texture and structure, as well as on the antecedent soil moisture content (FAO 2003). The highest infiltration capacities are found in loose sandy soils while heavy clay or loamy soils have considerable smaller infiltration capacities. The amount of rainfall that infiltrates soil will be governed by the intensity of the rainstorm in relation to the soil's infiltration rate. When rainfall intensity is greater than soil infiltration rate, runoff will occur, reducing amount of water that could have been used in saturating soil to induced instabilities (FAO 2003).

From adopted Moi university rainfall occurrence chart (see section 3.6.3), it was established that rainfall tended to fall following Gamma distribution and this assumption was adopted for this study. Distribution of probability of rainfall occurrence is as shown in Figure 4. 12, whereby 60% of the anticipated rainfall would fall within the first 20 minutes of rainfall time. Rainfall intensity exceeds infiltration capacity of soils when heavy amount of rainfall is received resulting in generation of surface runoffs. In the study area, most of the escarpment is covered with clay loam soils which have low infiltration capacity (hydraulic conductivity) which can be easily exceeded by rainfall intensity. This explains why for the case of 21st April, skewed rainfall pattern gave small percentage of unstable areas though it had high cumulative for both weekly and total, as the high amount rainfall of 59 mm received on 16th April (see *Appendix F*) for skewed rainfall ended up generating lots of surface runoff as opposed to saturating soils to induce slope instabilities.

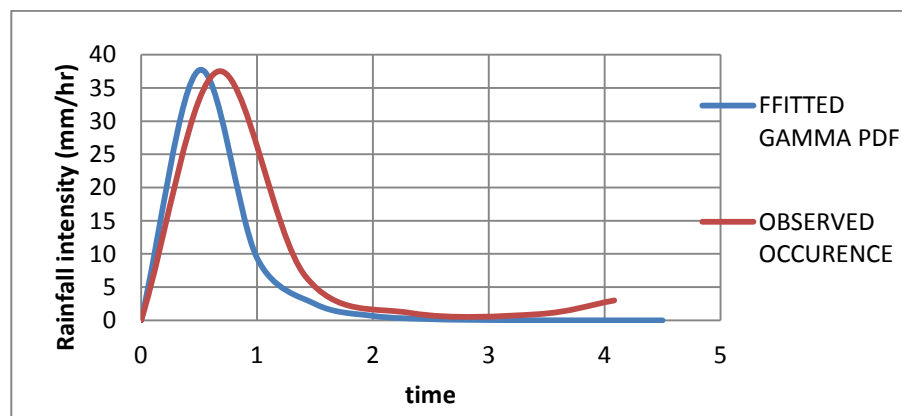


Figure 4. 12: Probability distribution of rainfall occurrence

4.4.2 Evaluating Effects of Land Use Change on Slope Stability

Vegetation roots are known to stabilize, or, improve the bearing in forest soils and therefore any action taken to destroy vegetation would result in increase in slope failures. In this study, procedures in section 4.4.1 was repeated and only that the

rainfall data applied were the areal rainfall data (see *Appendices B and C* for modelled suction stress and soil water content results respectively) and two assumed scenarios were taken into consideration. These scenarios are;

- a) Complete adoption of Agriculture as land use in the whole of study area
- b) Complete adoption of forest as land use in the whole of study area

4.4.2.1 Complete adoption of forest (pine or fir plantation) as land use in the whole of study area

In this scenario, it was assumed that the study area is covered with forest (pine or fir plantation) and from *appendix E* and Table 3.3, root tensile strength and RAR were chosen respectively for use in calculating the roots cohesion strength contribution using equation (3.42). The adopted values for root tensile strength and RAR are 30 MPa and 0.0075 respectively. The analysis results for this scenario were as shown in Figure 4.13, in which the percentage of unstable and critical areas was found to be 0.05% and 1.81% respectively.

4.4.2.2 Complete adoption of Agriculture as a land use for the study area

In this scenario, it was assumed that the study area is covered with maize plantation and from *Appendix E* and Table 3. 3, the adopted root tensile strength and RAR for use in calculating the roots cohesion strength contribution using equation (3.42) was 5 MPa and RAR of 0.001 respectively. For the month of April (planting season), it was assumed that maximum rooting depth for maize is zero. The analysis results for this scenario were as shown in Figure 4.14, in which the percentage of unstable and critical areas was found to be 0.69% and 5.35% respectively.

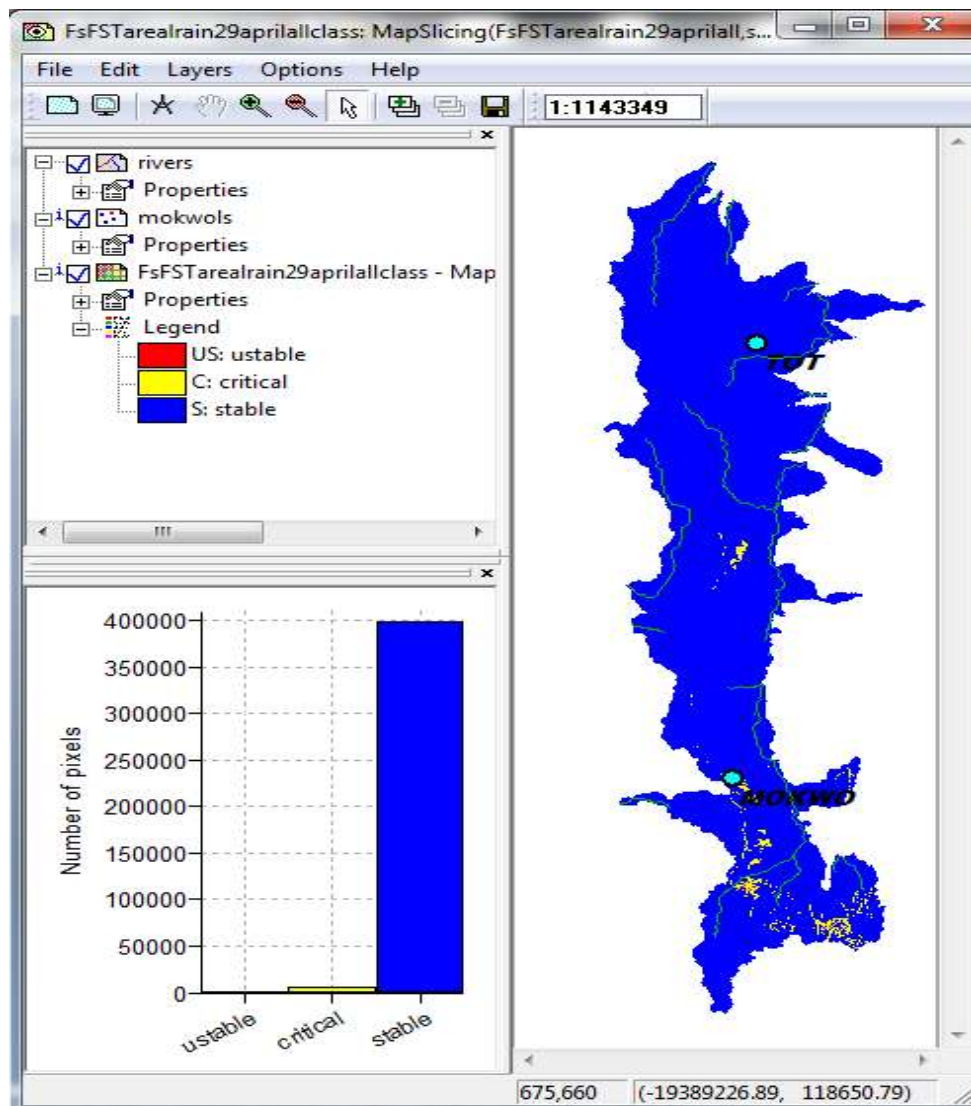


Figure 4.13: Hazard map for complete forestation of study area as on 29th April 2007

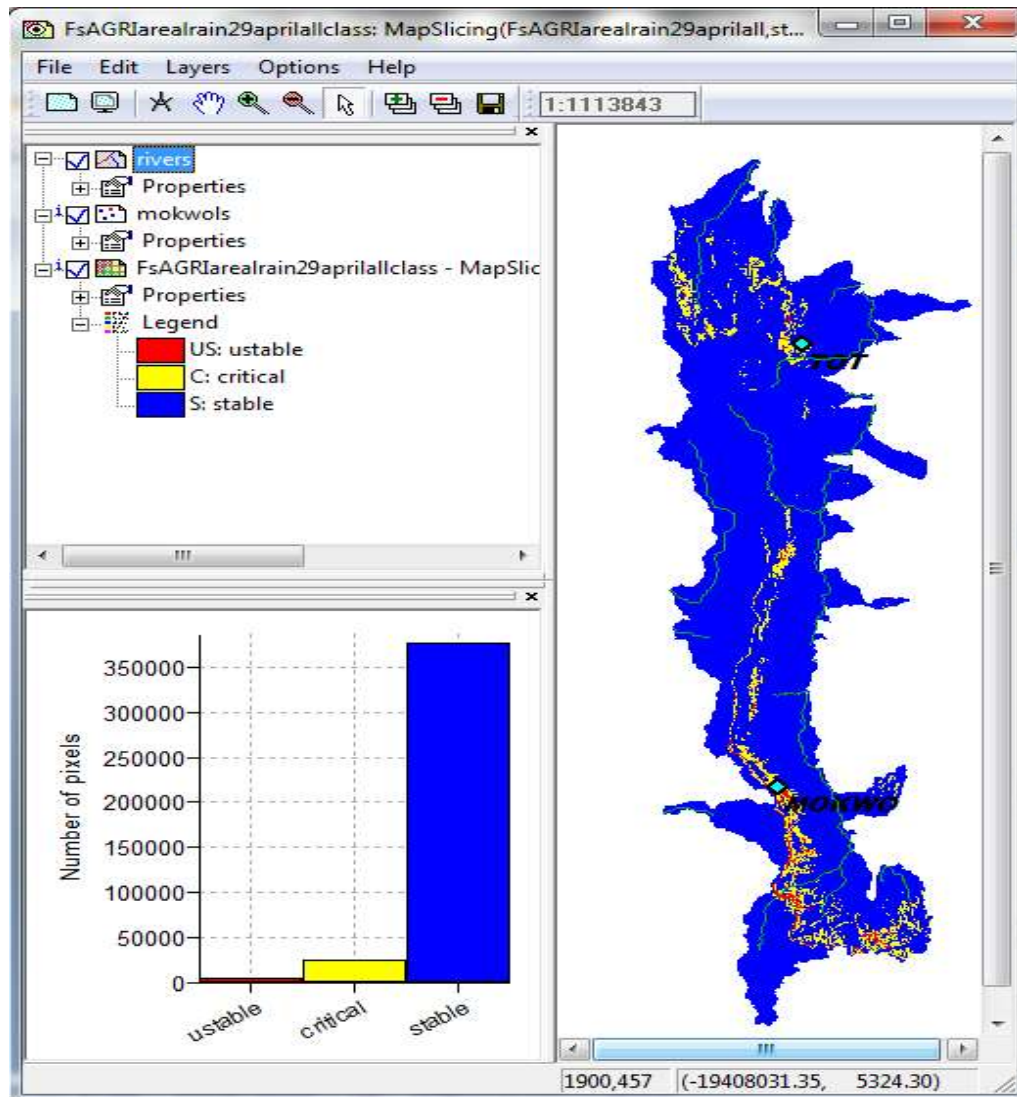


Figure 4.14: Hazard map for complete denudation of study area as on 29th April 2007

4.4.2.3 Discussion

Comparing percentages of unstable area in section 4.4.2.1 and 4.4.2.2 reveals that adoption of forest as a land use would greatly improve the stability of the study area as compared to case when area is bare land (agriculture). If the rainfall of HYDROID 8935184 for year 2007 is applied in the analysis, the percentage of unstable and critical areas for the case when the whole study area is forested would only be 0.05% and 1.81% respectively, while for the case when whole study area is bare (agriculture) the percentage of unstable and critical areas would increase to 0.69% and 5.35%.

4.5 GROUND TRUTHING OF GENERATED HAZARD MAPS

The ability of ILWIS GIS to allow draping of raster, vector as well as point maps in the 3D display generated from area DEM would assist in verifying the accuracy of mapping before actual site visit is undertaken. Figure 4.15 below show some of the 3D display of hazard areas in and around historical occurrence sites and it can be established from these maps that the hazardous areas are located only in steep areas (escarpment) meaning that ILWIS GIS mapping formulation used in methodology is correct as none of the hazard zones was shown to lie on relatively flat areas.

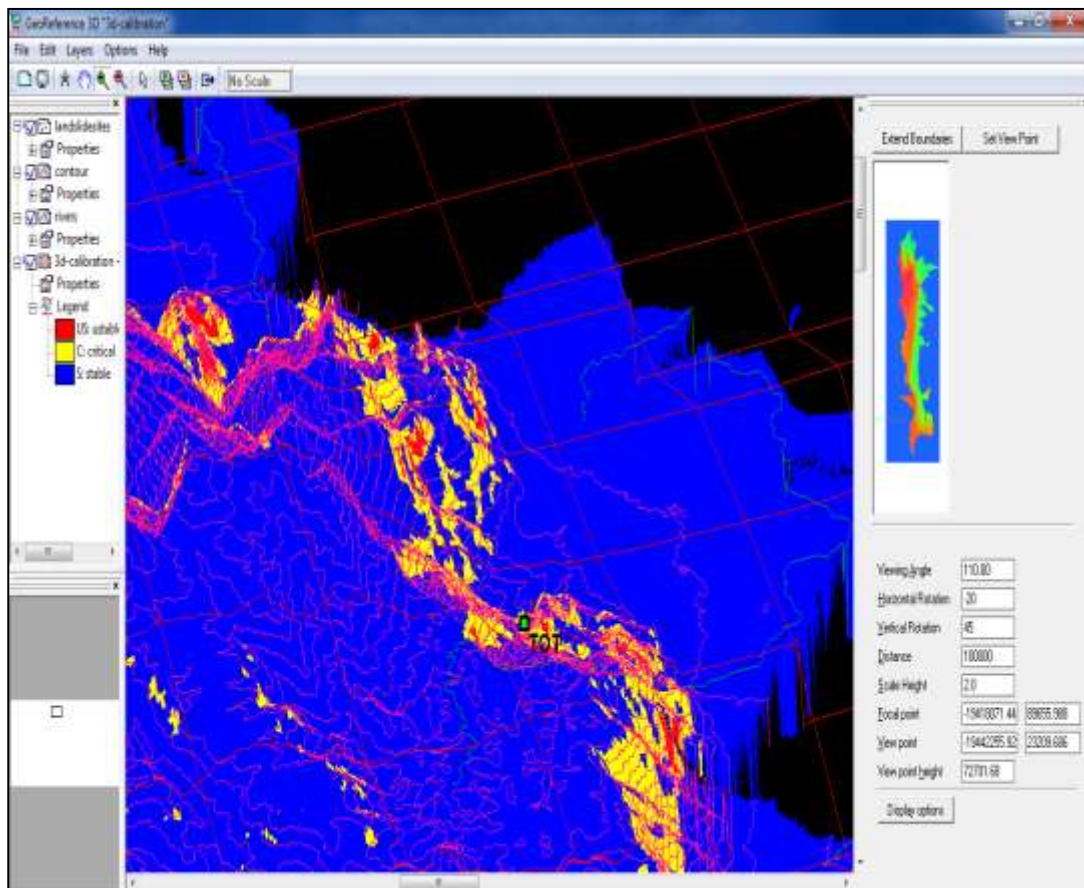


Figure 4.15: 3D display of generated hazard map in Tot area

CHAPTER FIVE: CONCLUSIONS AND RECOMMENDATIONS

5.1 CONCLUSIONS

Landslide occurrences are natural phenomena which often have detrimental consequences. Landslide hazards can be systematically modelled by using different methods depending on the available data and resources. For this study we developed Landslide Prediction Model (LPM) to suit parameters being analyzed. The results obtained from LPM were fairly conclusive as it predicted rainfall induced landslides. Also the information provided by hazard maps could form a basis of decision making to residents (in identifying habitable areas), environmentalists (in expounding importance of tress), rescuers (e.g. Red Cross in marshalling resources) and engineers (in establishing major projects) in reducing, preventing and mitigating losses caused by landslides. Our objectives were successfully met as follows;

5.1.1 Developing Model for Rainfall Induced Landslides:

The formulated landslide prediction model (LPM) was successfully formulated and calibrated, and since the standard models applied in this study were not commercial, it can thus provide an effective and cheap method of predicting landslides. HYDRUS 1D model made it possible to analyze the subsurface water movement with ease and ILWIS GIS made it possible to understand the spatial distribution of unstable slopes which could not have been possible with Ms-EXCEL LPM (1 dimensional formulated model). Integration of ArcGIS and ILWIS models in preparation and analysis of spatial data made it easy to undertake spatial mapping since ILWIS provided a platform for developing with ease mapping functions (combination of Infinite slope model and suction stress equation) while ArcGIS assisted in watershed delineation and processing of topographic maps and SRTM DEM maps.

5.1.2 Sensitivity of Slope Stability to Change in Variables

The analysis involving evenly and skewed distributed rainfall showed that magnitude of day's rainfall as well as the antecedent rainfall are important landslides triggering factors. High persistence of wet spells is a major cause of landslides as was realized from the different factors of safety, F_s , that were calculated for the two cases of rainfall events (skewed and evenly distributed rainfall patterns); though their total rainfall amount for analysis period were nearly equal. For stability analysis that were undertaken on 13th April for the two cases of rainfall patterns, the skewed rainfall pattern gave higher percentage of unstable and critical areas because of higher antecedent rainfall as compared to evenly distributed rainfall. Also on 6th May, evenly rainfall pattern gave higher percentage of unstable areas because of the same reason. Rainfall intensity that exceeds infiltration capacity of soils results in generation of surface runoffs and this explains why for the case of 21st April analysis, skewed rainfall pattern gave small percentage of unstable areas though it had high cumulative for both weekly and total rainfall.

The analysis involving assumed change of land use to agriculture (maize plantations) and forest (pine plantation) showed that forest cover is an important factor in as far as slope stabilization is concerned and this stems from reinforcement of soils by roots. It is also known that trees stabilize slopes by removing soil moisture build up through evapotranspiration and also forest canopies do modify intensity of precipitation by lowering it, such that their presence may prevent sliding in some instances, even though these were not included in this research.

5.2 RECOMMENDATIONS

Based on the findings of the study presented in this research, the following recommendations are given for future landslide hazard assessment project:

- a) Any landslide study in future should divide a soil layer under analysis into many sections as possible so as to improve accuracy of the results.
- b) Scenario analysis involving combined effect of land use and wet spell variables should be undertaken in future to optimize on landslide triggering parameters.
- c) Future studies should consider application of HYDRUS 2D model, high resolution DEM (i.e. ASTER DEM 30m) and land use maps of the same year as analysis period so as to reduce bias in the analysis results.
- d) Rainfall generating model should be improved such that it can be able extrapolate yearly historical rain storm intensities to more extreme conditions (i.e. intensities of given return period) and resulting rainfall of extreme conditions be applied in landslide modelling. Also in modelling of areal rainfall, Kriging method of interpolation should be used so as to limit errors associated with Thiessen polygon method.
- e) Future research should consider incorporation into the model the ability of trees to stabilize slopes by lowering pore water pressure build up in soils through transpiration and also the ability of various trees to lower intensity of precipitation reaching soil surface through canopy storage.
- f) Most of the analyses were based on values obtained from existing literature and may not apply to Kerio escarpment. These parameters include; RAR values, soil type including their properties, and root distribution with depth. Therefore, research should be done to establish accurate values of these parameters as these may have led to over or underestimation of the stability of the slope.
- g) Any future landslide occurrence must be Geo-referenced and documented by relevant institutions in order to assist in assessing the quality and validation of landslide studies.

REFERENCES

- Abernethy B. and Rutherford I. D. "The distribution and strength of riparian tree roots in relation to riverbank reinforcement." *Journal of Hydrological Processes* 15(2001):63–79
- Abramson L.W. (2002). *Slope stability and stabilization methods*. New York; Wiley.
- Barkotulla .M. A. B. "Stochastic generation of the occurrence and amount of daily rainfall." *Pak.j.stat.oper.res.* 1.1 (2010):61-73
- Bogardi J.J. and Rumambo H., "Practical generation of synthetic rainfall time series in a semi-arid climatic zone." *Journal of Hydrology*, 103(1988): 357-373
- Brooks, R.H., and Corey, A.T., *Hydraulic properties of porous medium*. Colorado State University (Fort Collins), Hydrology paper, Nr. 3, March 1964.
- Cammeraat, C.; van Beek, R. & Kooijman, A. "Vegetation succession and its consequences for slope stability in SE Spain." *Plant and Soil*, 278.1 (2005):135-147
- Carsel, R.F., and R.S. Parrish., "Developing joint probability distributions of soil water retention characteristics." *Water Resour. Res.* 24(1988):755–769.
- Celia, M. A., and E. T. Bououtas, R. L. Zarba, "A general mass-conservative numerical solution for the unsaturated flow equation", *Water Resour. Res.*, 26(1990):1483-1496.
- Corominas J. and Moya J. "Historical landslides in the Eastern Pyrenees and their relation to rainy events." *In* J Chacon, C Irigaray and T Fernandez (eds.) *Landslides*. Balkema, 1996:125 - 132.
- Corominas, J. and Moya, J. "Reconstructing recent landslide activity in relation to rainfall in the Lobregat River basin, Eastern Pyrenees, Spain." *Geomorphology* 30.(1-2) (1999): 79-93.
- Croney,D and Coleman, J.D., "Pore pressure and suction in soils" *Proceedings, conference on pore pressure and suction in soils*. Butterworths, London. 1961:31-37
- Crosta G.B. and Frattini P. "Rainfall-induced landslides and debris flows." *Hydrol Process* 22.4 (2008):473–477
- Crozier M. J., "Prediction of rainfall-triggered landslides: a test of the antecedent water status model." *Earth Surf Proc Land* 24.9 (1999):825–833

- Crozier M.J., Glade T “Landslide hazard and risk: issues, concepts, and approach.”
In Glade T, Anderson M, Crozier MJ (eds) *Landslide hazard and risk*.
 Wiley, New York, 2005:1–40.
- Darcy, H., (1856). *Les Fontaines Publiques de la Ville de Dijon*, Paris; Dalmont.
- Dawes, W. R. and Hatton T. J. “TOPOG_IRM, 1, Model description.” Tech.
 Memo. 93/5, Commonwealth, Sci. and Ind. Res. Organ., Div. of Water
 Resourc., Canberra, A. C. T., 1993.
- De Baets S., Poesen J, Knapen A, Barberá G.G, Navarro J.A. “Root characteristics
 of representative Mediterranean plant species and their erosion-reducing
 potential during concentrated runoff.” *Plant Soil* 294(2008):169-183
- Duncan, J. M., and Wright S. G. (2005). *Soil Strength and Slope Stability*. 297
 pp., Hoboken, N. J.; John Wiley.
- Eigenbrod, KD. and Kaluza, O., “Shallow Slope Failures in Clays as a Result of
 Decreased Evapotranspiration Subsequent to Forest Clearing.” *50th
 Canadian Geotechnical Conference of the Canadian Geotechnical Society*,
 2(1997):823-830.
- El-Keshky M. (2012). “Temperature Effect on the Soil Water Retention
 Characteristic.” thesis report, Arizona State University.
- Emba T. A. (2010). “Determining rainfall threshold for landslide initiation.” Mphil
 Thesis. Yogyakarta, Indonesia; Gadjah Mada University (GMU).
- FAO, *Optimizing soil moisture for plant production, The significance of soil
 porosity*. Food and Agricultural Organization of The United Nations, Rome,
 2003.
- FAO/UNEP “Terminology for integrated resources planning and management.” *In*
 Choulhury K. and Loisa J.M.J. (eds) *Soil resources, management and
 conservation service*. FAO land and water development division, 1999.
- Feddes, R. A., P. J. Kowalik and Zaradny H. (1978). *Simulation of Field Water
 Use and Crop Yield*. New York; John Wiley & Sons.
- Flentje, P.N. and Chowdhury, R.N., “A landslide database for landslide hazard
 assessment.” Proceedings of the Second International Conference on
 Environmental Management. February 10-13. Wollongong Australia:
 Sivakumar, M. and Chowdhury, R. N.(eds) 1998:1229 - 1239. *Elsevier*,
 London.
- Fraedrich K. and Leslei L. M., “Evaluation of techniques for the operational,
 single station, short-term forecasting of rainfall at a midlatitude station
 (Melbourne)” Bureau of Meteorology Research Centre, Melbourne,
 Victoria, 3001 Australia, 1987.

- Fredlund D.G. and Rehardjo H. (1993). *Soil mechanics for unsaturated soils*. New York; Willey publications.
- Fredlund D.G., Anqing Xing, and Shangyan Huang, “Predicting the permeability function for unsaturated soils using the soil-water characteristic curve” *Can. Geotech. J.* 31(1994). 533-546
- Gardner W. R. “Steady state solutions of the unsaturated moisture flow equation with application to evaporation from a water table.” *Soil Science* 85(1958):228–232.
- Gowdish I. C., “An Improved Green-Ampt soil infiltration and redistribution method and its application to 1-dimensional and quasi 3-dimensional (point source) flow domains” A dissertation, University of Florida, 2007.
- Gray D. H. and Leiser A. T. (1982). *Biotechnical Slope Protection and Erosion Control*. New York; VanNostrand Reinhold.
- Gray D.H. and Sotir R.B. (1996). *Biotechnical and soil bioengineering slope stabilization: a practical guide for erosion control*. New York, USA; J. Wiley and sons.
- Griffiths D. V. and Lu N., “Unsaturated slope stability analysis with steady infiltration or evaporation using elasto-plastic finite elements.” *Int. J. Numer. Anal. Meth. Geomech.* 29(2005):249–267)
- Gurrapu S., “Estimation of soil moisture in unsaturated zone and irrigation scheduling” A master thesis at department of applied mechanics & hydraulics, National Institute of Technology Karnataka, (A Deemed University) INDIA, 2005.
- Gustafson, D., J. Anderson, A. Amoozegar, and D.L. Lindbo. (2005). “Water Movement & Soil Treatment Text.” in D.L. Lindbo and N.E. Deal eds. *Model Decentralized Wastewater Practitioner Curriculum. National Decentralized Water Resources Capacity Development Project*. North Carolina State University, Raleigh, NC.
- Hales, T. C., C. R. Ford, T. Hwang, J. M. Vose, and L. E. Band, “Topographic and ecologic controls on root reinforcement”, *J. Geophys. Res.*, 114(2009), F03013, doi:10.1029/2008JF001168.
- Hossain M. M. and Anam S., “Identifying the dependency pattern of daily rainfall of Dhaka station in Bangladesh using Markov chain and logistic regression model”, *Agricultural Sciences* 3.3(2012):385-391
doi:10.4236/as.2012.33045

- Inter-American Development Bank (2000). *Natural disasters in Latin America and the Caribbean: an overview of risk*, IADB 1300 New York Avenue, Washington, D.C.
- Joanne E. Norris, Alexia Stokes, L.P.H. van Beek, Thom Bogaard, Erik Cammeraat, Slobodan B. Mickovski, Anthony Jenner, Antonino Di Iorio and Thierry Fourcaud., "Slope stability and erosion control: Ecotechnological solutions." 65–118. © 2008 *Springer*
- Kanungo, D.P., Arora M.K., Sarkar S. and Gupta R.P. "A comparative study of conventional, ANN black box, fuzzy and combined neural and fuzzy weighting procedures for landslide susceptibility zonation in Darjeeling Himalayas" *Engineering Geology* 85(2006): 347–366.
- Karsli, F., Atasoy, M., Yalcin, A., Reis, S., Demir, O. and Gokceoglu, C. "Effects of Land-use Changes on Landslides in a Landslide-prone Area (Ardesen, Rize, NE Turkey)." *Environmental Monitoring and Assessment (Springer Science)*. DOI (2008): 10.1007/s10661-008-0481-5
- Lakhan R. R., "Landslide susceptibility mapping through enhanced dynamic slope stability analysis using earth observing satellite measurements", Ph.D. dissertation, University of New Hampshire, 2009, 201 pages; 3383325: ISBN 9781109461336
- Lam, N.S. "Spatial interpolation methods: A review." *Cartogr. Geogr. Inf. Sci.*, 10(1983): 129-150.
- Lu N. and Likos W.J. (2004). *Unsaturated Soil Mechanics*. NJ; Wiley: Hoboken.
- Lu, N., and Likos W. J. "Suction stress characteristic curve for unsaturated soil." *J. Geotech. Geoenviron. Eng.*, 132.2 (2006): 131– 142.
- Mattia, C.; Bishetti, G. & Gentile, F. "Biotechnical characteristics of root systems of typical Mediterranean species." *Plant and Soil* 278.1(2005): 23-32.
- Mavimbela S.S.W and L.D. Van Rensburg, "Evaluating models for predicting hydraulic characteristics of layered soils." *Hydrol. Earth systems* 9(2012): 301- 336
- Morgan, R., "Vegetative-based technologies for erosion control", in Stokes, A. (eds), *Eco - and Ground Bioengineering: The use of vegetation to Improve Slope Stability*, Dordrecht, London, 2007:265 -272.
- Muchemi J., Mwangi W. & Greijn H., "GIS in support of participatory land use planning in the Districts Keiyo & Marakwet, Kenya." Proceedings GISDECO Seventh International Seminar on GIS in developing countries, Venue: International Institute for Geo-Information Science and earth Observation (ITC) Enschede, The Netherlands, 15 - 18 May 2002.

- Musy, A. (2001). "e-drologie. Ecole Polytechnique Fédérale." Lausanne; Suisse.
- Naoum S. and I.K. Tsanis, "Ranking Spatial Interpolation Techniques Using A GIS-Based DSS", *Global Nest: the Int. J.* 6.1 (2004): 1-20
- Navarro V., Yustres A., Candel M., López J. and Castillo E. "Sensitivity analysis applied to slope stabilization at failure." *Comput Geotech* 37.(7-8) (2010):837-845
- Ochola W. O. and Kerkides P. "A markov chain simulation model for predicting critical wet and dry spells in Kenya: Analyzing rainfall events in the kano plains." *Journal of Irrigation And Drainage.* 52(2003): 327-342.
- Ogden, F.L., Sagharian, B. "Green and Ampt Infiltration with Redistribution." *Journal of Irrigation and Drainage Engineering* 123.5 (1997):386-393.
- Osman, N. and Barakabah, S. "Parameters to predict slope stability – Soil water and root profiles." *Ecological Engineering*, 28.1(2006):90-95.
- Pack, R. T., Tarboton, D. G. and Goodwin, C. N., "Assessing Terrain Stability in a GIS using SINMAP." The 15th Annual GIS Conference: GIS: 19-22 February, 2001. Vancouver, British Columbia, 2001.
- Perry, J., Pedley, M., and Reid, M. (2003). *Infrastructure embankments condition appraisal and remedial treatment.* South Wales; MWL Digital, Pontypool.
- Petley, D.N. and Bulmer, M.H.K., "The application of Earth observation technologies for landslide disaster mitigation." *The proceedings of the CEOS Workshop*, Beijing, November, 2004.
- Pollen N. and Simon A. "Estimating the mechanical effects of riparian vegetation on stream bank stability using a fiber bundle model." *Water Resources* 41(2005):1-11
- Priyaranjan R. D., "A Markov chain modelling of daily precipitation occurrences of Odisha." *International Journal of Advanced Computer and Mathematical Sciences* 3.4(2012):482-486 ISSN 2230-9624.
- Rahardjo H. et al, "Effectiveness of horizontal drains for slope stability." *Engineering Geology* 69 (2003): 295-308
- Rawls, W.J., Brakensiek, D.L., and Miller, N. "Green-Ampt Infiltration Parameters from Soils Data." *Journal of Hydraulic Engineering* 109.1 (1983):62 – 70
- Rawls, W.J., D.L. Brakensiek, and K.E. Saxton. "Estimation of soil water properties." *Trans. ASAE* 25 (1982):1316-1328.

- Refsgaard, J. C., and Storm B. "MIKE SHE." *In* Singh V. P., ed, *Computer models of watershed hydrology*, Highlands Ranch, CO: Water Resources Publications, 1995.
- Richards, B.G. "Measurement of the free energy of soil moisture by the psychrometric technique using thermistors." *In* Aitchison G.D. (eds) *Moisture equilibria and moisture changes in soils beneath covered areas*. Butterworth & co. Ltd., Sydney, Australia, (1965):39-46.
- Ritter J. B., "Landslides and Slope Stability Analysis; Using an Infinite Slope Model to Delineate Areas Susceptible to Translational Sliding in the Cincinnati, OH Area." Department of Geology, Wittenberg University. 2004
- Schmidt K. M., Roering J. J., Stock J. D., Dietrich W. E., Montgomery D. R. and Schaub T., "The variability of root cohesion as an influence on shallow landslide susceptibility in the Oregon Coast Range." *Can. Geotech. J.* 38(2001) 995–1024.
- Sidle, R.C., Pearce, A.J., and O'Loughlin, C.L. (1985). *Hillslope stability and land use*. Water Resources Monograph Series 11, Washington, D.C.; American Geophysical Union.
- Simon A., Pollen N., Langendoen E., "Influence of two woody riparian species on critical conditions for streambank stability: upper Truckee river, California." *J Am Water Resour Assoc* 42(2006):99–113
- Šimůnek, J., M. Šejna, H. Saito, M. Sakai, and van Genuchten M. Th. "The HYDRUS-1D Software Package for Simulating the Movement of Water, Heat, and Multiple Solutes in Variably Saturated Media, Version 4.08, HYDRUS Software Series 3." Department of Environmental Sciences, University of California Riverside, Riverside, California, USA, 2009
- Skaggs, R.W. and Khaleel, R. "Infiltration" *In*: C.T. Haan, H.P. Johnson, D.L. Brakensiek, Eds., *Hydrologic Modelling of Small Watersheds*, ASAE Monograph No. 5, St. Joseph, Michigan, (1982):21-166.
- Skaggs, R.W., Huggins, L. F., Monke, E.J., Foster, G.R. "Experimental Evaluation of Infiltration Equations." *Transactions of the ASAE* 12.6 (1969):822-828.
- Soeters R, Van Westen CJ "Slope instability recognition, analysis, and zonation." *In* Turner A.K. and Schuster R.L. (eds) *Landslides: investigation and mitigation (Special Report). National Research Council, Transportation and Research Board Special Report 247, steep land forests. In Carbon uptake and allocation in subalpine ecosystems as a key to management. Edited by R.H. Waring*. Oregon State University, Corvallis, Oreg., 1996:70-78.
- Terlien M.T. "The determination of statistical and deterministic hydrological landslide triggering thresholds." *Env Geol* 35.2 (1998):124–130

- Thiebes B. "Landslide Analysis and Early Warning Systems." *Springer Theses*, DOI: 10.1007/978-3-642-27526-5_1, © Springer-Verlag Berlin Heidelberg, 2012.
- Trotta, P.D., J.O. Ramsey and Cooper C., "Hydraulics IV: Groundwater and Onsite Text." in M.A. Gross and N.E. Deal, (eds) *University Curriculum Development for Decentralized Wastewater Management. National Decentralized Water Resources Capacity Development Project*. University of Arkansas, Fayetteville, AR (2005).
- United Nation Development Programme; *Kenya Natural Disaster Profile*, Nairobi Kenya, 2005.
- Van Asch Th. and Sukmantalya I. N. "The modelling of soil slip erosion in the upper Komering area, South Sumatra Province, Indonesia." *Geogr. Fis. Din. Quat.* 16(1993):81-86.
- van Genuchten M.Y. "A closed form equation for predicting the hydraulic conductivity of unsaturated soils." *Soil Science Society of America Journal* 44(1980):892–898.
- Van Westen, C.J. and M.T.J. Terlien, "Deterministic landslide hazard analysis in GIS. A case study from Manizales (Colombia)." *Earth surface processes and landforms* 21 (1996):853-868.
- Verruijt A., (2001). *Soil Mechanics*. Delft University of Technology, pp 273
- Vogel, T., K. Huang, R. Zhang, and M. Th. van Genuchten, "The HYDRUS code for simulating one-dimensional water flow, solute transport, and heat movement in variably-saturated media," Version 5.0, Research Report No 140, U.S. Salinity Laboratory, USDA, ARS, Riverside, CA, 1996.
- Waldron L.J. and Dakessian S. "Effect of grass, legume and tree roots on soil shearing resistance." *Soil Sci Soc Am J* 46(1982):894-899
- Wasterlund I. "Strength components in the forest floor restricting maximum tolerable machine forces." *J Terramech* 26(1989):177-182
- Wieczorek, G.F., Effect of rainfall intensity and duration on debris flows in central Santa Cruz Mountains, California. In: (Costa and Wieczorek editors) *Debris flows/avalanches: processes, recognition and mitigation. Reviews in Engineering Geology, Geological Society of America*, 7(1987):23-104.
- Willatt S.T. and Sulistyaningsih N. "Effect of plant roots on soil strength." *Soil Till Res* 16(1990):329-336
- Williams, P.J. (1982). *The surface of the earth, an introduction to geotechnical science*. New York; Longman Inc.

Wu TH., McKinnell W.P III., Swanston D.N. “Strength of tree roots and landslides on Prince of Wales Island, Alaska.” *Can Geotech J* 16(1979):19–33

Yeh H. F., J. F. Chen, and Lee C. H. “Application of a Water Budget Model to Evaluate Rainfall Recharge and Slope Stability.” *Journal of the Chinese Institute of Environmental Engineering* 14 .4 (2004): 227-237.

Yeh Hsin-Fu., Chen-Chang L. and Cheng-Haw L., “A rainfall-infiltration model for unsaturated soil slope stability.” *Journal of Environmental Engineering Management* 18.4(2008): 261-268.

INTERNET SOURCES

BBC news (2010), Kenya villagers die in Rift Valley landslide, Available: <http://news.bbc.co.uk/2/hi/8655298.stm>; accessed on 20/06/2012. Page last updated at 18:50 GMT, Friday, 30 April 2010 19:50 UK

Bloomberg (2010), Death toll of China’s Gansu mudslide may rise, disaster relief chief says- Bloomberg [Online] Available: <http://www.bloomberg.com/news/2010-08-11/death-toll-of-china-s-gansu-mudslide-may-rise-disaster-relief-chief-says.html> Accessed 20 June 2012

Boston Globe (2010) Landslides strike Zhouqu County, China—the big picture— Boston.com [Online]. Available: http://www.boston.com/bigpicture/2010/08/landslides_strike_zhouqu_count.html; Accessed 20 June 2012

Azizul (2009), Landslides, Last updated on December 20, 2009, available; <http://drazizul.wordpress.com/>; last checked on 13th October 2012.

EDGE ,2005: Response of Suction, Moisture and Temperature of Unsaturated Granitic Residual Soil to Rainfall, available: <http://www.ejge.com/2005/Ppr0545/Ppr0545.htm>, last accessed on 2/8/2012

ESRI, 2008. Last updated January 3, 2008. An overview of the Interpolation tools, available; http://webhelp.esri.com/arcgisdesktop/9.2/index.cfm?TopicName=An_overview_of_the_Interpolation_tools; Last accessed 10/10/2012.

Food and Agriculture Organisation of the United Nations (2007), Introduction to Evapotranspiration. Available at; <http://www.fao.org/docrep/X0490E/x0490e04.htm>; last viewed 20 June 2012

KAGOECH (2012), Keiyo Climatic Conditions & Economic Development, available, <http://www.demo.co.ke/kagoech/section.asp?id=13>; last accessed 13th October 2012

- Kalenjinonline (2012), Keiyo district, (online) Available:
http://www.kalenjin.org/index.php?option=com_content&view=article&id=27:keiyo-district&catid=902:keiyo&Itemid=251; last accessed 20 June 2012
- Mckinney D. C., Groundwater hydraulics, available online
www.ce.utexas.edu/prof/mckinney/ce374l/ce374l.html; last checked on 19th July 2012
- Pack R.T., Tarboton D.G., Goodwin C.N., and Prasad A. (2005) SINMAP 2-A stability index approach to terrain stability hazard mapping.
<http://www.hydrology.neng.usu.edu/sinmap2/sinmap2.pdf>; 26th Oct 2010
- Pavement manual (2007), Available:
http://www.dot.state.mn.us/materials/pvmtdesign/docs/Chapter_3-2.pdf;
last assessed on 20th July, 2012
- Standardmedia (2010), Ten killed in mudslide, 20 missing after heavy rains;
available
<http://www.standardmedia.co.ke/?id=2000008797&cid=4&articleID=2000008797>; last assessed 19th July, 2012
- Standardmedia (2011), Landslide claims 3 lives as floods destroy property;
available
<http://www.standardmedia.co.ke/?articleID=2000047721&pageNo=1>; last assessed on 19th July 2012
- United Nation Office for the Coordination of Humanitarian Affairs (UN-OCHA),
available: <http://ochaonline.un.org/Portals/42/maps/LANDSLIDE.JPG>; last assessed on 19th July, 2012
- United States Geological Survey (USGS), available;
<http://geology.com/usgs/landslides/>; last assessed on 10th July 2012

$$\begin{aligned}
& io \leq 1.5, WC4B, WC4C) - residualWC) / (porosity - residualWC)^{n/(n-1)}) - \\
& 1)^{(1/n)/\alpha}, 100)) - 0/Ks) / (1 + (\alpha * (-1/\alpha) * \ln(\exp(-10 * \alpha * 0) * (0/Ks + \exp(- \\
& \alpha * (IFF(IFUNDEF(((1/((\\
& IFF(sdmkerio \leq 1, WC4A, IFF(sdmkerio \leq 1.5, WC4B, WC4C) - residualWC) / (porosity - \\
& residualWC)^{n/(n-1)}) - \\
& 1)^{(1/n)/\alpha}, 100) > 100, 100, IFUNDEF(((1/((IFF(sdmkerio \leq 1, WC4A, IFF(sdmkerio \\
& io \leq 1.5, WC4B, WC4C) - residualWC) / (porosity - residualWC)^{n/(n-1)}) - \\
& 1)^{(1/n)/\alpha}, 100)) - 0/Ks)))^{n * (n-1)/n})) * TANPI) \\
& / (((IFF(sdmkerio \leq 1, (10 * (SGs / (1 + VR) + WC1A)), IFF(sdmkerio \leq 1.5, (10 * (SGs / (1 + VR) \\
& R) + WC1B)), (10 * (SGs / (1 + VR) + WC1C)))) * (0.2 * sdmkerio) * Si * Co) + ((IFF(sdmkerio < \\
& = 1, (10 * (SGs / (1 + VR) + WC2A)), IFF(sdmkerio < 1.5, (10 * (SGs / (1 + VR) + WC2B)), (10 * (\\
& SGs / (1 + VR) + WC2C)))) * (0.5 * sdmkerio) * Si * Co) + (IFF(sdmkerio <= 1, \\
& (10 * (SGs / (1 + VR) + WC3A)), IFF(sdmkerio < 1.5, (10 * (SGs / (1 + VR) + WC3B)), \\
& (10 * (SGs / (1 + VR) + WC3C)))) * (0.3 * sdmkerio) * Si * Co)), 100, (\\
& ((coheskerio + soilcohes) + ((IFF(sdmkerio \\
& <= 1, (10 * (SGs / (1 + VR) + WC1A)), IFF(sdmkerio < 1.5, (10 * (SGs / (1 + VR) + WC1B)), (10 * \\
& (SGs / (1 + VR) + WC1C)))) * (0.2 * sdmkerio) * Co2) + \\
& (IFF(sdmkerio <= 1, (10 * (SGs / (1 + VR) + WC2A)), IFF(sdmkerio < 1.5, (10 * (SGs / (1 + VR) \\
& + WC2B)), (10 * (SGs / (1 + VR) + WC2C)))) * (0.5 * sdmkerio) * Co2) + \\
& (IFF(sdmkerio <= 1, (10 * (SGs / (1 + VR) + WC3A)), IFF(sdmkerio < 1.5, (10 * (SGs / (1 + VR) \\
& + WC3B)), (10 * (SGs / (1 + VR) + WC3C)))) * (0.3 * sdmkerio) * Co2)) - (IFF(sdmkerio <= 1, \\
& (IFF((WC3A = porosity) AND (q3A = 0), (10 * 0.3 * SDMKERIO), \\
& IFF((WC2A = WC3A) = POROSITY) AND \\
& ((q2A = q3A) = 0), (10 * 0.8 * SDMKERIO), IFF(((WC1A = (WC2A = WC3A)) = POROSITY) \\
& AND ((q1A = (q2A = q3A)) = 0), (SDMKERIO * 10), 0))), IFF(sdmkerio <= 1.5, \\
& (IFF((WC3B = porosity) AND (q3C = 0), (10 * 0.3 * SDMKERIO), \\
& IFF((WC2B = WC3B) = POROSITY) AND \\
& ((q2B = q3B) = 0), (10 * 0.8 * SDMKERIO), IFF(((WC1B = (WC2B = WC3B)) = POROSITY) \\
& AND ((q1B = (q2B = q3B)) = 0), (SDMKERIO * 10), 0))), (IFF((WC3C = porosity) AND \\
& (q3C = 0), (10 * 0.3 * SDMKERIO), IFF(((WC2C = WC3C) = POROSITY) AND \\
& ((q2C = q3C) = 0), (10 * 0.8 * SDMKERIO), IFF(((WC1C = (WC2C = WC3C)) = POROSITY) \\
& AND ((q1C = (q2C = q3C)) = 0), (SDMKERIO * 10), 0)))))) \\
&) + (IFF((-1/\alpha) * \ln(\exp(-10 * \alpha * 0) * (0/Ks + \exp(-\alpha * (IFF(IFUNDEF(((1/((\\
& IFF(sdmkerio <= 1, WC4A, IFF(sdmkerio <= 1.5, WC4B, WC4C) - residualWC) / (porosity - \\
& residualWC)^{n/(n-1)}) - \\
& 1)^{(1/n)/\alpha}, 100) > 100, 100, IFUNDEF(((1/((IFF(sdmkerio <= 1, WC4A, IFF(sdmkerio \\
& io <= 1.5, WC4B, WC4C) - residualWC) / (porosity - residualWC)^{n/(n-1)}) - \\
& 1)^{(1/n)/\alpha}, 100)) - 0/Ks) \\
& <= 0, (-((-1/\alpha) * \ln(\exp(-10 * \alpha * 0) * (0/Ks + \exp(-\alpha * (IFF(IFUNDEF(((1/((\\
& IFF(sdmkerio <= 1, WC4A, IFF(sdmkerio <= 1.5, WC4B, WC4C) - residualWC) / (porosity - \\
& residualWC)^{n/(n-1)}) - \\
& 1)^{(1/n)/\alpha}, 100) > 100, 100, IFUNDEF(((1/((IFF(sdmkerio <= 1, WC4A, IFF(sdmkerio \\
& io <= 1.5, WC4B, WC4C) - residualWC) / (porosity - residualWC)^{n/(n-1)}) - \\
& 1)^{(1/n)/\alpha}, 100)) - 0/Ks))), ((-1/\alpha) * \ln(\exp(-10 * \alpha * 0) * (0/Ks + \exp(-\alpha * (\\
& IFF(IFUNDEF(((1/((IFF(sdmkerio <= 1, WC4A, IFF(sdmkerio <= 1.5, WC4B, WC4C) - \\
& residualWC) / (porosity - residualWC)^{n/(n-1)}) - \\
& 1)^{(1/n)/\alpha}, 100) > 100, 100, IFUNDEF(((1/((IFF(sdmkerio <= 1, WC4A, IFF(sdmkerio \\
& io <= 1.5, WC4B, WC4C) - residualWC) / (porosity - residualWC)^{n/(n-1)}) - \\
& 1)^{(1/n)/\alpha}, 100)) - 0/Ks) / (1 + (\alpha * (-1/\alpha) * \ln(\exp(-10 * \alpha * 0) * (0/Ks + \exp(-
\end{aligned}$$

$$\begin{aligned}
& \text{alpha} * (\text{IFF}(\text{IFUNDEF}(\frac{1}{((1 - \text{IFF}(\text{sdmkerio} \leq 1, \text{WC4A}, \text{IFF}(\text{sdmkerio} \leq 1.5, \text{WC4B}, \text{WC4C}) - \text{residualWC}) / (\text{porosity} - \text{residualWC}))^{n/(n-1)}) - 1)^{1/n}) / \text{alpha}, 100) > 100, 100, \text{IFUNDEF}(\frac{1}{((1 - \text{IFF}(\text{sdmkerio} \leq 1, \text{WC4A}, \text{IFF}(\text{sdmkerio} \leq 1.5, \text{WC4B}, \text{WC4C}) - \text{residualWC}) / (\text{porosity} - \text{residualWC}))^{n/(n-1)}) - 1)^{1/n}) / \text{alpha}, 100))) - 0 / \text{Ks}))^{n/(n-1/n)}) * \text{TANPI} \\
& / (((\text{IFF}(\text{sdmkerio} \leq 1, (10 * (\text{SGs} / (1 + \text{VR}) + \text{WC1A})), \text{IFF}(\text{sdmkerio} \leq 1.5, (10 * (\text{SGs} / (1 + \text{VR}) + \text{WC1B})), (10 * (\text{SGs} / (1 + \text{VR}) + \text{WC1C})))) * (0.2 * \text{sdmkerio}) * \text{Si} * \text{Co}) + ((\text{IFF}(\text{sdmkerio} \leq 1, (10 * (\text{SGs} / (1 + \text{VR}) + \text{WC2A})), \text{IFF}(\text{sdmkerio} \leq 1.5, (10 * (\text{SGs} / (1 + \text{VR}) + \text{WC2B})), (10 * (\text{SGs} / (1 + \text{VR}) + \text{WC2C})))) * (0.5 * \text{sdmkerio}) * \text{Si} * \text{Co}) + (\text{IFF}(\text{sdmkerio} \leq 1, (10 * (\text{SGs} / (1 + \text{VR}) + \text{WC3A})), \text{IFF}(\text{sdmkerio} \leq 1.5, (10 * (\text{SGs} / (1 + \text{VR}) + \text{WC3B})), (10 * (\text{SGs} / (1 + \text{VR}) + \text{WC3C})))) * (0.3 * \text{sdmkerio}) * \text{Si} * \text{Co})) , ?)
\end{aligned}$$

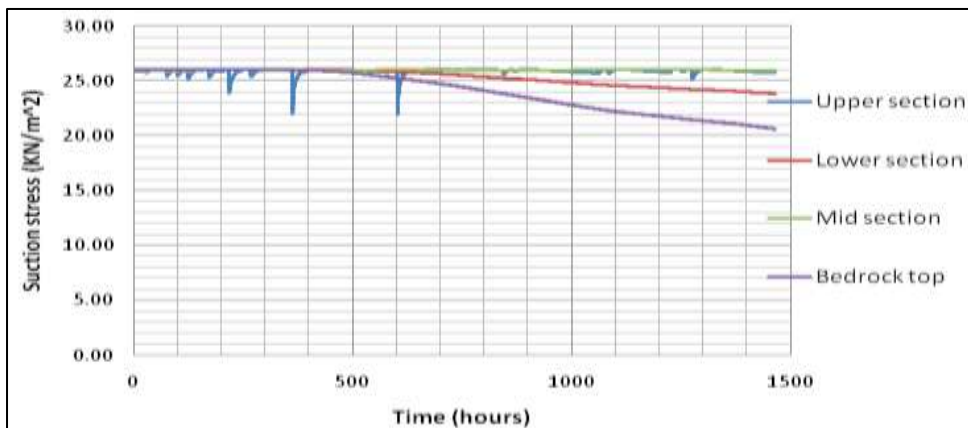
Appendix A (iii): Temporal parameters required by ILWIS GIS Functions in every section of soil

		Thickness of soil under analysis		
Parameter name	Soil section	< 1m	1m ≤ thickness ≤ 1.5m	>1.5M
Volumetric soil water content, θ	Upper	WC1A	WC1B	WC1C
	Mid	WC2A	WC2B	WC2C
	Lower	WC3A	WC3B	WC3C
	Bedrock top	WC4A	WC4B	WC4C
Water flow flux, q	Upper	q1A	q1B	q1C
	Mid	q2A	q2B	q2C
	Lower	q3A	q3B	q3C
Hydraulic conductivity, K	ALL	HC		

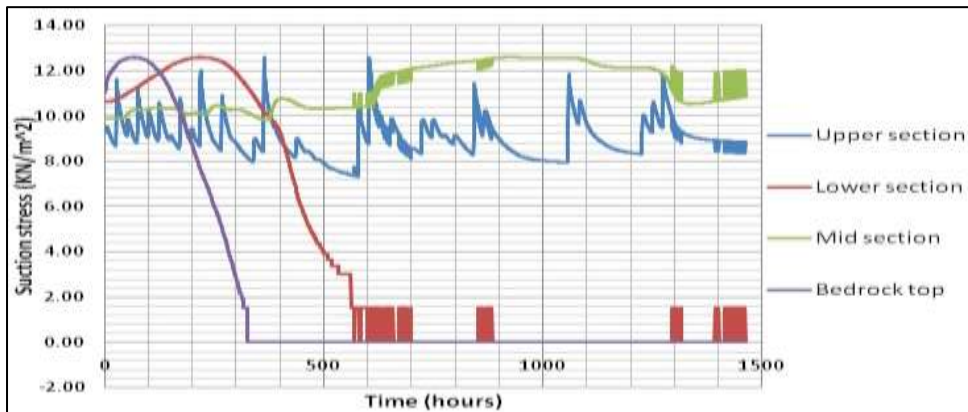
Appendix A (iv): Raster maps required by mapping functions in ILWIS GIS

NO.	RASTER MAP NAME	PARAMETER
1	Ks	Hydraulic conductivity
2	coheskerio	Root cohesion strength contribution
3	soilcohes	Soil cohesion strength
4	sdmkerio	Soil depth
5	Porosity	Soil porosity
6	SGs	Soil specific gravity (2.65)
7	VR	Soil void ratio
8	Co2	Cosine square of slope obliquity
9	alpa	Soil parameter α
10	residualWC	Residual water content
11	n	Soil parameter n
12	TANPI	Tangent of angle of friction
13	Si	Sine of slope obliquity
14	Co	Cosine of slope obliquity
15	RMD	Root maximum depth
16	ROOTTENSILESTRENGTH	Tensile strength of plant species roots

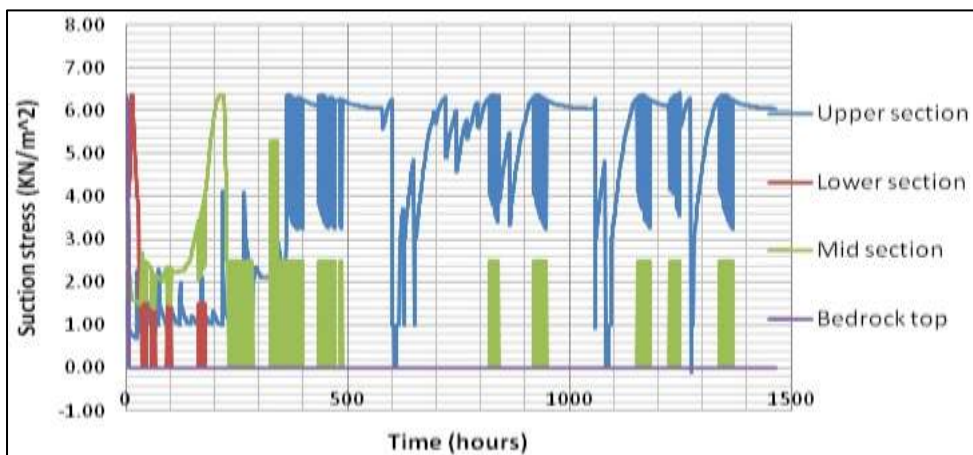
Appendix B: Modelled suction stress results for areal rainfall data



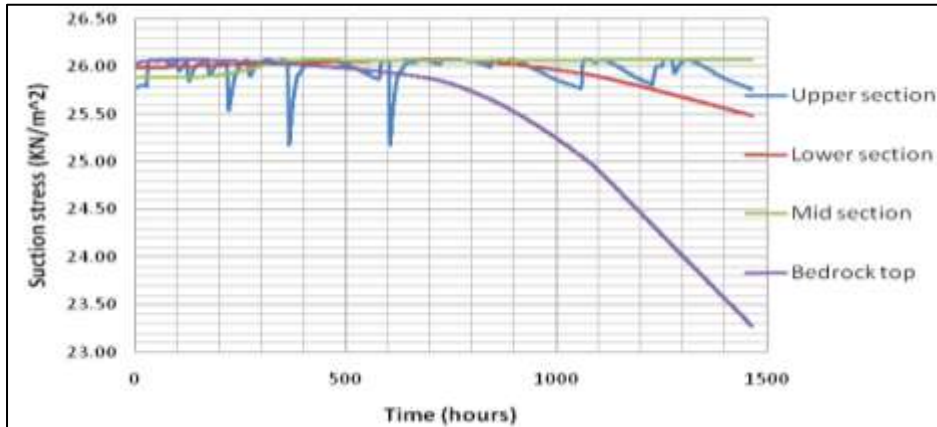
B.1: variation of suction stress with time for clay loam soil of depth 1m



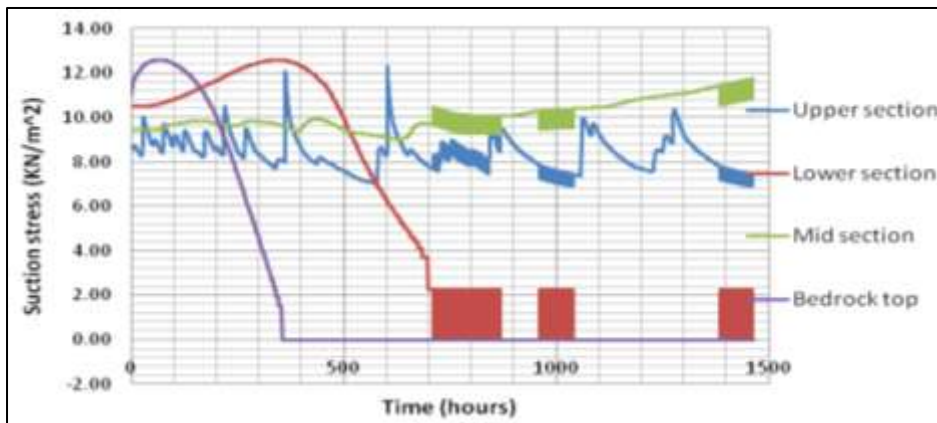
B.2: variation of suction stress with time for loam soil of depth 1m



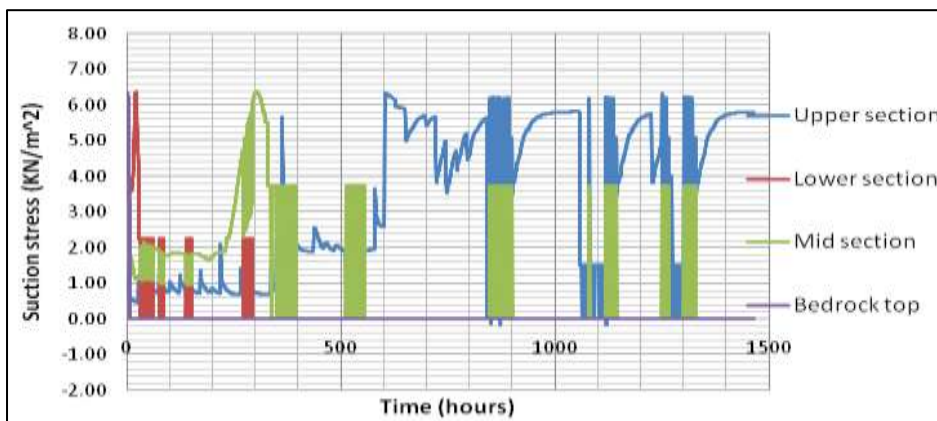
B.3: variation of suction stress with time for sandy loam soil of depth 1m



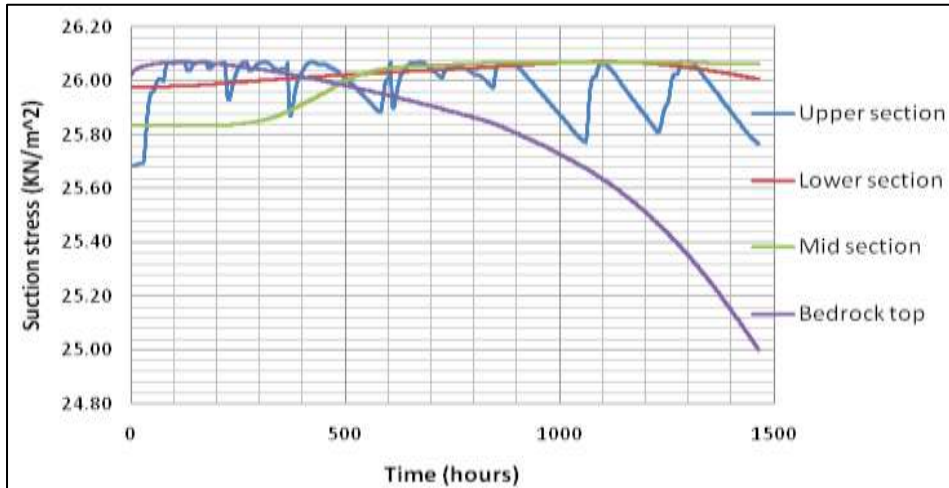
B.4: variation of suction stress with time for clay loam soil of depth 1.5 m



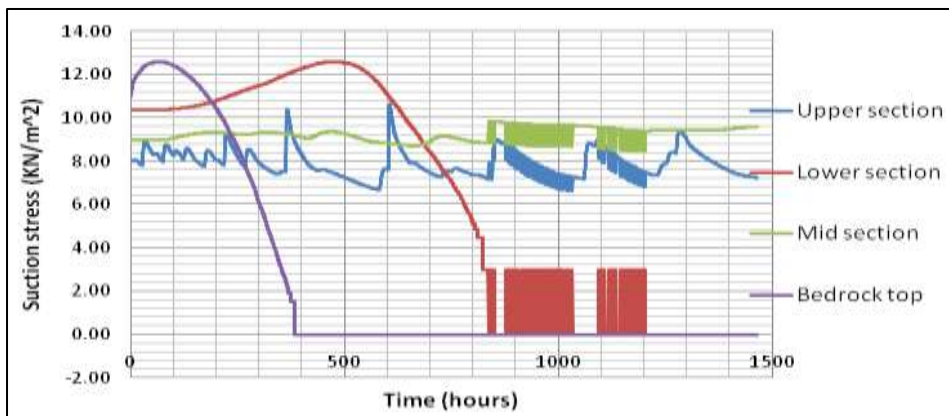
B.5: variation of suction stress with time for loam soil of depth 1.5m



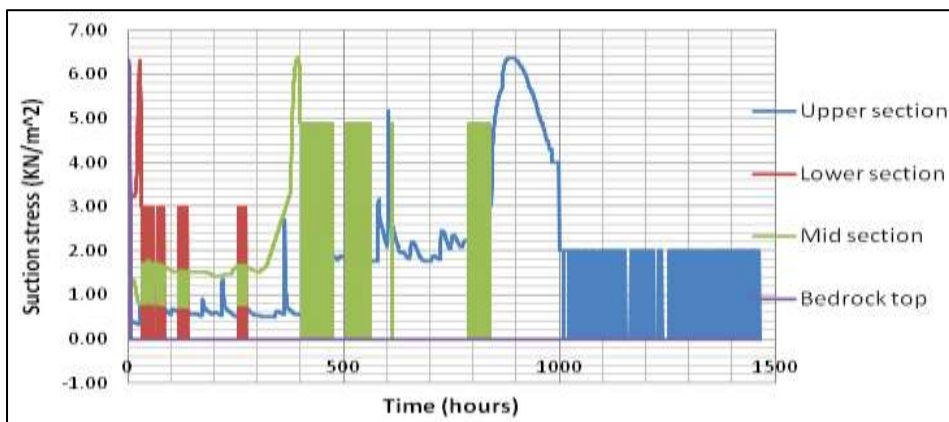
B.6: variation of suction stress with time for sandy loam soil of depth 1.5m



B.7: variation of suction stress with time for clay loam soil of depth 2m

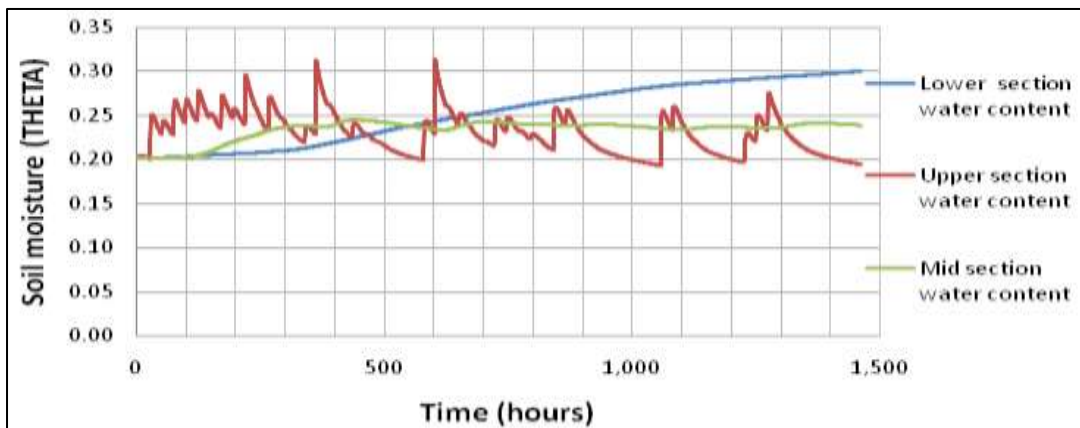


B.8: variation of suction stress with time for loam soil of depth 2m

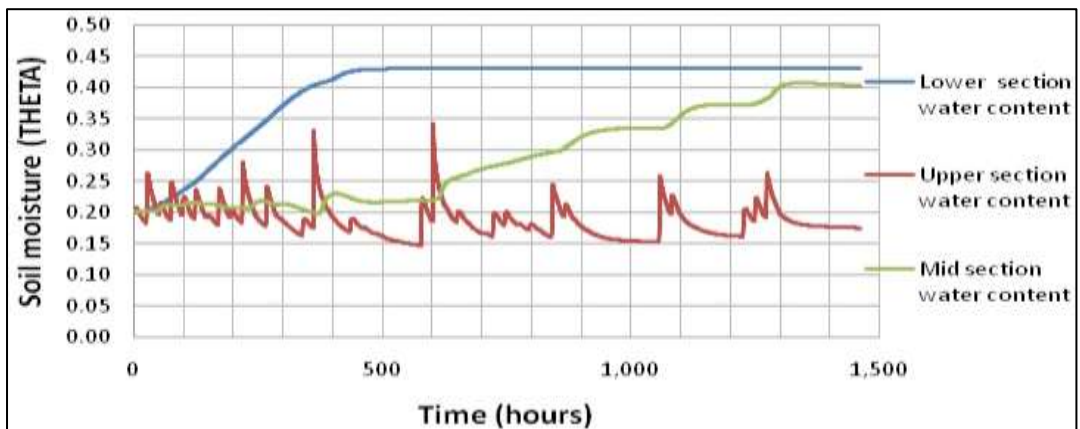


B.9: variation of suction stress with time for sandy loam soil of depth 2m

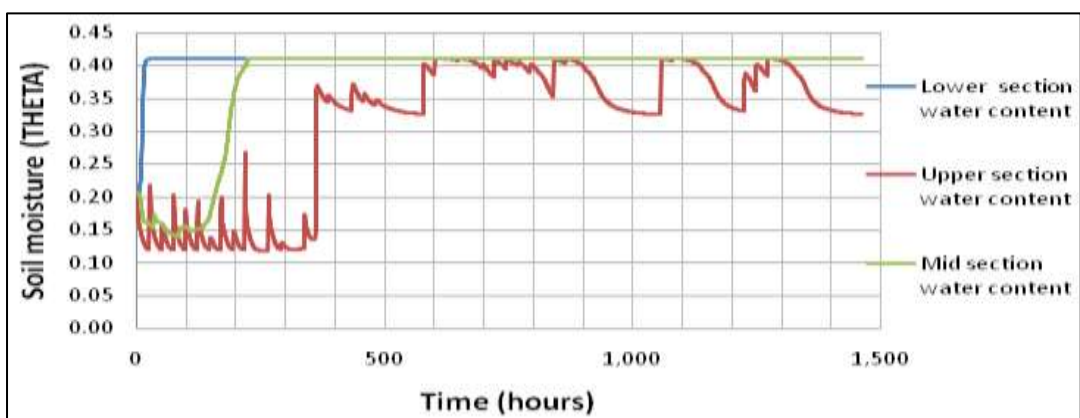
Appendix C: Modelled soil water content for areal rainfall data



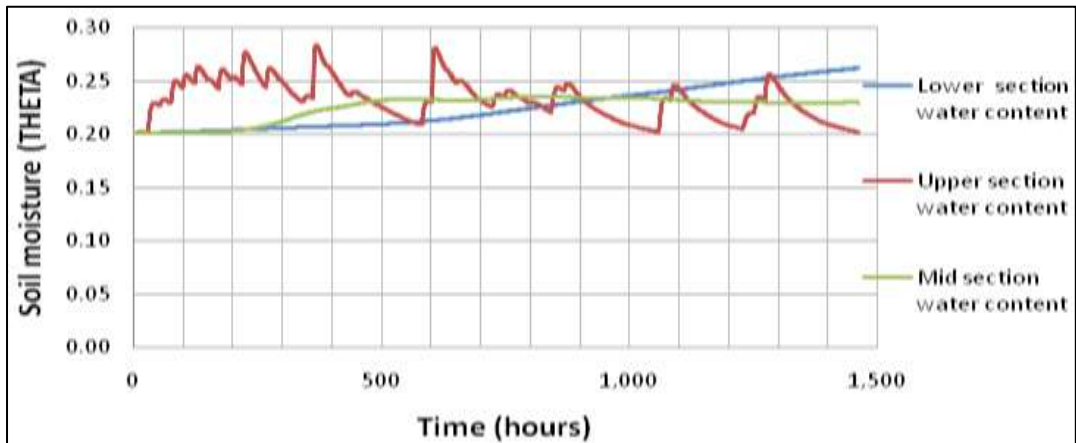
C.1: variation of soil moisture with time for clay loam soil of depth 1m



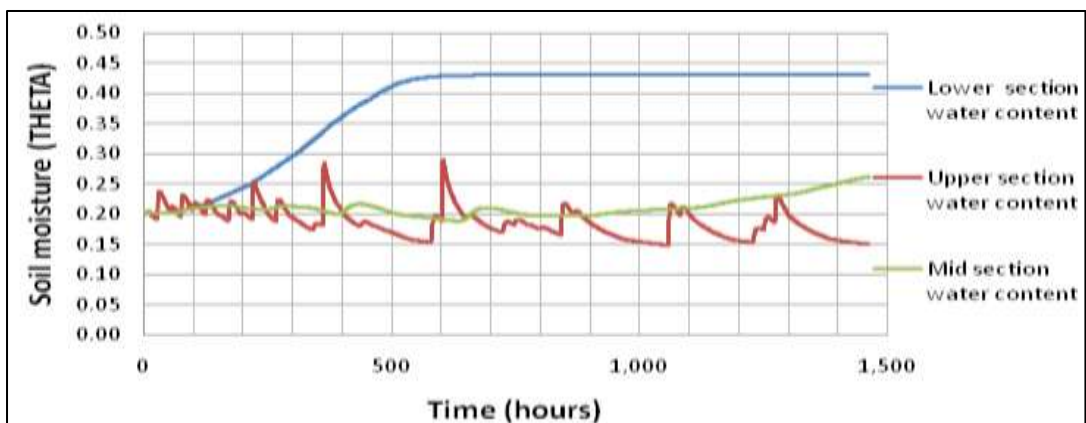
C.2: variation of soil moisture with time for loam soil of depth 1m



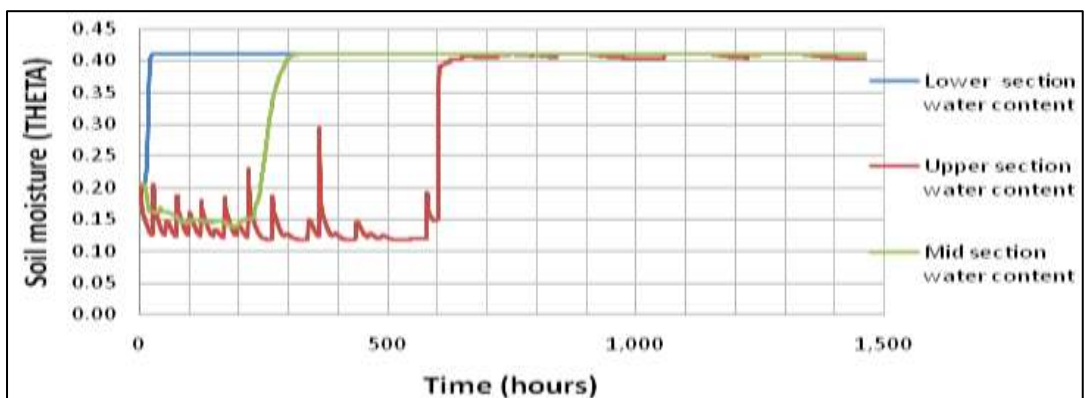
C.3: variation of soil moisture with time for sandy loam soil of depth 1m



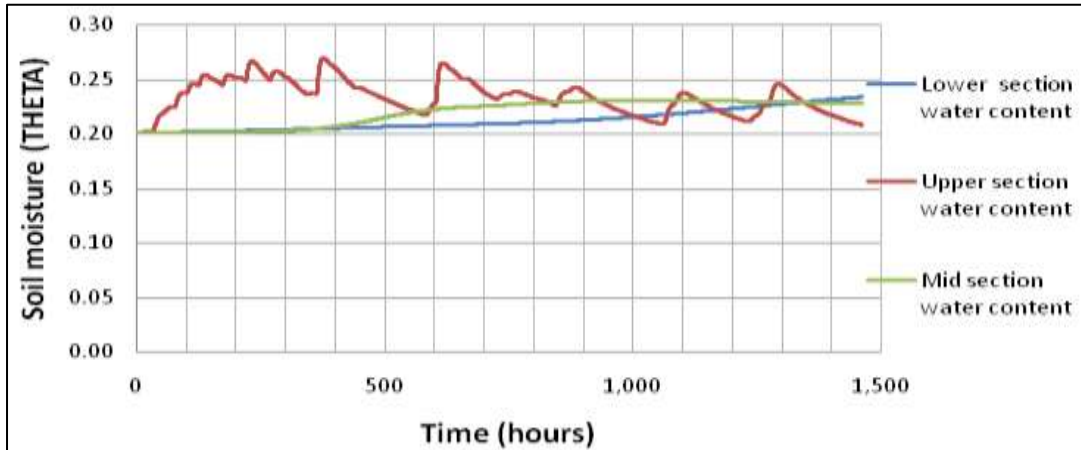
C.4: variation of soil moisture with time for clay loam soil of depth 1.5m



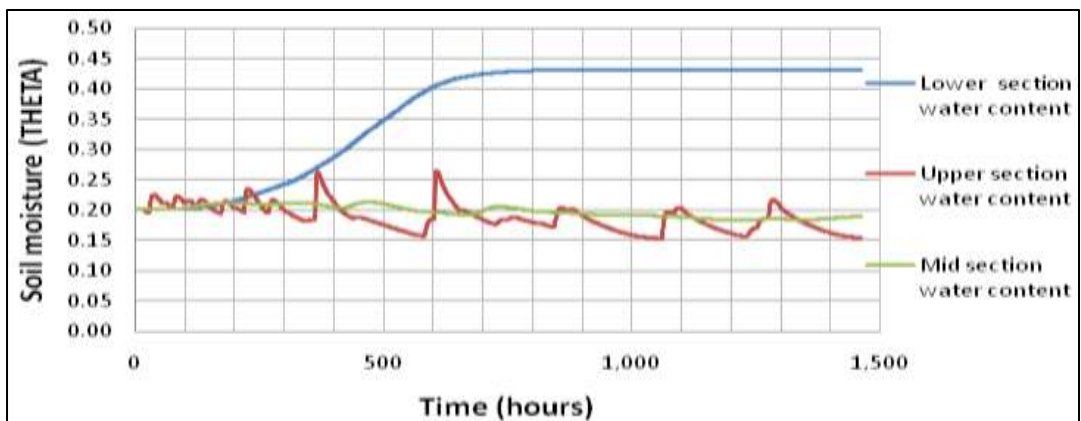
C.5: variation of soil moisture with time for loam soil of depth 1.5m



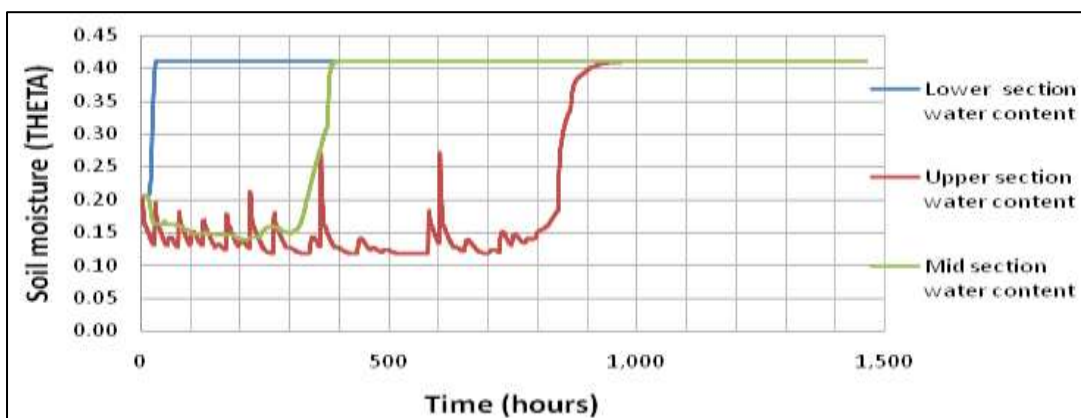
C.6: variation of soil moisture with time for sandy loam soil of depth 1.5m



C.7: variation of soil moisture with time for clay loam soil of depth 2m

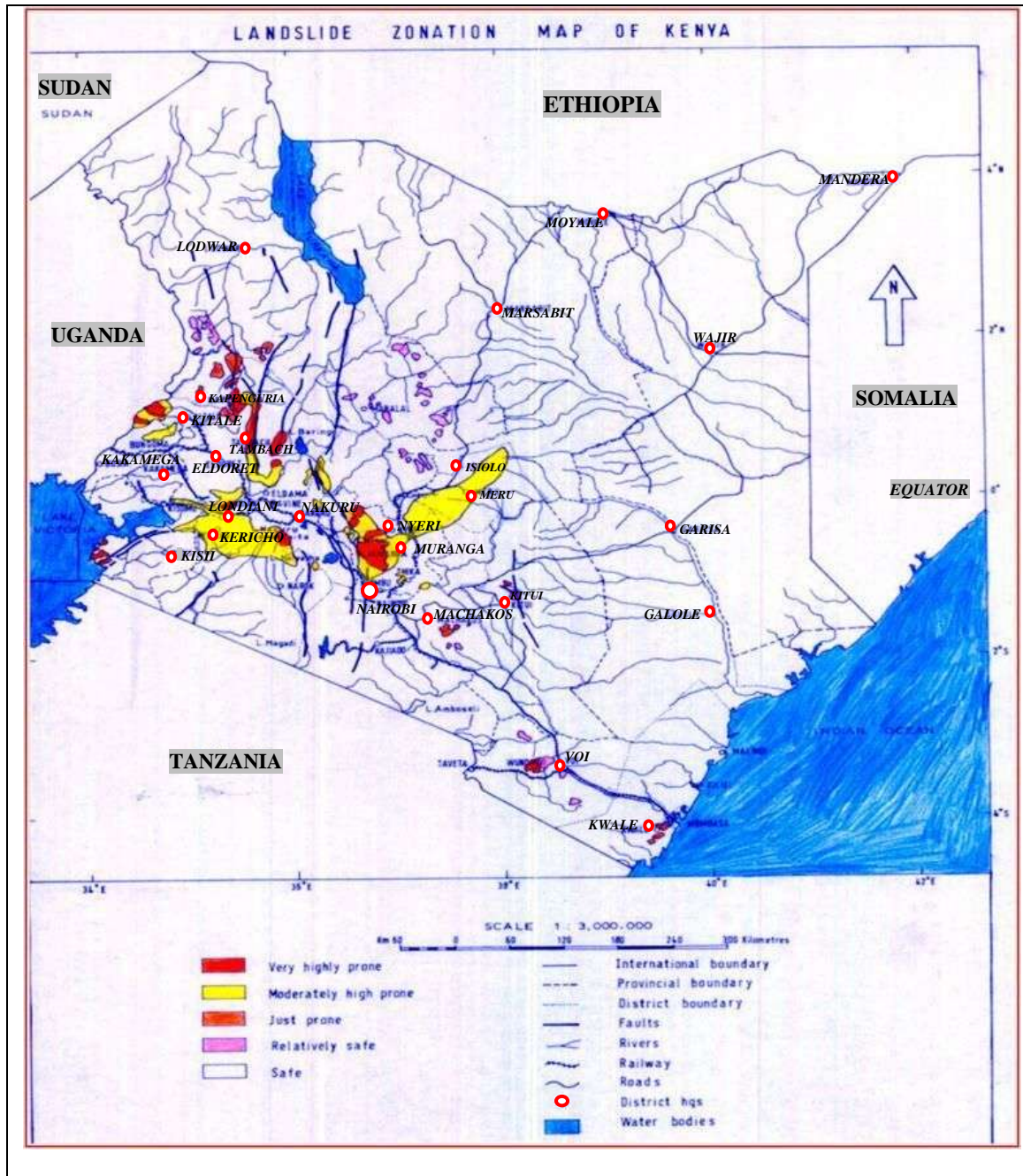


C.8: variation of soil moisture with time for loam soil of depth 2m



C.9: variation of soil moisture with time for sandy loam soil of depth 2m

Appendix D: landslide prone areas of Kenya



(Source: <http://ochaonline.un.org/Portals/42/maps/LANDSLIDE.JPG>)

Appendix E: Root tensile strength for various plant species

author	species	Common name	σ_T	σ_C	σ_B
SHRUBS					
Mattia et al. (2005)	Atriplex halimus	Mediterranean saltbush	57		
Schiechtl (1980)	Castanopsis chrysophylla	Golden chinkapin	18		
Schiechtl (1980)	ceanothus velutinus	ceanothus	21		
Norris (2005a)	Crataegus monogyna	hawthorn	8		
Schiechtl (1980)	Cytisus scoparius	Scotch broom	32		
Mattia et al. (2005)	Pistacia lentiscus	Gum mastic	55		
Norris and Greenwood (2003)	Spartium junceum	Spanish broom	17		
Schiechtl (1980)	Lespedeza bicolor	Scrub lespedeza	71		
Norris and Greenwood (2003)	Phillyrea latifolia	privet	11		
Schiechtl (1980)	Vaccinium spp.	huckleberry	16		
TREE SPECIES: CONIFER					
Stokes (unpublished data)	Abies alba	Silver fir	31	26	
Riedl (1937)	Abies brachyphylla	Nikko fir	28		
Schiechtl (1980)	Abies georgi 3400m a.s.l 4330m a.s.l		28 13		
Genet et al. (2006a)	Cryptomeria japonica	Japanese cedar	8-88		
Stokes & Mattheck (1996)	Larix decidua	European larch	66-428	25	5
Schiechtl (1980) Bischetti et al. (2005) Genet et al.(2005) Turmanina (1965) Mattheck (1996)	Picea abies	European spruce	28 86-650 20-155	27	6, 28
Riedl (1937)	Picea excelsa	Bhutan pine	28		
Coppin & Richards (1990) Schiechtl (1980) Coutts (1983b) Parr and Cameron (2004) Lewis (1985)	Picea sitchensis	Sitka spruce	23 16 35 40	14- 50	
Schiechtl (1980)	Pinus densiflora	Japanese red pine	32		
Norris (unpublished)	Pinus halepensis	Aleppo pine	29, 47		

DECIDUOUS					
Schiechtl (1980)	Acacia confuse	Acacia	11		
Nikla (1999)	Acer saccharum	Sugar maple		35	
Riedl (1937)	Acer plantanoides	Norway maple	27		
Norris (unpublished)	Acer pseudoplatanus	Sycamore	2		
Riedl (1937) Bieshetti et al. (2005) Stokes & Mattheck (1996)	Fraxinus excelsior	Ash	26 37-297	26	12
Schiechtl (1980)	Nothofagus fusca	Red beech	36		
O'Loughlin & Watson (1979)	Nothofagus sp.	Southern beech	31		
Schiechtl (1980)	Populous deltoides	poplar	37		
Schiechtl (1980)	Populous euramericana	American poplar	32		
Coppin & Richards (1990) Stokes & Mattheck (1996)	Populous nigra	Black poplar	5- 12	20	5.5
Hathaway & Penny (1975)	Populous yunnanensis	Poplar	41		
Norris & Greenwood (2003)	Quercus coccifera	Oak	13		
Schiechtl (1980)	Quercus robur	English oak	32		
Turmanina (1965)	Quercus rubra	Red oak	7		
Norris (2005a)	Quercus sp.	Oak	7		
Coppin & Richards (1990)	Robinia pseudoacacia	Black locust	68		

(Source: Norris J.E. et al. (eds.), 2008)

Key to *appendix E*

σ_T is the mean tensile strength (MPa);

σ_B is the mean bending strength (MPa);

a.s.l. imply, “above sea level”.

σ_C is the mean compression strength (MPa);

Appendix F: Rainfall data applied in analysis

DATE	AREAL RAIN DATA (mm)	EVEN RAIN DATA (mm)	SKEWED RAIN DATA (mm)	MOKWO RAIN DATA (mm)
01-Apr	0.3	0.0	2.3	0.0
02-Apr	0.2	17.9	18.7	0.0
03-Apr	0.1	27.6	7.3	0.0
04-Apr	0.1	0.0	15.6	0.0
05-Apr	0.5	11.6	9.7	0.0
06-Apr	3.4	0.0	12.7	9.5
07-Apr	12.3	5.6	4.2	9.8
08-Apr	20.8	0.0	14.8	8.1
09-Apr	5.7	0.0	5.9	0.0
10-Apr	5.9	24.4	25.6	11.5
11-Apr	5.0	0.0	2.2	0.7
12-Apr	4.7	17.5	15.6	0.5
13-Apr	11.6	7.3	2.5	16.6
14-Apr	7.1	0.0	0	10.0
15-Apr	7.1	22.4	8.2	9.0
16-Apr	11.4	0.0	59	23.4
17-Apr	11.1	10.7	2.6	19.5
18-Apr	11.6	0.0	0	28.4
19-Apr	27.7	23.9	7.5	17.1
20-Apr	9.0	0.0	2.8	17.0
21-Apr	5.3	16.8	2.2	18.2
22-Apr	0.2	0.0	0	12.7
23-Apr	2.0	22.5	0	11.4
24-Apr	0.3	17.3	0	0.5
25-Apr	0.7	11.2	16.4	0.2
26-Apr	0.0	24.4	59	0.0
27-Apr	1.0	0.0	2.6	0.1
28-Apr	0.0	5.4	6.9	0.0
29-Apr	0.2	0.0	0	0.0

30-Apr	3.2	11.4	2.3	0.0
01-May	13.7	0.0	10.3	12.7
02-May	20.1	0.0	7.6	9.5
03-May	4.6	12.4	3.4	13.7
04-May	11.4	6.6	5.1	0.1
05-May	10.1	0.0	0	0.2
06-May	7.8	11.3	18.7	18.4
07-May	13.4	0.0	7.5	14.1
08-May	14.5	5.3	0	0.2
09-May	18.1	0.0	0	0.1
10-May	16.0	13.0	0	17.9
11-May	9.9	24.3	0	9.3
12-May	10.5	0.0	0	0.0
13-May	12.7	12.3	0	15.8
14-May	12.9	0.0	0	8.1
15-May	7.8	6.5	25.6	0.2
16-May	6.5	0.0	9.7	1.2
17-May	2.6	0.0	0	0.2
18-May	3.9	0.0	0	1.2
19-May	3.4	6.8	0	9.0
20-May	6.7	0.0	0	9.2
21-May	22.0	0.0	0	15.7
22-May	1.6	7.6	11.2	11.5
23-May	4.7	6.8	10.9	0.0
24-May	1.1	6.0	17.1	17.7
25-May	3.3	0.0	0	10.4
26-May	1.5	0.0	0	19.1
27-May	0.2	11.2	0	0.2
28-May	0.2	0.0	0	0.1
29-May	J7	0.0	0	0.5
30-May	1.0	7.6	0	0.1
31-May	1.7	12.7	0	1.3
	416.9	428.6	433.7	442.0

Appendix G: Moi University Rainfall Occurrence Charts

